Determination of Energy Requirements for Submarine Operations in Shallow Water: An Investigation of the Contribution of Environmental Forces and Seabed Effect.

Maria-Eleni Margeti

Delft University of Technology

TU Delft

Determination of Energy Requirements for Submarine Operations in Shallow Water: An Investigation of the Contribution of Environmental Forces and Seabed Effect.

by

Maria-Eleni Margeti

performed at

C-Job Naval Architects

to obtain the degree of Master of Science in Marine Technology
in the specializations of Ship Design and Marine Engineering
at the Delft University of Technology

This thesis MT.23/24.003 is classified as confidential in accordance with the general conditions for projects performed by TUDelft.
To be defended publicly on Tuesday October 24, 2023

Student number: 5248523
Project duration: December 23, 2022 – October 24, 2023
Thesis committee:

Dr. A. Coraddu,	TU Delft Supervisor, Chair
Dr.ir. R.L.J Helmons,	TU Delft, external member
Ing. R. Hijdra,	C-Job Supervisor

An electronic version of this thesis is available at: http://repository.tudelft.nl/.

TU Delft C-JOB DEDICATED NAVAL ARCHITECTS

Preface

Back in 2021, before I came to the Netherlands and specifically joined TU Delft, I could never have envisioned myself being a part of such an incredible project. My fascination with submarines had always been a personal passion, but the idea of working on them as a mechanical engineer felt like an unattainable dream. Yet, here I am today! The concept design project involving the submarine dredger, aimed at achieving sustainable dredging, seemed like a monumental undertaking at the time, as it allowed me to contribute to the ambitious zero-emission goal.

It's been a full year since I embarked on my internship within the same project, albeit in a different capacity, and then continued with my thesis. I owe a debt of gratitude to C-Job Naval Architects, with a special mention for Rolph Hijdra, who not only placed his trust in me but also provided me with the opportunity to be a part of this remarkable team. I understand that supervising me may have presented its challenges, so I want to express my sincere appreciation for his patience and unwavering guidance throughout the project. Our collaboration has undoubtedly shaped me into a better engineer and has heightened my awareness of the imminent practical and societal challenges within the shipping industry.

Additionally, I am thankful for all the colleagues I encountered at the Rotterdam office, who illuminated even the gloomiest of days with their presence. A heartfelt thanks goes to Ricardo and Mark, who patiently fielded my seemingly trivial inquiries and helped me surmount the now minor obstacles that, back then, appeared insurmountable. I am equally appreciative of their emotional support during this journey.

Of course, this project would not have reached completion without the invaluable contribution of Dr. Andrea Coraddu, my supervisor from TUDelft. I owe him a profound debt of gratitude for consistently being there to provide guidance and support whenever I needed it. I will always remember his favorite expressions that characterized my work: *"When life gives you lemons, make Limoncello,"* and *"Imagine your thesis as a BBQ, if you put too much meat, you will burn it; if you put too little, people will be hungry."*

Turning to my everyday supporters, my friends, both from the MSc Marine Technology program and other departments, I extend my heartfelt thanks to all of you for being my biggest source of strength and encouragement. I cherish the memories of our shared moments and the days and nights spent studying together, striving to meet deadlines.

I wish to express my profound gratitude to the esteemed organizations and companies that placed their trust in me and honored me with the following scholarships: the prestigious *G. P. Livanos HELMEPA Scholarship*, the esteemed *Scholarship of the UGS in memory of Ioannis Angelicoussis*, and the coveted *HelleniQ Energy Scholarship*. Your generous financial support has been instrumental in my academic journey, and I wholeheartedly acknowledge that I wouldn't have achieved this milestone without your unwavering belief in my potential. Thank you for your invaluable contribution to my education.

Last but certainly not least, my deepest gratitude goes to my family for their unwavering love and support. Thank you all for being there and believing in me, even in my wildest dreams. While the completion of this thesis may not automatically repay the investments you've made in me, I hope that the overwhelming sense of pride and happiness is undoubtedly there! Although it was a journey full of emotions and I jumped through hoops, or, if I directly translate it from Greek, *I went through 40 waves*, I finally made it!

Maria-Eleni Margeti
Delft, October 2023

Summary

It is known that the Dutch North Sea coast consists mostly of sand, which creates the need for continuous maintenance. For the time being, these maintenance activities are carried out with the aid of trailing suction hopper dredgers (TSHDs), which emit greenhouse gases during dredging operations. As the world continues to prioritize sustainability, the field of marine engineering is no exception. The Dutch Rijkswaterstaat goal is to reduce these emissions to zero by 2030 at the latest. For this reason, C-Job Naval Architects has designed the Autonomous Low Energy Replenishment Dredger (ALERD) to meet the anticipated increase in Dutch coastal maintenance while simultaneously providing sustainable and cost-effective solutions for such maintenance work. The development of autonomous replenishment dredgers has to be further investigated in order to determine the energy requirements and if it is a worthy future investment.

Regarding the research's approach, first, the environmental conditions need to be determined in order to identify the environment in which these submarines will operate and the relevant destabilizing forces that they create. Ocean currents, ocean waves, as well as seabed interaction with submarines and generally underwater vehicles will be reviewed with respect to modelling, as they can have a significant impact on stability and manoeuvrability. In order to counteract the developed forces, forward thrusters, vertical tunnel thrusters, and the trim tanks will be modelled. Investigating the aforementioned topics, the simultaneous research about the modelling of the environmental forces and the seabed interaction on underwater vehicles and the existence of a model that can estimate the energy consumption is recognized as a "gap" in the literature. As a result, a simulation model for an underwater vehicle, especially a submarine that operates in shallow water, that takes into account all the previously mentioned destabilizing factors and counteracting forces, will contribute to the advancement of a model that effectively estimates the required energy, using Matlab, Simulink.

In the developed model, three PID controllers in the three different degrees of freedom, surge, heave and pitch, are applied. They control the rpm for the forward thrusters and the vertical tunnel thrusters in surge and heave respectively. The PID controller in pitch direction adjusts the water mass that needs to be transferred from one trim tank to another in order to handle the pitch motion. The ALERD is used as a case study for the generated model.

At the present phase of the ALERD concept, detailed hydrodynamic characteristics remain unavailable. The undertaking of CFD simulations or scale-model tests is deemed undesirable due to their perceived expense and time-consuming nature, particularly given the incomplete status of the ALERD's key parameters. The mathematical equations that describe the former are modelled in Matlab, Simulink to perform time-domain simulations. The ALERD has an unique operational profile in which it operates underwater in all three of its operational modes: transit, dredging, and discharge. This operational profile for the ALERD is based on conventional dredgers working in coastal replenishment along the Dutch coastline. Each operating mode has its own set of criteria, such as the goal depth, desired speed, and operational time.

It is worth noting that given the operational profiles for the velocity in surge, the depth and the pitch, the ALERD follows them successfully. Nevertheless, the presence of the waves cause an oscillating behavior of the ALERD in heave and pitch directions which cannot be eliminated if only PID controllers are utilised. The PID controllers fail to cancel out the oscillations by themselves. Since the implementation of a different control strategy is not in the scope of this project, a different solution needs to be explored to estimate the required energy. For this reason, a low-pass filter is applied at the resultant rpm of the PID controller in heave direction in order to make the oscillating behavior of the rpm converge to a value, and calculate the required thrust. As a result, the consumed energy for a full dredging cycle is determined per actuator.

It needs to be mentioned that when factoring in all environmental conditions and seabed interactions, the ALERD exhibits a maximum overshoot of 6.25% when descending to a depth of 8 meters. This deviation is not considered critical, as it poses no risk of grounding. In the case of operation at a depth of 15 meters during dredging conditions, the combined maximum overshoot, which accounts for both the depth controller and pitch controller, is estimated at 7.3% (0.58m). This level of overshoot is

considered safe, given that the ALERD has a clearance of 2 meters. Regarding the energy results, it is concluded that the forward thrusters consume 4192kWh, the vertical tunnel thrusters 340kWh and the pump for the trim tank system 0.2kWh. These results cannot be verified since the ALERD is a unique concept design and there are no available data of similar submarine dredgers. However the developed model can be used for the estimation of the required energy of similar designs that are in a preliminary design phase. Furthermore, the maximum demanded power for the thrusters and the pump can be determined using the model, in order to define the size of the necessary machinery.

The concluding recommendations mostly revolve around the functionality improvement of the tool, in order to increase its quality and generate models of higher accuracy. An adaptive PID controller is recommended to be implemented, since the gains for the PIDs can change dynamically. By using adaptive coefficients, a PID controller can be made more robust and versatile, able to handle nonlinearities, and changes in system dynamics. Furthermore, a state-observed is suggested to be applied in combination with the already existed PID controllers in order to estimate and compensate for unknown environmental forces in real-time and eliminate the oscillating behavior. Last but not least, the hydrodynamic coefficients should be improved to the actual hull shape of the submarine in further investigation.

Contents

List of Figures

List of Tables

1 Introduction

1.1. Background & Motivation

As it is widely known, the Dutch North Sea coast consists mostly of sand. By applying beach, shoreface, and coastal foundation nourishments, Rijkswaterstaat maintains the coastline and regularly nourishes erosional hotspots. Currently, 12 million m^3 of sand is replenished annually [1] depending on market conditions, and an increase to 20 million m^3 is required for the entire coastal base to grow in parallel with the current rise in sea levels. The volume of sand required to maintain the coastal base grows in synch with the rising sea level. According to preliminary estimates, this can range from 30 million m^3 per year in 2050 to 65 million m^3 per year in 2100 [2].

For the time being, these maintenance activities are carried out with the aid of trailing suction hopper dredgers (TSHDs), which emit greenhouse gases during dredging operations. The Dutch Rijkswaterstaat goal is to reduce these emissions to zero by 2030 at the latest. In times of increasing environmental awareness and a continuous focus on economic interest, a balance should be found between these two. C-Job Naval Architects started contributing to the aforementioned program and initiated the Autonomous Underwater Maintenance Dredger (AUMD). This is a concept design that according to [3] shows promising, both from an operational as well as sustainability point of view. In continuation of this project, C-Job Naval Architects developed another concept design, the Autonomous Low Energy Replenishment Dredger (ALERD) for coastal replenishment. This built on the work for the AUMD but with a different operational profile; coastal replenishment instead of maintenance work in ports and harbours.

The research is motivated by the critical need for sustainable and efficient energy usage in the maritime industry. Submarine operations in shallow waters are complicated due to environmental forces and seabed effects, which can affect a vessel's energy requirements. Furthermore, being aware of the highly nonlinear equations of motion that characterize a submarine, and the coupled motions, it is concluded that the development of a simulation model, although challenging, will contribute to the maritime industry. For analyzing the efficiency of the model, the Autonomous Low Energy Replenishment Dredger (ALERD) can be used as a case study, that aims to address these issues by providing a more sustainable and efficient dredging solution. This research seeks to improve understanding of the factors that affect the energy efficiency of underwater vessels by investigating the contribution of environmental forces and seabed effects on the energy requirements of submarines. After reviewing the literature study and the state-of-the-art approaches with respect to modeling these destabilizing forces on a submarine, it was noted that there is no such simulation model that can be used to assess the energy requirements for the aforementioned underwater vehicle. Recent advancements in autonomy, navigation, and communication enable autonomous missions that would otherwise require constant operator control. Although ALERD is the triggering concept design for this research and also the development of a simulation model, more underwater vehicles will benefit from the former. For instance, the MUM, Large Modifiable Underwater Mothership, the project represents a new class of autonomous working platforms that are supposed to deliver a system capable of solving relevant tasks of the offshore and deep-sea market effectively with a minimum of engineering effort after the initial product development [4]. Furthermore, in [5] a novel subsea shuttle tanker (SST) concept was pro-

posed as a cost-effective alternative to subsea pipelines and tanker ships for liquid CO2 transportation between a source facility and a subsea well. As is verified from the previous studies, autonomous underwater submarines are an expanding field, resulting in the need for the development of a simulation model that will provide them with accurate results for the energy requirements. Through this review, the development of a control system will enable the accurate determination of the energy requirements of a submarine, which can then be used to optimize its performance and energy usage. Ultimately, the results of this research have the potential to contribute to the development of more sustainable and efficient maritime technologies, which can have significant environmental and economic benefits.

1.2. Case Study-ALERD

1.2.1. C-Job Naval Architect's Vision - Autonomous shipping

In the last few years, autonomous shipping has been a hot topic that is discussed more and more every day. As it is said, it can provide better efficiency, reliability, safety, and sustainability. In line with this statement, C-Job's vision is that autonomy could provide alternative solutions that support the development of sustainable solutions. For this reason, and after exploring the possibilities of the former, the idea of AUMD was developed. Although it is an extreme concept design for dredging, it can contribute to the sustainable dredging operations of the future. In continuation of AUMD's idea, ALERD's idea started being developed for delivering sediment to coastlines to protect the land. Both the AUMD and the ALERD concept designs will be briefly explained further below.

1.2.2. Autonomous Underwater Maintenance Dredger (AUMD)

The Autonomous Underwater Maintenance Dredger (AUMD) is a proposed submarine design that has the capability to perform dredging activities without requiring a crew. This design offers several advantages, including reduced power consumption for the dredging pumps due to the reduced suction head, as stated by the authors of [6]. The AUMD is fully submerged and thus does not experience wave resistance, resulting in reduced propulsion power. Additionally, the AUMD has the same loading capacity as manned dredgers but incurs reduced operational costs as it does not require a crew on board. According to C-Job Naval Architects, a 16 MWh battery pack is sufficient for AUMD which makes it able to perform 12 hours of (continuous) dredging operations. These advantages of the AUMD concept design have significant implications for both sustainability and economic considerations in terms of operational costs.

1.2.3. Autonomous Low Energy Replenishment Dredger (ALERD)

In order to protect the land in a sustainable manner and as a foster of AUMD, the Autonomous Low Energy Replenishment Dredger (ALERD), is built on AUMD's concept idea with a different operational profile and the main goal of the replenishment of the coastline. According to [7], [8] ALERD can operate autonomously underwater, saving energy during the dredging process and transit. The need for energy saving created the ambition of further research of state-of-the-art energy supplies. In [7] a literature review was performed regarding the Li-ion batteries and the Proton Exchange Membrane Fuell Cell (PEMFC). Not taking into account the weight and stability calculations, from [7] it is concluded that the hybrid types of ALERD have the best characteristics for coastal maintenance. More specifically, it is stated that the implemented system depends on the development of ammonia SOFC, if it is ready to supply energy, or if the hydrogen PEMFC is the best solution. After further research, it was demonstrated that both power sources could deliver lower operational costs compared to the benchmark provided by the IKZ program.

ALERD's concept idea is still ongoing and the research around it has not ended. Further studies for the stability, the optimal hopper's volume, etc. need to be defined in order to obtain the final dimensions of the former. Nevertheless, a preliminary design is depicted in Figure [1.1], and this research aims to proceed one step further with this idea, analyzing the energy requirements and evolving the motion control system which is developed in [9]. This will be achieved considering the environmental forces and the seabed interaction, forces that need to be counteracted for the operability of ALERD.

Figure 1.1: Preliminary design of the outer shell and the inner layout of ALERD

1.3. Problem Formulation

In the pursuit of reducing energy consumption in offshore operations, C-Job Naval Architects is conducting research on the benefits and challenges of autonomous/unmanned submarine operations. However, operating near the surface and seabed poses critical conditions for submarines due to environmental forces and seabed effects, which affect the resistance, heel, and trimming moment. The former need to be quantified in order to define to what extent they affect a submarine's energy requirements. This dissertation aims to investigate not only the theoretical background but also the different approaches researchers followed to model the environmental forces, the seabed interaction, and the different actuators to simulate an accurately challenging environment and underwater vehicle models.

Modeling and simulation will be used to implement the behavior and contribution of these disturbances to submarines, with consideration given to computational cost, implementation, and precision. The first-order motions caused by these disturbances will be addressed through the development of an appropriate control system for submarines. This research will investigate the challenges and potential solutions associated with these issues in the context of submerged dredging. Nevertheless, for the specific case study that will be used for the evaluation and results of the model, ALERD will be utilized and the research, in the end, will be focused on its specifications. It needs to be mentioned that it is in the initial design phase, so the dimensions are not finalized yet, but it can be considered that it is going to operate around 8-10 knots, with Froude numbers being in the range from 0.15 to 0.19, considering the overall length of $L_{oa} = 80m$. Similarly, CFD analysis or a model test is not the most suitable method to obtain results. Nevertheless, the model will be available to be used for every submarine similar to ALERD, regarding the dimensions and the displacement. Consequently, the integration of the environmental forces, as well as the seabed effect into an underwater vehicle's motion control system and the calculation of the energy required are essential studies to be carried out.

1.3.1. Research aim & questions

The aim of this research is to integrate environmental forces and seabed effects into the motion control system, modelling motion compensating actuators such as vertical thrusters and control planes, and investigating the energy required for stable submarine operation during dredging and transit operations in shallow waters. The submarine must maintain a prescribed height above the seabed to ensure safe clearance for the dredging process.

Therefore, ***the primary objective of this research is to develop a model that accurately determines the energy required to compensate for environmental forces and seabed effects on a submarine, operating in shallow water.*** This will contribute to a better understanding of the energy requirements of submarines and enable the development of more energy-efficient solutions.

Additionally, the research questions are defined below in order to guide the research in the desired direction.

Research Questions:

1. What are the environmental forces in the North Sea operating area that need to be considered?

    a. What are the main environmental forces that affect submarine operations in shallow waters both in transit as well as in dredging conditions?

   b. How can the environmental forces be included in the mathematical model?

2. How does the seabed contribute to the overall forces on a submarine in shallow waters?

   a. How can the effect on resistance and surge, pitch and heave by the seabed be included in the mathematical model?

3. How many DOFs should be included in the model?

   a. What is the most significant direction in terms of the impact on the submarine of the seabed effect?

4. What are the best control strategies that can be implemented in the mathematical model considering energy requirements and operability?
5. Should / How can the non-linearities be included in the motion control?
6. A case study will be performed for the application within ALERD, determining the energy requirements.

1.4. Literature Review

This literature review aims to investigate not only the theoretical background but also the different approaches researchers followed to model the environmental forces, the seabed interaction, and the different actuators to simulate an accurately challenging environment and an underwater vehicle model. The obtained knowledge will be properly utilized to answer the research question which addresses developing a model that accurately determines the energy required to compensate for environmental forces and seabed effects on a submarine, operating in shallow water. For the verification of the model, the case study of ALERD will be employed, which is going to be the first autonomous underwater unmanned replenishment dredger, developed by C-Job Naval Architects.

Underwater vehicles are complex and primarily characterized by non-linear and highly coupled dynamic systems. Nevertheless, it is proven that the critical directions being affected by the environmental forces, such as the ocean currents and waves, as well as by the seabed interaction, are the surge, heave, and pitch. Thus, the created forces need to be compensated in the aforementioned directions. Correspondingly, the developed model for a submarine can be represented by two non-interacting longitudinal and lateral subsystems, with a coupled 3 degrees of freedom 2D model. CFD analysis and model tests are cutting-edge methods for simulating underwater vehicles and determining their hydrodynamic properties. Taking into account the fact that some submarines might be in an initial design phase, the aforementioned approaches will be hard to apply, due to the computational cost. Consequently, regarding the hydrodynamic coefficients, they will be reduced considering the symmetrical hull shape of submarines and by the linearization of the system. Moreover, the assumption of the ellipsoidal shape of the hull will be done and analytical formulas will be used to determine the hydrodynamic coefficients.

It is reviewed that the ocean currents and the ocean waves can create a very challenging environment for the operation of underwater vehicles. Furthermore, underwater vehicles that operate in shallow water, especially close to the surface and seabed, are affected by forces such as resistance, lift, and pitching moment. These forces vary with the different Froude numbers and depth. In order to develop a precise model including randomness, Fossen's approach will be followed, integrating a stochastic current signal and a stochastic Jonswap wave spectrum. For the specific case study of ALERD which is going to operate in the North Sea, it is believed that the Jonswap spectrum and a current signal from this area will create suitable conditions for the simulation. Simultaneously, using coefficients from already existing CFD studies, the seabed interaction and the near-surface operation will be included in the model.

Since the developed destabilizing forces need to be compensated, stabilizing systems are required. The most common actuators on underwater vehicles are the control planes, the tunnel thrusters, and the ballast tanks. They are reviewed and the state-of-the-art approaches are described. Control surfaces are used to control the vertical motion when operating at high speeds while the vertical tunnel thrusters are utilized at low speeds. Regarding the control planes, one of the cutting-edge approaches is the integration of controllers in order to change the pitching angle, while more precise equations that describe more accurately the behavior of the thrusters have been developed. Automated ballast tank systems have been studied and integrated into underwater vehicles, applying a depth controller,

and aiming to achieve and maintain setpoint depth while using a minimum amount of water and air mass resources. In the case study of ALERD, the main ballast tank system is used to compensate for the forces created by the loading and discharge of the soil in the hopper. For a wide applicability of the motion control system, the mass in the ballast tank system will remain constant. In this way, submarines similar to ALERD can utilize the motion control system independently of the ballast tank one. The underwater environment, mainly characterized by currents and waves, is challenging. Thus, the developed forces will have a frequency of adjustment in an order of minutes, which might make the tanks insufficient to compensate on time for the former, however, an integrated automated ballast tank system is not the scope of this work. Additionally, as ALERD is still in the initial design phase, is armed with neither control surfaces nor vertical tunnel thrusters. Notwithstanding, in order to develop a more realistic simulation, and broaden the applicability of the motion control system integrating submarines that already have these actuators, assumptions regarding the implementation of tunnel thrusters will be made. The control planes will be excluded for the simplification of the model. Simple models will be established to control the motions and in the end, an assessment of the energy requirements for controlling these motions can be done.

Last but not least, the commonly used as well as cutting-edge motion control methods for underwater vehicles are discussed. One of the most common controllers is the PID controller, being applied to underwater vehicles but it has been reviewed that sometimes fails due to the non-linearities of the system. As mentioned previously, the PID is tuned under specific conditions. These conditions change, due to the fact that they are affected by currents and waves, which vary with time, resulting in insufficient results being provided by the controller. In order to deal with this issue, researchers developed more complex control strategies, combining the PID controller with state, and disturbance observers, or applying adaptive PID control methods. Furthermore, control methods such as MPC, SMC, and Fuzzy logic controllers are implemented into underwater vehicles providing satisfactory results. Considering the motion control system which aims at the energy assessment, the development of a complex control strategy is out of the scope of this study. Hence, the model will be provided by three PID controllers for the three different degrees of freedom, to verify the results being found in the literature about the insufficiency of the former. In continuation, after capturing the motions the assessment of the required energy of the submarine will take place.

1.5. Research Reflection

1.5.1. Importance of dredging

Waterborne transportation has achieved substantial commercial viability and environmental preference as a means of transportation in the modern landscape. Maintenance and development of access channels and basins near waterside facilities are crucial to facilitating and ensuring the continued viability of this form of transportation. The significance of such dredging cannot be emphasized, as it is critical in optimizing waterborne transit and providing effective waterside services. The expansion in coastal urbanization has raised the demand for property for residential, commercial, and recreational purposes. Modern advances in dredging technology have changed the once-expensive process of land reclamation into a financially viable possibility for new land development endeavors.

Coastal communities face several environmental challenges, such as rising sea levels, stronger and more frequent storms, and erosion, which pose significant threats to human safety and health. Dredging meets the demand of coastal populations for more beach protection against floods and other health and safety concerns, by removing sediment buildup in waterways and creating deeper channels to allow for better water flow and reduced tidal surge.

Beach nourishment is another objective of integrated coastal zone management. The artificial placing of sand on an eroding shore to preserve the amount of presented sand is referred to as beach nourishment. As the name implies, this technique includes dredging material, such as sand, which is distributed over the beach to compensate for coastline erosion and restore the beach's recreational value. Beach erosion is widely recognized as a serious problem. To be more specific, when the shoreline recedes, the sea barriers collapse, endangering coastal properties. Beach replenishment is not a long-term erosion-control option. The erosive pressures of waves, storms, and increasing sea levels do not subside after nutrition, which is why nourishment is typically a recurrent procedure.

In conclusion, dredging is a crucial component of modern coastal and maritime infrastructure, essential for the smooth and efficient operation of waterways, ports, and harbors and for supporting the

sustainable development of the maritime sector. Dredging helps prevent silting, which can affect the stability of docks and other coastal structures, and ensures the ongoing functionality of access channels and basins near waterside facilities. Last but not least, beach replenishment is a necessary procedure that needs to be continued and dredging plays a crucial role in the former. The necessity of continuing maintenance dredging for these facilities cannot be overstated since it is essential for the optimization of waterborne transportation and the provision of functional waterside facilities.

1.5.2. Maintenance of the Dutch coast

Half of the Dutch coastline is protected by natural dunes and the densely populated Randstad area almost entirely. To preserve the dunes and coastline periodically sand is supplied. It is widely known that climate change threatens the Dutch coastline as the sea level rises and periodic nourishment in smaller time intervals will be required.

The Dutch Rijkswaterstaat, is responsible, for construction, management, and coastal maintenance. For this reason, many projects approved by the former, aim to beach replenishment. According to [10] and regarding the Quality Status Report around the Wadden Sea, several small dikes were strengthened and many relevant projects are in progress aiming at the improvement of the dikes and the protection of the Dutch coastline. On the Wadden Sea islands, sand nourishment and dune strengthening are needed in order to protect the coastline against erosion and to guarantee the functionality of dunes as flood protection elements [10]. The nourishment of larger amounts of sand evokes fewer disturbances in the soil environment and provides coastal recreation opportunities. The Dutch National Innovation Platform has therefore proposed the pilot Zandmotor (Sand Engine).

In 2011, Rijkswaterstaat and the Provincial Authority of South Holland agreed to construct a hook-shaped peninsula of about 21.5 million m3 of sand. In this way, the waves, winds, and tides transport the sand to the right place and the replenishment would not be necessary for a long time. In line with this project, more scientific research projects were developed to integrate model tools on coastal morphology, aeolian transport, and fresh underwater resources at the Sand Engine.

In addition, the Hollands Noorderkwartier Water Board (HHNK) reinforced the seawall with sand in 2014-2015 as part of the coastal reinforcement ('Coast on strength') to absorb the wave and wind forces that carry sand from the coast.

The main goal of the Rijkswaterstaat is to make beach replenishment activities in the Netherlands carbon neutral by 2030 [11]. They aim to reduce emissions and ecological impacts by exploring alternative maintenance strategies. Especially, in 2020, together with MARIN, C-Job Naval Architects submitted the concept design of the Autonomous Underwater Maintenance Dredger (AUMD) as part of the "Innovaties in de Kustlijnzorg" (IKZ). In continuation of the work, Rijkswaterstaat was interested in the design which led C-Job to further develop the design into the Autonomous Low Energy Replenishment Dredger (ALERD). This autonomous underwater dredger runs on battery power and will sustainably nourish the coastlines.

1.5.3. Autonomous Shipping

The fast-changing and rapid uptake of technologies emerged with the potential of autonomous shipping which contributes to safe sailing and to low-cost investments and operations. The elimination of the need for crew accommodation and safety provisions such as air conditioning and sanitary systems has resulted in a decrease in the overall construction costs of ships. Furthermore, the partial or complete replacement of onboard crew with shore-based support teams has significantly reduced operational costs. This shift not only provides greater convenience for sailors, who no longer need to spend extended periods of time away from their families but also enables more efficient use of human resources in the industry.

According to ICS and BIMCO Manpower Report 2015, there will be a forecasted global shortage of approximately 150.000 seagoing officers by 2025. Autonomous shipping provides the solution to this emerging problem, as unmanned vessels can replace the former. Studies show that 75% of maritime accidents are caused by human errors due to fatigue and attention deficit. Collision avoidance methods using AI data in conjunction with machine learning are piloted by shipping companies. Based on the position, speed, and heading of the vessel, they aim to hazard's predictions, alerting operators of possible collisions. On the other hand, the authors of [7] do not confirm these studies, considering that the former may be exaggerated in the case of inland navigation on the Danube and the Sava. Quantifying the results in [7], human failures caused less than 60% of accidents in Austria and less

than 20% in Serbia.

T. Porathe et al. [12] state that although automation can decrease accidents caused by human error, new accidents are likely to be created due to the transition between automatic and manual control. Investigating the impact of constrained autonomy on ships is necessary to determine if it increases the likelihood of certain types of accidents compared to traditional manned ships. Nevertheless, it's important to acknowledge that the implementation of new technology may result in the emergence of new types of incidents [12].

In [13] it is emphasized that in case an abnormal situation occurs, supervisors of these operations will need to think "out of the box" in order to take control because the system is simply not designed to act in these situations and it is deficient. This is also in line with [7], in which it is stated that in case the waterway and the ship are not properly maintained, an accident is less predictable and cannot be resolved by an unmanned system. It is also stated that human contribution is significant since it can mitigate the consequences of an upcoming accident or turn it into a near-miss [7].

According to [14], autonomous ships that are unmanned or low-manned will reduce the number of people at risk at sea. Due to the fact that the increase in safety is not quantified, in [14] the distribution of human casualties and lost ships are investigated. It has been revealed that 44% of all accidents are due to navigation issues, but it remains unclear what portion of these accidents might be prevented through the use of autonomous navigation technology. As is concluded in [7], autonomous shipping may save lives and be beneficial where accident records are dominated by collisions, allisions or groundings. Nevertheless, in other cases, the removal of the crew would be critical regarding safety. For this reason, extended and further research needs to be carried out in order to specify the removal of the human operator.

1.5.4. Sustainability

As the world continues to prioritize sustainability, the field of marine engineering is no exception. Submarines with zero emissions are being developed to lessen the environmental effects of undersea activities. One of the most promising breakthroughs in this respect is sustainable dredging. Dredging, which is required for the maintenance of rivers and ports, is normally carried out with diesel-powered vessels, which generate damaging greenhouse gases. Sustainable dredging options, on the other hand, include the use of electric dredgers driven by renewable energy sources such as wind or solar power. Using these technologies might significantly lower the carbon footprint of dredging operations while also mitigating the detrimental impacts on the coastal environment. As maritime engineering evolves, it becomes clear that sustainability must be at the forefront of each new development, such as the deployment of zero-emission submarines and sustainable dredging.

In order to confirm that autonomous submarines will contribute to a more sustainable way of living, the energy they consume needs to be assessed and compared with conventional vessels. To meet these requirements, a motion control system that will take into account the environmental conditions and the modeling of the submarine needs to be developed. In this way, the energy requirements will be quantified and the general energy assessment of the submarine will be performed, evaluating if the former contributes or not to the sustainable goals of the maritime industry.

For this reason, and in order to implement the motion control system in a case study, ALERD will be utilized. The autonomous low-energy replenishment dredger is one of the solutions that contribute to the mitigation of the carbon footprint. Additionally, since ALERD will operate underwater and it will be fully electric, it will be not visible and will create less noise than a conventional dredger. Underwater noise can have severe impacts on marine life, particularly on animals that rely on sound for communication, navigation, and survival. Thus, ALERD mitigates underwater noise pollution. Furthermore, the near seabed operation of ALERD benefits the more precise discharge of the soil through the bottom doors. Compared to conventional dredgers, dumping from the water surface using their bottom doors to discharge the soil, ALERD uses less power and releases the soil closet to the seabed, creating less dredge plume, which benefits the underwater life. In collaboration with Rijkswaterstaat, ALERD can actively engage in the future, in a more sustainable replenishment of the Dutch coastline.

1.6. Report Outline

The report outline is defined below. In Chapter 2 some general assumptions for ALERD and its main parameters are mentioned. In Chapter 3, the hydrodynamic modelling of the ALERD and the implementation of the mathematical equations in MATLAB, Simulink are analysed in order to perform time-domain simulations for a given time period. Chapter 4 refers to the modeling of the environmental forces and the seabed interaction. Moreover, the modeling of the actuators and their physical constraints are analyzed in Chapter 5. In Chapter 6 the operational profile of ALERD is analysed. Furthermore, the general overview and a description of how the model works are presented. Also, the energy analysis per actuator is determined. In Chapter 7, the behavior of the ALERD is presented and further explained, regarding the position and the velocity with respect to the PID gains. Also, the energy consumption is analyzed per actuator as well and an overview of the model is given. In Chapter 8 the conclusions and some future recommendations are presented.

2

Autonomous Low Energy Replenishment Dredger (ALERD)

This chapter presents the profile of the ALERD which is used as a case study for the development of the simulator, as well as its main dimensions, displacement, and characteristics. Furthermore, information about the buoyancy and gravity centers is provided, along with assumptions that have been made for the simplification of the problem.

2.1. Model Code

The simulator code was developed using Matlab/Simulink. Although MATLAB runs slowly compared to other compilers, the program greatly facilitates data visualization. While most of the previous work that has been done in Matlab, Simulink for underwater vehicles includes assumptions such as deeply submerged conditions, avoiding the contribution of the seabed and the surface, or no experience of underwater currents, these are key topics in the present study.

2.2. Assumptions

For the simplification of the model, there have been done some assumptions.

2.2.1. Environmental Assumptions

- One of the environmental assumptions is that the vehicle does not experience memory effects. As a result, the simulator neglects the effects of the vehicle passing through its own wake.
- Fluid properties are considered constant.
- Local variances of the gravitational field are ignored.

2.2.2. Vehicle Assumptions

- The underwater vehicle is a rigid body of constant mass, whose distribution does not change during operation.
- **Control surfaces:** There is no design study conducted for the optimal dimensions of the control surfaces and their position on the hull. It is assumed that they do not stall regardless of the angle of attack. The response time is small compared to the underwater vehicle response time.
- **Vertical thrusters:** There is no design study conducted for the optimal dimensions of the vertical thrusters and their position on the hull. It is assumed that they can provide constant thrust and torque. And they do not influence each other, nor does the seabed or water surface influence the thrust provided.
- The drag coefficient C_D is considered constant and independent of orientation.
- The lift coefficient C_L is considered constant and independent of orientation

2.3. Vehicle Profile

As mentioned in the introduction, ALERD is the continuation of AUMD. The ALERD's hull is presented in Figure [2.1].

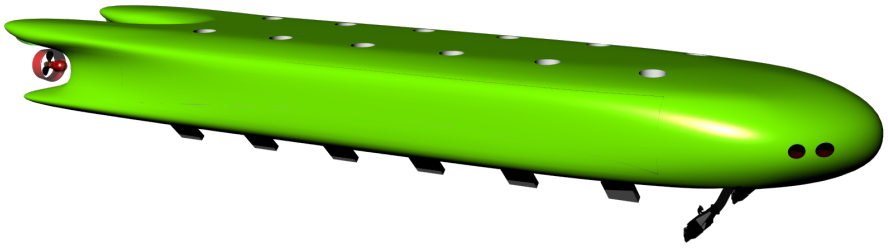

Figure 2.1: Preliminary design of ALERD's hull

Although ALERD has a different operational profile than AUMD the hull is the same, since it is still in an initial design phase. The main dimensions are not finalized yet but with the simulator's development, the behavior of the underwater vehicle will be easy to be checked, when the former is completed. The hopper, Figure 2.2 is compartmentalized into six cells in the longitudinal direction and two in the transverse direction in order to ensure proper stability. It is used for the storage of the dredged soil, which will enter the hopper through the drag-heads and the pipes that lead to each compartment. The flooding holes, where the remaining water will leave the hopper, as well as the bottom doors that will be used for the soil discharge, are depicted in Figure 2.1.

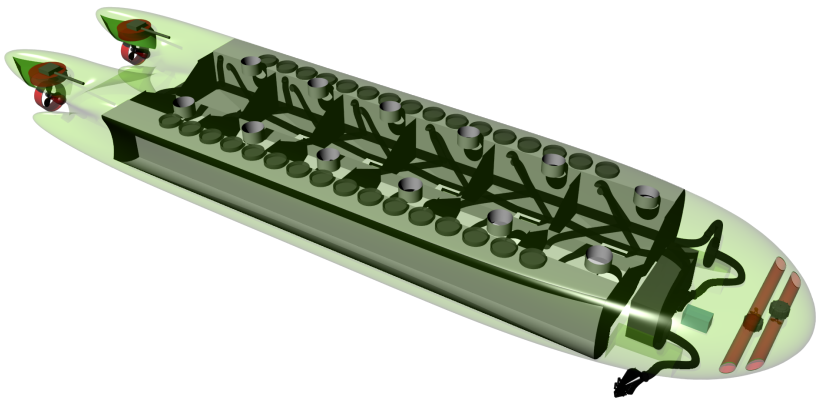

Figure 2.2: Preliminary design of the inner layout of ALERD

Table 2.1 gives the main dimensions for ALERD, which are used in the time-domain simulations.

Parameter	Value	Unit	Description
Loa	80	m	Overall length
B	20	m	Width
D	8.5	m	Depth
Δ	10830	tonnes	Displacement
BG	0.43	m	Vertical distance between COG and COB

Table 2.1: ALERD's Main Dimensions

2.4. Centers of Buoyancy and Gravity

Due to the asymmetrical mass distribution of the underwater vehicle, the center of gravity and the center of buoyancy do not coincide. Furthermore, due to the hull shape and the vertical distribution of mass, there exists a difference in CoG and CoB. As mentioned previously in Table 2.1 their in-between distance is $BG = 0.43m$.

For the modeling of underwater vehicles, it is a common approach to assume that the center of buoyancy coincides with the center of the origin of the body-fixed frame $\{b\}$ $(CO = CB)$, resulting in the vector $r^b_{bb} = [0, 0, 0]$. The center of gravity is defined as $r^b_{bg} = [x_g, y_z, z_g]$ and due to the multiple planes of symmetry, the vector is reduced to $r^b_{bg} = [0, 0, BG]$.

2.5. Ellipsoidal Hull Form Assumption

As mentioned previously, the ALERD is in an initial design phase, so the use of hydrodynamic software for CFD analysis or scale model tests to obtain the required hydrodynamic data is not an option. These are time-consuming and expensive approaches that need to be done in the basic design phase. In order to properly model the characteristics of the underwater vehicle, such as the moment of inertia, it is generally considered sufficiently accurate to use the values for an ellipsoid of revolution with the same length and diameter.

In Figure 2.3 the ellipsoid of revolution is presented. This prolate ellipsoid is obtained by setting $b = c$ and $a > b$. Using these assumptions, the mass and the moments of inertia are calculated.

$$m = \frac{4}{3}\pi\rho abc = \frac{4}{3}\pi\rho ab^2 \tag{2.1}$$

$$I_{xx} = \frac{1}{5}m(b^2 + c^2) = \frac{2}{5}mb^2 \tag{2.2}$$

$$I_{yy} = \frac{1}{5}m(a^2 + c^2) = \frac{1}{5}m(a^2 + b^2) \tag{2.3}$$

$$I_{zz} = \frac{1}{5}m(a^2 + b^2) = I_{yy} \tag{2.4}$$

The mass of the prolate ellipsoid needs to meet the requirements of the mass of ALERD. For this reason, $b = c = \frac{\bar{d}}{2}$ where $\bar{d}$ is calculated by:

$$\bar{d} = \sqrt{\frac{6\Delta}{\pi\rho L_{oa}}} \tag{2.5}$$

where Δ is the ALERD's displacement in kg, ρ is the water density in kg/m^3 and Loa is the total length of ALERD in m. Moreover, $a = \frac{L_{oa}}{2}$

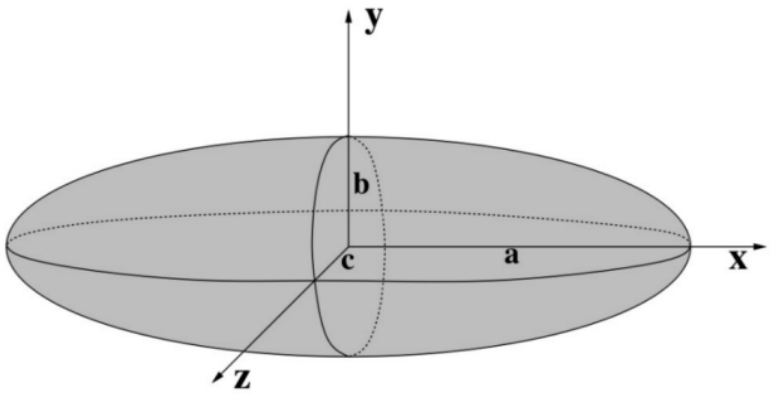

Figure 2.3: Ellipsoid of revolution

3 Methodology

This chapter presents a method for mathematically modelling underwater vehicles, which is essential for accurately simulating the motions of submarines in a time-domain simulation model. This modelling approach is especially helpful when the design phase of the submarines is in an early stage because their final main dimensions and hull form are still unknown. In this way and by employing mathematical formulas within a time-domain simulation model, parametric modelling of underwater vehicles becomes possible. This approach makes it possible to compare many design variations by allowing the alteration of major variables like length or displacement.

In this chapter, the governing equations of motion of the vehicle are defined. These equations consist of the following:

- Kinematics: the geometric aspects of motion
- Rigid-body Dynamics: the vehicle inertia matrix
- Mechanics: forces and moments causing motion

3.1. Vehicle Kinematics

In order to model underwater vehicles, multiple reference frames can be used. The motion of the body-fixed frame of reference (BODY), in this simulation, is described relative to an inertial or earth-fixed reference frame, North-East-Down (NED). To specify this, the NED reference frame is fixed, while the BODY reference frame is fixed to the underwater vessel and moves with it.

The used notation for the positions, velocities, forces, and moments can be found in Table 3.1 and the positive directions, rotations, and different reference frames are depicted in Figure 3.1.

DOF	Motion	Force	Linear Velocity	Position
1	Surge	X	u	x
2	Sway	Y	v	y
3	Heave	Z	w	z
	Rotation	**Moment**	**Angular velocity**	**Rotation angle**
4	Roll	K	p	ϕ
5	Pitch	M	q	θ
6	Yaw	N	r	ψ

Table 3.1: Notation

Normally, the mathematical modelling of a submarine in 6DOF follows the approach that is presented below, [15]. The nonlinear dynamic equations of motion could be written:

$$[M_{RB} + M_A]\dot{v} + [C_{RB}(v) + C_A(v)]v + D(v)v + g(\eta) = \tau_E + \tau \tag{3.1}$$

where:

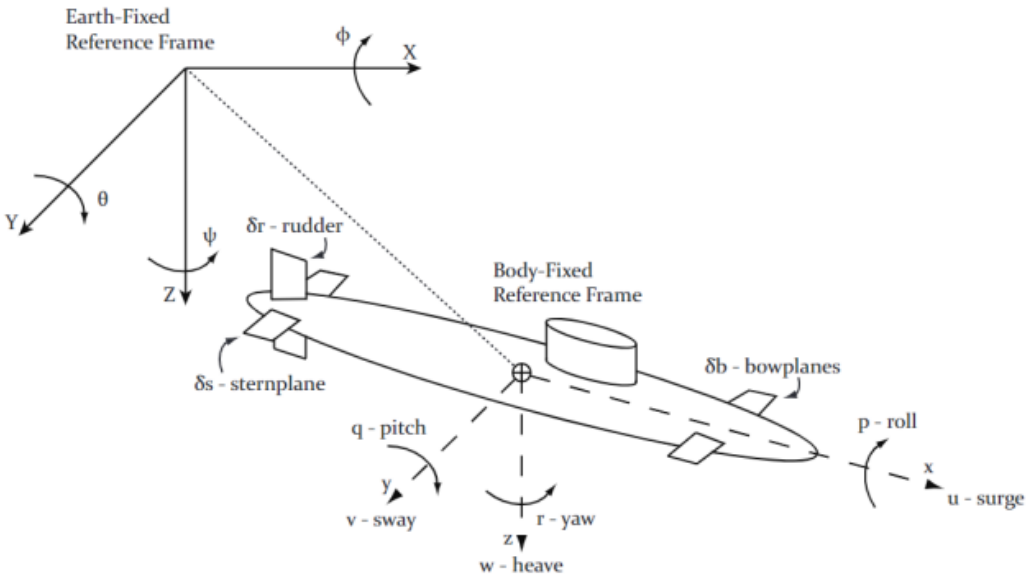

Figure 3.1: NED and BODY coordinate frames

- $M = M_{RB} + M_A$ - system inertia matrix
- $C(v) = C_{RB} + C_A$ - Coriolis-centripetal matrix
- $D(v)$ - damping matrix
- $g(\eta)$ - vector of gravitational/buoyancy forces and moments

$$\eta = [x \quad y \quad z \quad \phi \quad \theta \quad \psi]^T \tag{3.2}$$

$$v = [u \quad v \quad w \quad p \quad q \quad r]^T \tag{3.3}$$

$$\tau = [X \quad Y \quad Z \quad K \quad M \quad N]^T \tag{3.4}$$

where η denotes the position and orientation of the vehicle with respect to the inertial frame, v the translational and rotational velocities of the vehicle with respect to the body-fixed reference frame and τ the total forces and moments acting on the vehicle with respect to the body-fixed reference frame. However, according to the literature review, the degrees of freedom that are mostly affected by the ocean waves, ocean currents and seabed interaction are the surge, heave and pitch. Consequently, the developed model will investigate the behaviour of a submarine, in these 3DOF where the forces being developed lead to larger responses and higher energy consumption to compensate for them.

As a result, the vectors will be formed as follows:

$$\eta = [x \quad z \quad \theta]^T \tag{3.5}$$

$$v = [u \quad w \quad q]^T \tag{3.6}$$

$$\tau = [X \quad Z \quad M]^T \tag{3.7}$$

The following coordinate transform relates translational velocities between body-fixed and inertial or earth-fixed coordinates:

$$\begin{bmatrix} \dot{x} \\ \dot{z} \\ \dot{\theta} \end{bmatrix} = \boldsymbol{J}(\boldsymbol{\eta}) \begin{bmatrix} u \\ w \\ q \end{bmatrix} \tag{3.8}$$

where J is given in:

$$J(\eta) = \begin{bmatrix} cos\theta & sin\theta & 0 \\ -sin\theta & cos\theta & 0 \\ 0 & 0 & 1 \end{bmatrix} \tag{3.9}$$

3.1.1. Cross-Product Operator

The cross-product operator is included in the MSS toolbox as Smtrx.m. It is possible to calculate a cross-product with any other vector using this S-matrix as a cross-product operator.

Equation 3.10 contains the cross-product operator, where the vector λ is an arbitrary vector used to compute the cross-product.

$$\begin{gathered} \lambda \times a := S(\lambda)a \\ S(\lambda) = -\boldsymbol{S}^{\top}(\lambda) = \begin{bmatrix} 0 & -\lambda_3 & \lambda_2 \\ \lambda_3 & 0 & -\lambda_1 \\ -\lambda_2 & \lambda_1 & 0 \end{bmatrix} \\ \lambda = \begin{bmatrix} \lambda_1 \\ \lambda_2 \\ \lambda_3 \end{bmatrix} \end{gathered} \tag{3.10}$$

3.1.2. H-matrix

The H-matrix is a function that is obtained from the MSS Toolbox and is required to translate the inertia matrix from CG to any given location, including CO. In order to build it, S-matrix is used as well. It is derived following the equation below 3.11.

$$\begin{gathered} \vec{r}_{g/n} = \vec{r}_{b/n} + \vec{r}_g \\ \boldsymbol{v}^b_{g/n} = \boldsymbol{v}^b_{b/n} + \boldsymbol{\omega}^b_{b/n} \times \boldsymbol{r}^b_g \\ = \boldsymbol{v}^b_{b/n} - \boldsymbol{r}^b_g \times \boldsymbol{\omega}^b_{b/n} \\ = \boldsymbol{v}^b_{b/n} + \boldsymbol{S}^{\top}\left(\boldsymbol{r}^b_g\right)\boldsymbol{\omega}^b_{b/n} \\ \begin{bmatrix} \boldsymbol{v}^b_{g/n} \\ \boldsymbol{\omega}^b_{b/n} \end{bmatrix} = \boldsymbol{H}\left(\boldsymbol{r}^b_g\right) \begin{bmatrix} \boldsymbol{v}^b_{b/n} \\ \boldsymbol{\omega}^b_{b/n} \end{bmatrix} \\ \boldsymbol{H}\left(\boldsymbol{r}^b_g\right) := \begin{bmatrix} \boldsymbol{I}_{3\times3} & \boldsymbol{S}^{\top}\left(\boldsymbol{r}^b_g\right) \\ 0_{3\times3} & \boldsymbol{I}_{3\times3} \end{bmatrix} \end{gathered} \tag{3.11}$$

3.1.3. Rigid-Body Matrix

The rigid-body kinetics can be expressed in vectorial form according to [15]. M_{RB} is the rigid-body inertia matrix, and for the 6DOF is presented in equation 3.12, expressed with respect to CG.

$$M^{CG}_{RB} = \begin{bmatrix} m & 0 & 0 & 0 & 0 & 0 \\ 0 & m & 0 & 0 & 0 & 0 \\ 0 & 0 & m & 0 & 0 & 0 \\ 0 & 0 & 0 & I_x & 0 & 0 \\ 0 & 0 & 0 & 0 & I_y & 0 \\ 0 & 0 & 0 & 0 & 0 & I_z \end{bmatrix} \tag{3.12}$$

In order to transform it from CG to CO the equation 3.13 is used.

$$M^{CO}_{RB} = H^T(r^b_{bg}) M^{CG}_{RB} H(r^b_{bg}) \tag{3.13}$$

As a result, the rigid-body matrix with respect to CO is given in Equation 3.14.

$$M_{RB}^{CO} = \begin{bmatrix} m & 0 & 0 & 0 & mz_g & 0 \\ 0 & m & 0 & -mz_g & 0 & 0 \\ 0 & 0 & m & 0 & 0 & 0 \\ 0 & -mz_g & 0 & I_x & 0 & 0 \\ mz_g & 0 & 0 & 0 & I_y & 0 \\ 0 & 0 & 0 & 0 & 0 & I_z \end{bmatrix} \tag{3.14}$$

It is clear that there are two planes of symmetry, and that CG is located below CB, which is equal to CO. The off-diagonal terms are due to the location of z_g, which does not coincide with CB (and thus CO). The operations described here are executed in the Matlab function Spheroid.m. The elements of the rigid body matrix can be filled in using the mass of the submarine and the moments of inertia corresponding to a prolate ellipsoid, which are already derived in Chapter 2.

3.1.4. Coriolis-centripetal Matrix

Equation 3.15 contains the Coriolis-centripetal matrix that corresponds to CO. The Coriolis-centripetal matrix results from the rotation of the body-fixed reference frame with regard to the inertial reference frame, as was discussed in the previous sections.

$$C_{RB}^{CO}(v_r) = H^T(r_{bg}^b) \begin{bmatrix} 0 & -mr & mq & 0 & 0 & 0 \\ mr & 0 & -mp & 0 & 0 & 0 \\ -mq & mp & 0 & 0 & 0 & 0 \\ 0 & 0 & 0 & 0 & I_z r & -I_y q \\ 0 & 0 & 0 & -I_z r & 0 & I_x p \\ 0 & 0 & 0 & I_y q & -I_x p & 0 \end{bmatrix} H(r_{bg}^b) \tag{3.15}$$

Equation 3.16 is the Coriolis-centripetal matrix in CG.

$$C_{RB}^{CG} = \begin{bmatrix} 0 & -mr & mq & 0 & 0 & 0 \\ mr & 0 & -mp & 0 & 0 & 0 \\ -mq & mp & 0 & 0 & 0 & 0 \\ 0 & 0 & 0 & 0 & I_z r & -I_y q \\ 0 & 0 & 0 & -I_z r & 0 & I_x p \\ 0 & 0 & 0 & I_y q & -I_x p & 0 \end{bmatrix} \tag{3.16}$$

The Matlab function Spheroid.m executes the operations and fills in the coriolis-centripetal matrix in a manner similar to that described above.

3.1.5. From 6DOF to 3DOF

From the literature review that was performed, surge, heave and pitch are the critical directions for modelling submarines that operate near the seabed in shallow water. These interactions create an added resistance, a suction force, towards the surface or seabed, from the surface and seabed respectively, and a pitch moment. Additionally, due to the operation near the surface, the submarine is affected by the waves, which create a heave force and a pitch moment on the former.

Since the surge, heave and pitch are the critical directions affected by the environmental conditions, the 6DOF is decided to be reduced to 3DOF. Furthermore, this is a way to simplify the model. Consequently, the rigid-body matrix and the Coriolis-centripetal matrix are given in the equations 3.17 and 3.18 respectively.

$$M_{RB}^{CO} = \begin{bmatrix} m & 0 & mz_g \\ 0 & m & 0 \\ mz_g & 0 & I_y \end{bmatrix} \tag{3.17}$$

$$C_{RB}^{CO}(v_r) = \begin{bmatrix} 0 & mq & 0 \\ -mq & 0 & -mz_g q \\ 0 & mz_g q & 0 \end{bmatrix} \tag{3.18}$$

3.2. Hydromechanics of Underwater Vehicles

In order to derive the hydrostatic restoring forces and moments, the added mass coefficients and the linear damping coefficients for the studied submarine need to be defined.

3.2.1. Added Mass Matrix

The off-diagonal terms of the added mass matrix are ignored because it is assumed that the hull form will be a prolate ellipsoid and that the ALERD will only be moving at low to medium speed. Three planes of symmetry are presumed for the added mass matrix, as opposed to two for the rigid-body matrix. This is because mathematical formulas cannot be used to determine off-diagonal terms. According to the literature, the diagonal structure of the damping and added mass matrices is considered to be a quite good approximation for underwater vehicles operating at low to medium speed [15].

Consequently, the added mass matrix in 6DOF is presented in equation 3.19.

$$M_A = \begin{bmatrix} X_{\dot{u}} & 0 & 0 & 0 & 0 & 0 \\ 0 & Y_{\dot{v}} & 0 & 0 & 0 & 0 \\ 0 & 0 & Z_{\dot{w}} & 0 & 0 & 0 \\ 0 & 0 & 0 & K_{\dot{p}} & 0 & 0 \\ 0 & 0 & 0 & 0 & M_{\dot{q}} & 0 \\ 0 & 0 & 0 & 0 & 0 & N_{\dot{r}} \end{bmatrix} \tag{3.19}$$

To acquire the added mass coefficients, numerous hydrodynamic programs are available. Given that ALERD is currently in its preliminary design phase, the determination of these coefficients was beyond the scope of this study. Consequently, the responsibility for this task was delegated to an external partner. WAMIT was used to compute frequency-dependent added mass M_A.

After obtaining the added mass coefficients, they should be transformed to be placed in the added mass matrix. Following WAMIT's manual the added mass is calculated as can be seen in equation 3.20

$$A_{ij} = \overline{A_{ij}} \rho L^k \tag{3.20}$$

where $k = 3$ for $i, j = 1, 2, 3$, $k = 4$ for $i = 1, 2, 3$, $j = 4, 5, 6$ or $j = 1, 2, 3$, $i = 4, 5, 6$ and $k = 5$ for $i, j = 4, 5, 6$

3.2.2. Added Mass Coriolis-Centripetal Matrix

Equation 3.21 shows the equivalent additional mass Coriolis-centripetal matrix for CO. Similar to the method stated for the rigid body mass and Coriolis-centripetal matrix, which are illustrated in the previous sections, the added mass coriolis-centripetal matrix was derived. The Matlab function Imlay61.m, in conjunction with the function m2c.m, calculates the corresponding Coriolis-centripetal matrix using the added mass matrix and the velocity vector (translational and rotational). The mathematical derivation of the relationship between the matrices that correspond to the definition of the function m2c.m is given in [15].

$$C_A(v_r) = \begin{bmatrix} 0 & 0 & 0 & 0 & -Z_{\dot{w}} w_r & Y_{\dot{v}} v_r \\ 0 & 0 & 0 & Z_{\dot{w}} w_r & 0 & -X_{\dot{u}} u_r \\ 0 & 0 & 0 & -Y_{\dot{v}} v_r & X_{\dot{u}} u_r & 0 \\ 0 & -Z_{\dot{w}} w_r & Y_{\dot{v}} v_r & 0 & -N_{\dot{r}} r & M_{\dot{q}} q \\ Z_{\dot{w}} w_r & 0 & -X_{\dot{u}} u_r & N_{\dot{r}} r & 0 & -K_{\dot{p}} p \\ -Y_{\dot{v}} v_r & X_{\dot{u}} u_r & 0 & -M_{\dot{q}} q & K_{\dot{p}} p & 0 \end{bmatrix} \tag{3.21}$$

3.2.3. Damping Matrix

Due to the lack of CFD calculations or scaled model tests, the damping coefficients need to be defined using another approach. To specify this, Froude scaling will be implemented. The original geometric and inertial values of the HRC-AUV are provided in [16]. Taking into account the symmetry of the hull, $Y_v = Z_w$ and $M_q = N_r$. According to [15], when operating at high speed, the damping of underwater vehicles is highly non-linear and coupled, and the non-linear damping coefficients are dominant. In order to avoid this phenomenon, and simplify the problem, it is assumed that the ALERD operates at low to medium speed, where the linear damping terms are dominant. According to [15], decoupled motions

for underwater vehicles and for damping is a good approximation, so the motions are decoupled and only the diagonal terms are present.

$$D = \begin{bmatrix} X_u & 0 & 0 & 0 & 0 & 0 \\ 0 & Y_v & 0 & 0 & 0 & 0 \\ 0 & 0 & Z_w & 0 & 0 & 0 \\ 0 & 0 & 0 & K_p & 0 & 0 \\ 0 & 0 & 0 & 0 & M_q & 0 \\ 0 & 0 & 0 & 0 & 0 & N_r \end{bmatrix} \tag{3.22}$$

The Froude numbers for both the HRC-AUV and ALERD are comparable using their design speeds and lengths.

$$Fr = \frac{V_s}{\sqrt{gL}} \tag{3.23}$$

$$Fr_{ALERD} = Fr_{AUV} \tag{3.24}$$

$$\lambda = \frac{L_{ALERD}}{L_{AUV}} \tag{3.25}$$

Consequently, in order to obtain the damping coefficients for ALERD, the following equations are derived:

$$X_u = \frac{\lambda^3}{\sqrt{\lambda}} X_u \tag{3.26}$$

$$Z_w = \frac{\lambda^3}{\sqrt{\lambda}} Z_w \tag{3.27}$$

$$M_q = \frac{\lambda^4}{\sqrt{\lambda}} M_q \tag{3.28}$$

It is known that Froude scaling is not used for submerged vehicles due to the absence of waves and free surface. When an underwater vehicle is submerged, only frictional and viscous damping terms are present.

Following the method of Reynolds similarity the damping coefficients from the model in [VALERI-ANOO 28] can be theoretically scaled. However, a novel concern arises due to the infeasibility of achieving analogous Reynolds numbers across the prototype and actual scale due to the non-scalable nature of viscosity.

In [17] it is stated that if the Reynolds number of the model is $Re \geq 5 * 10^6$ and the Reynolds of the actual vessel is $Re \geq 1 * 10^8$ estimations of the viscous and frictional damping terms can be estimated with an acceptable error lower than 20%. These criteria find fulfilment in both the LAUV and the ALERD. Consequently, Reynolds similarity can be invoked, employing identical equations as those utilized in Froude scaling.

3.2.4. From 6DOF to 3DOF

As mentioned previously, surge, heave and pitch are the critical directions for modelling submarines that operate in shallow water. For this reason and for the simplification of the model, the 6DOF matrices reduce to 3DOF.

Consequently, the added mass matrix, the added mass Coriolis-centripetal matrix and the damping matrix are given in the equations 3.29, 3.30 and 3.31 respectively.

$$M_A = \begin{bmatrix} X_{\dot{u}} & 0 & 0 \\ 0 & Z_{\dot{w}} & 0 \\ 0 & 0 & M_{\dot{q}} \end{bmatrix} \tag{3.29}$$

$$C_A = \begin{bmatrix} 0 & 0 & -Z_{\dot{w}} w_r \\ 0 & 0 & X_{\dot{u}} u_r \\ 0 & -X_{\dot{u}} u_r & 0 \end{bmatrix} \tag{3.30}$$

$$D = \begin{bmatrix} X_u & 0 & 0 \\ 0 & Z_w & 0 \\ 0 & 0 & M_q \end{bmatrix} \tag{3.31}$$

3.3. Restoring Forces and Moments

The $g(\eta)$ term is used to characterize the gravitational buoyancy vector exerted on the submarine in the water. The gravitational and buoyancy forces are functions of orientation and are independent of vehicle motion.

For the ALERD, the formulation of the restoring forces and moments vector ensues under the assumption that the initial weight aligns with the buoyancy, expressed as $W = B = \rho g \nabla$, where ρ is the water density and the ∇ is the displaced volume by ALERD.

Expressing the restoring force vector in the body-fixed coordinate system, it yields:

$$g(\eta) = \begin{bmatrix} (W-B)\sin\theta \\ -(W-B)\cos\theta\sin\phi \\ -(W-B)\cos\theta\cos\phi \\ -(y_G W - y_B B)\cos\theta\cos\phi + (z_G W - z_B B)\cos\theta\sin\phi \\ (z_G W - z_B B)\sin\theta + (x_G W - x_B B)\cos\theta\cos\phi \\ -(x_G W - x_B B)\cos\theta\sin\phi - (y_G W - y_B B)\sin\theta \end{bmatrix} \tag{3.32}$$

The simplified buoyancy and gravitational force vector $g(\eta)$ was obtained using the following rules. As was stated previously, the most critical degrees of freedom for a submarine that operates near the seabed are the surge, heave and pitch, so sway, roll and yaw are excluded and the related angles ϕ and r are considered zero. Moreover, as mentioned in the previous chapter, the centre of gravity does not coincide with the centre of buoyancy and their in-between distance is described by the vector [x_G y_G z_G] = [0 0 BG]. For this reason, the vector $g(\eta)$ is simplified more to 3.33. Consequently, the hydrostatic loads in the three directions are simplified and written as:

$$g(\eta) = \begin{bmatrix} (W-B)\sin\theta \\ (B-W)\cos\theta \\ z_g W \sin\theta \end{bmatrix} = \begin{bmatrix} 0 \\ 0 \\ z_g W \sin\theta \end{bmatrix} \tag{3.33}$$

3.4. Hydrodynamic Forces and Moments

The right-hand part of the equations of motion consists of the forces and moments acting on the submarine. Especially, these are the cross-flow drag, the viscous drag and the control forces and moments.

3.4.1. Cross-Flow Drag

According to [18] for relative current angles $|\beta_c - \psi| \gg 0$, where β_c is the current direction, the cross-flow drag principle may be applied to calculate the nonlinear damping force in sway and yaw moment. Although the model calculates the motions in surge, heave and pitch, the cross-flow vector is included in case of extension of the current model in the future. The function that estimates the cross-flow in Matlab is the crossFlowDrag.m It is a function of the beam B, and draft T of the vessel. Moreover, a 2-D drag coefficient is used and is calculated using another function called Hoerner.m It has to be stated that for the current model, the generated forces and moments are zero due to the fact that these degrees of freedom were decided not to be included.

3.4.2. Hull Resistance

The authors in [3] have already calculated the resistance in order to estimate the required propulsion power but they are slightly adjusted. In [19] the authors have conducted a study that compares calculations of underwater ships' bare hull resistance using analytical methods with results from computational fluid dynamics (CFD) simulations. The conclusion drawn is that the equations used in the analysis provide accurate outcomes. Additionally, the total resistance coefficient C_T, as defined in equation 3.36, is utilized to calculate the overall resistance of the ships.

The total resistance acts only in the surge direction and is estimated using the equation 3.34.

$$R_T = \frac{1}{2} \cdot \rho \cdot V_s^2 \cdot S \cdot C_T \cdot (1+k) \tag{3.34}$$

where ρ is the water density, $V_s = 8.5knots$ is the vessel's speed, $S = 3900m^2$ is the wetted surface, and from ICCT $(1+k) = 1.1$. The skin friction coefficient is given from equation 3.35. Moreover, the kinematic viscosity used for the calculation of Reynolds number is $\nu = 1.354 * 10^-6m^2/s$ at 10° C.

$$C_{F0} = \frac{0.075}{(\log Re - 2)^2} \tag{3.35}$$

$$C_T = C_{F0}(1 + 1.5(\frac{D}{L})^1.5 + 7(\frac{D}{L})^3) \tag{3.36}$$

The equations used above are implemented in the Matlab function ResistanceCalculation.m, which is used in the main function ALERD.m. Consequently, the vector that yields from this equation is given in equation 3.37.

$$\tau_{R_T} = \begin{bmatrix} -R_T \\ 0 \\ 0 \end{bmatrix} \tag{3.37}$$

In order to calculate the total resistance, the forward speed is utilised and the total force is already expressed in body-frame. As a result, there is no need to use the rotational matrix to convert it into body-frame coordinates. Moreover, when considering small angles, the use of rotation matrices to alter the force's orientation, as might be required with a pitch angle, becomes unnecessary.

3.4.3. Control Forces and Moments

Furthermore, the τ vector apart from the hydrodynamic forces and moments, includes the control forces for the pitch and heave. The ALERD was designed in such a way that the heave motion is controlled by two vertical tunnel thrusters that both operate with the same number of rpm in order to create only a vertical force and not any pitch moment. This is done for the simplification of the model and for the decoupling of the heave and pitch degrees of freedom. The tunnel thrusters model is analytically described in Chapter 5. Furthermore, the ALERD is equipped with two trim tanks that are responsible for the control of pitch. The water mass change in this closed system generates a moment which is able to compensate for the created pitch moment on the submarine. The model of the trim tanks is further analysed in Chapter 5. Both the forces and moments that are used to control the ALERD are expressed in the fixed body-frame. Moreover, the main propeller is equipped with a nozzle and it is capable of controlling the forces in the surge direction using the RPM as an input.

3.5. State-Space Model

Consider the model:

$$M\dot{\nu} + C(\nu)\nu + D(\nu)\nu + g(\eta) = \tau + \tau_{R_T} + \tau_{crossflow} \tag{3.38}$$

$$\dot{\eta} = J_\Theta(\eta)\nu \tag{3.39}$$

which can be expressed in time-invariant system:

$$\dot{x} = f(x,u) \tag{3.40}$$

where $x = [\eta^T, \nu^T]^T$ The state-space model of the submarine is expressed in the equation 3.41 and it is solved in Simulink.

$$f(x,u) = \begin{bmatrix} J_\Theta(\eta)\nu \\ M^{-1}[\tau + \tau_{R_T} + \tau_{crossflow} - C(\nu)\nu - D(\nu)\nu - g(\eta)] \end{bmatrix} \tag{3.41}$$

Although this state-space model can be applied to the 6DOF model, in this case, the vectors are:

$$J(\eta) = \begin{bmatrix} cos(\theta) & sin(\theta) & 0 \\ -sin(\theta) & cos(\theta) & 0 \\ 0 & 0 & 1 \end{bmatrix} \tag{3.42}$$

$$\eta = [x \quad z \quad \theta]^T \tag{3.43}$$

$$\nu = [u \quad w \quad q]^T \tag{3.44}$$

The state-space model consists of the acceleration and velocity vectors when the derivatives of the equations 3.44 and 3.43 are considered. Using the Euler angle transformation matrix 3.42, the translational and rotational velocities are transferred from fixed body-frame $\{b\}$ to the inertial frame $\{n\}$, and the $\dot{\eta}$ vector is obtained.

Simulink calculates the vector $\dot{x}$ and integrates it in order to obtain the position and velocity of the ALERD in the surge, heave and pitch in the inertial frame $\{n\}$. To accomplish this computation, an input vector necessitating initial conditions is required. At the beginning of the iterative procedure, all positional and velocity components within this vector are initialized to zero. This requirement is explained by using the initial conditions vector as described in Equation 3.45. This vector is then employed as the input for Simulink to solve the steady-state model, resulting in the computation of $\dot{x}$.

$$x_0 = [\eta_0, \quad \nu_0]^T \tag{3.45}$$

The integration of this vector yields an updated version of the vector x, which subsequently takes on the role of the novel input vector, thus establishing the initial conditions for the state-space model. By iteratively executing these procedural steps, a simulation in the time domain can be effectively executed.

4

External Disturbances

4.1. Ocean Current

The impact of ocean currents is one of the many challenges that submarines and underwater vehicles face. Currents are horizontal movements of water in the ocean caused by a variety of factors, including wind, temperature, and tides. Navigating through these currents can be difficult for submarines operating in shallow waters, where the currents are often stronger and more unpredictable. Tidal currents are weak in deep water but are of great importance close to shoreline configurations [20]. In inlets and straights in coastal regions, there are strong tidal currents [20]. The interaction of currents and submarines can have severe consequences for both the vessel's performance and the safety of its crew, so submarine operators and, thus, the autonomous navigation algorithm must understand and manage the impact of currents on their vessels.

4.1.1. Modeling of Ocean Currents in MATLAB, Simulink

There are two ways to model ocean currents, the deterministic and the stochastic approach. Following a deterministic approach the user has to define two input variables, V_c and β_c which represent the ocean's current speed and direction, respectively. With this approach, the speed and the direction of the current remain constant, while in reality, they change. According to [18] the ocean current velocity and the current direction can be generated by using the first Gauss-Markov process:

$$\begin{aligned} \dot{V}_c + \mu_1 V_c &= \omega_1 \\ \dot{\theta}_c + \mu_2 \theta_c &= \omega_2 \end{aligned} \tag{4.1}$$

where μ_1 and μ_2 are constants that determine the time constant of the Gauss-Markov process and is a non-negative value, while ω_1 and ω_2 are Gaussian white noises. In this way, randomness is included in the model.

Both μ_1, μ_2 values are chosen to be low $(= 1)$ since higher values can increase the rise time before a steady state current is reached. To simplify, two values for the inflow angle θ_c are selected 0 (following current) and π (heading current). It is noted that a mean current velocity at the center of the submarine is used; this means the effect of shear currents is not considered. Shear currents can give rise to a difference in hydrodynamic pressure between the top and bottom of the submarine, which can lead to a positive pitch moment. The initial stage of this model involved expressing the current velocity within the global frame. Subsequently, the relative velocity was ascertained by transforming the current velocity into the body-fixed frame and consequently adding it to the submarine's own speed. Following this, the calculations for hydrodynamic forces were carried out and presented below.

$$\begin{bmatrix} u_c \\ \omega_c \end{bmatrix} = \underbrace{\begin{bmatrix} \cos(\theta) & \sin(\theta) \\ -\sin(\theta) & \cos(\theta) \end{bmatrix}}_{\text{Transformation matrix}} \begin{bmatrix} \dot{x}_c \\ \dot{z}_c \end{bmatrix} \tag{4.2}$$

where θ is the pitch angle; u_c, ω_c are the current components in the body-fixed frame; $\dot{x}_c$, $\dot{z}_c$ are the current velocity components in the global frame and are given by the equations below.

$$\begin{aligned} \dot{x}_c &= V_c \cos(\theta_c) \\ \dot{z}_c &= V_c \sin(\theta_c) \end{aligned} \tag{4.3}$$

In [21], the author provided an illustrative depiction of the maximum tidal currents observed during spring tides. These currents exhibit their greatest strength along the coastline of Great Britain and in the southern regions of the North Sea, where they can surpass speeds of 1 meter per second in specific locations. Farther north maximum speeds are considerably lower, yet they remain in the range of several tens of centimeters per second, as illustrated in [22]. Nevertheless, in [23] the uncertainties in current measurements in the North Sea are studied, and the authors indicate that in the southern part, the current is around 0.2m/s to 0.5m/s.

Consequently, the mean value for the current speed is set to 0.5m/s. The angle of it is set to 0 rad and π rad for the simplification of the analysis.

Simulating equations 4.1 in Simulink, yields varying current speed and velocity with the mean values mentioned previously. The Band-Limited White Noise block generates normally distributed random numbers that are suitable for use in continuous systems and it was utilized in the simulation. A noise power value, representing the covariance of the distribution, was set at 0.1, and a sample time of 100 was defined. The latter means that a new value for both current speed and angle is generated every 100 seconds and in the current study it was chosen to be 100 in order to retain the generated value constant for 100s and not change it every 0.1s. This is beneficial for the current study but also is a way for the PID to handle these disturbances. To address the abrupt changes in the values, a moving average block was employed to achieve a smoother output. The resultant velocity components in the surge and heave direction are then subtracted from the velocity components of the submarine in the same directions in order to estimate the relative speed. The created vector 4.5 is applied to the steady-space model as follows:

$$M\dot{v_r} + C(v_r)v_r + D(v_r)v_r + g(\eta) = \tau + \tau_{R_T} + \tau_{crossflow} \tag{4.4}$$

$$v_r = \begin{bmatrix} u - u_c, & v - \omega_c, & 0 \end{bmatrix}^T \tag{4.5}$$

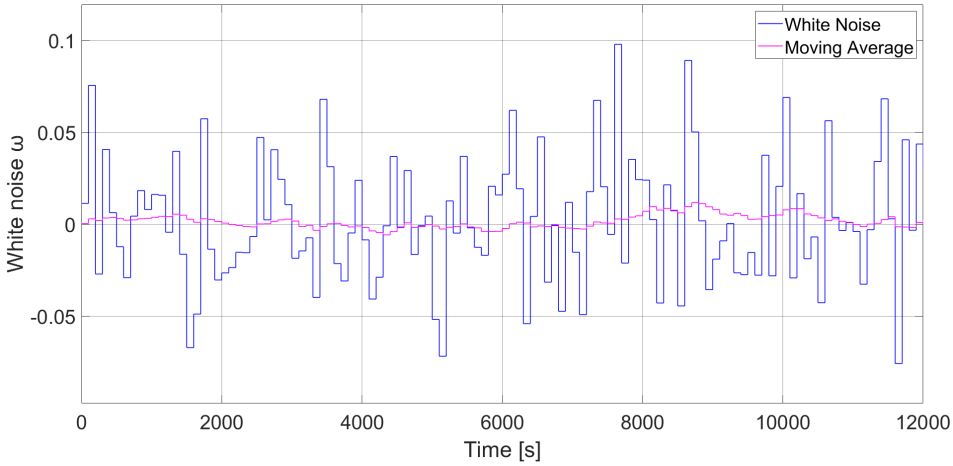

Figure 4.1: Generated signal from white noise and moving average blocks

4.1.2. Sanity Check

To ensure the accuracy of the analysis, a sanity check using a case study the ALERD was conducted. This involved utilizing its dimensions and parameters, as outlined in Table 2.1, to define the force and moment exerted on the ALERD. As previously discussed, these force and moment values vary with depth.

To validate the findings and confirm that they align with real-world scenarios, the operational profile of the ALERD needs to be established. An operational profile analysis conducted by C-Job is available in [24]. Furthermore, the depth operational profile created by the author in [9] relies on AIS data

analysis from conventional dredgers engaged in coastal replenishment along the Dutch coastline and is illustrated in Figure 6.2 which is explicitly described in Chapter 6. This analysis aids in assessing the dredger's performance in various operational conditions, ensuring that the force and moment calculations are in line with realistic scenarios.

As illustrated in Figure A.4 in the Appendix, it is observed that the highest force is exerted on the ALERD when it is at the surface. When the ALERD is in transit and maintains a constant depth, the force remains consistent. However, as the ALERD descends to greater depths, the heave force generated by the waves decreases. This pattern is logical, as waves gradually lose their energy at larger water depths.

4.1.3. Discussion

In conclusion, this chapter offers a detailed description of ocean current modeling, with a special emphasis on the stochastic technique recommended by Fossen [15]. By adopting the first-order Gauss-Markov process for simulating ocean current velocity and angle, Fossen's approach enables us to capture the inherent randomness and variability in real-world current patterns. This stochastic modeling technique has proven useful in providing realistic current data for use in many maritime applications, as evidenced by our simulations. Furthermore, the incorporation of additional control mechanisms, such as the moving average block, has been critical and is used as a temporary solution to solve the problem of the overshoot of the submarine due to the abrupt changes in the values. The PID controllers need more time in order to compensate for these fast changes and reinstate the submarine to the reference track. Future research can be done on the implementation of an adaptive PID controller which can be adjusted in different inputs, and respond more efficiently to the abrupt changes.

4.2. Ocean Waves

The ocean waves are a powerful and ever-present force that can have a significant impact on submarine movement and operations. Wind, tides, and other natural factors create waves, which can range from gentle ripples to massive swells. Many studies indicate that underwater vehicles operating near the surface are mainly affected by ocean waves, which cause undesirable motions creating turbulent conditions, affecting maneuverability, and making it more difficult to detect or avoid obstacles. The interaction of submarines with ocean waves is a critical aspect of submarine operations that requires careful consideration and planning to ensure mission safety and success. For the specific case study of ALERD, understanding how it interacts with ocean waves is critical to ensure safe and effective dredging operations, making it an ideal case study for investigating the complex relationship between submarines and ocean waves in shallow waters.

4.2.1. Modeling of Ocean Waves in MATLAB, Simulink

According to the literature review that was carried out, it is found that there are a couple of ways to simulate the wave's behavior and the created forces on the submarines. The authors of [25], modeled the wave forces acting on a submarine in two parts, using the Response Amplitude Operator (RAO) for each motion mode and the wave-induced steady force. The first is the 1st order wave-induced force caused by the high-frequency oscillatory wave exciting force depending on the wave encountering frequency. The second is the 2nd order wave-induced steady force that fluctuates over a long period. In order to check the wave effect, the operating depth of the submarine was set to 40m from the water's surface. According to [25], the wave-induced steady force in water causes relatively tiny changes in trajectory compared to the high-frequency oscillatory motions. For this reason and because the first-order waves are considered shallow water waves, [26] in the current study, it is decided to model the first-order waves as a disturbance. Especially, according to [27], the instantaneous force in heave on the vehicle is given by the first and second-order effects. Consequently, the first-order heave force acting on the submarine which is of great significance in the current study is given by:

$$Z_1(t) = \sum_{i=1}^{N} Z_{1i}(t) = \sum_{i=1}^{N} C_{Z1} \nabla \rho \left(1.5 \sin^2 \mu + 1\right) \cdot (1 - 0.02U \cos \mu) F_{1i} \sin \omega_{ei} t \tag{4.6}$$

Similarly, the moment created by the waves and exerted on the submarine is given by:

$$M_1(t) = \sum_{i=1}^{N} M_{1i}(t) = -\sum_{i=1}^{N} C_{M1} L \nabla \rho (1 - 0.02U \cos \mu) Sgn(\cos \mu) \cdot F_{1i} \cos \omega_{ei} t \tag{4.7}$$

where F_{1i} is the force due to the attenuated static head at the vehicle depth produced by each wave component. It is represented by the equation:

$$F_{1i} = a_i^2 \omega_{ei}^2 e^{-\omega_{ei}^2 \frac{H}{g}} \tag{4.8}$$

where a_i is given by:

$$a_i = \sqrt{2S(\omega_{ei})\delta\omega} \tag{4.9}$$

The forces on the submarine are dependent on the encounter frequency ω_{ei} rather than on the sea state alone, where:

$$\omega_{ei} = \omega_i - \frac{\omega_i U \cos(\mu)}{g} \tag{4.10}$$

The aforementioned parameters are:

- a_i - wave amplitude of the ith component, according to the Fourier-Stieltjes theorem
- ω_i - wave frequency of the ith component
- ∇ - submarine volumetric displacement
- C_{Z1}, C_{M1} - non-dimensional hydrodynamic coefficients
- μ - heading of the submarine relative to the waves

In [28] is stated that a typical wave spectrum for two different encounter angles is presented in Fig. 4.2 showing that the main peak of the spectrum is the highest in a following sea $(\mu = 0)$ and that there is also an additional peak at a higher frequency. As a result, the following sea is therefore the most difficult condition for the submarine to operate under. It is generally agreed that the controller must be designed for this encounter angle.

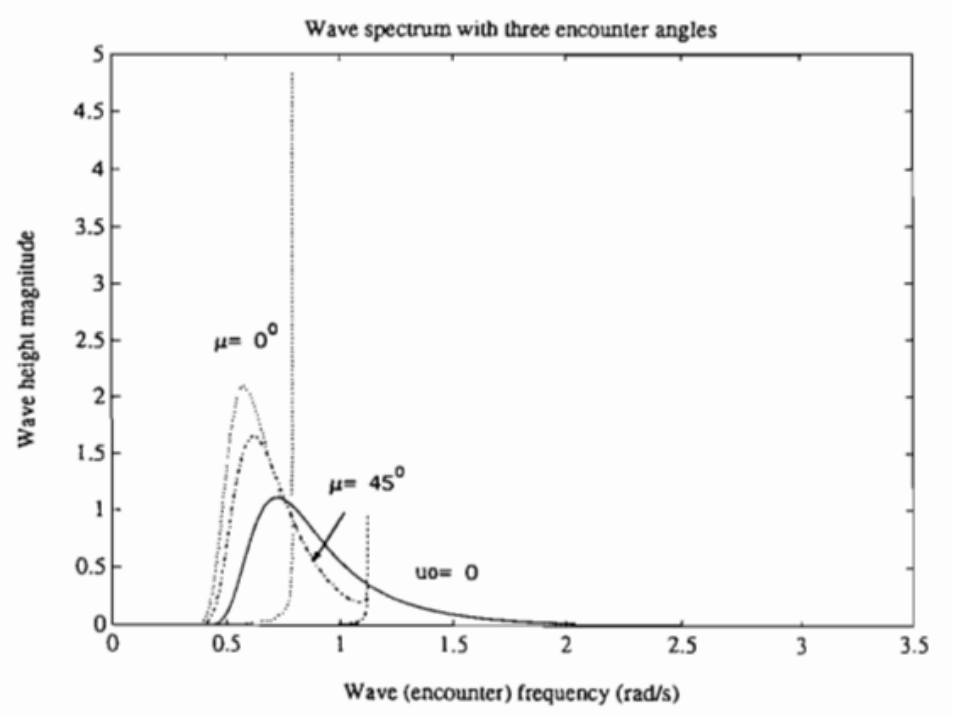

Figure 4.2: Effect of submarine heading on wave encounter frequency

Consequently, the heading angle is assumed to be $\mu = 0$.

It needs to be mentioned that the non-dimensional hydrodynamic coefficients are taken from [28] since in order to be properly defined a hydrodynamic software is required, as well as the final design phase of the submarine. Given that the dimensions of the submarine in [28] are similar to the ALERD, and the hydrodynamic coefficients are related to the shape of the submarine, this will be a fair assumption to start with, being at an early stage design phase.

4.2.2. Jonswap Wave Spectrum

To incorporate a realistic wave scenario, and taking into account that the North Sea (operating area of ALERD) is wind-dominated, a Jonswap spectrum will be employed, instead of the Pierson Moskowitz spectrum which is mainly used for ocean swell and developed seas. For the development of the Jonswap spectrum, the wavespec.m [15] function is utilized and modified with respect to the depth as mentioned below. The inputs in the function are the significant wave height in meters, the peak frequency in rad/s, and the factor γ.

The authors of [29] that studied wave-current interactions in the southern North Sea, which is also the area of interest of the current study, indicate that the significant wave height at the open sea can reach a maxima significant wave height of 5m. Nevertheless, at the southern part of the North Sea, the significant wave height is up to 3m with a period of up to 12sec. In [30] is stated that a relation between T_e and $T_{m0,2}$ has been derived based on a Jonswap frequency spectrum with γ = 3.3. The derivation of $T_{m0,2}$ relies on the second moment of spectral density, which implies sensitivity to high-frequency, low-energy fluctuations in the wave spectrum. However, a more universally recognized parameter for wave power computations is the energy period, denoted as T_e, which offers a more accurate representation of lower frequencies. In the context of peak periods falling within the 3 to 15-second range, the ratio between T_e and $T_{m0,2}$ converges to approximately 1.162. For the current study, the significant wave height that was used is 2m and the peak period is set to $T_e = 8.13s$. From the scatter diagram in [30]

the most probable peak period is 7s and this value is multiplied by 1.162 yielding to $T_e = 8.13s$. All the used parameters are summarized in Table 4.1.

Used Parameter	Unit	Value
H_s	m	2
T_e	s	8.13
γ	-	3.3

Table 4.1: Jonswap spectrum's wave-parameters

According to [31], the Jonswap spectrum and the waves are attenuated at depth z by the factor:

$$R(z) = e^{-\frac{\omega^2}{g}z} \tag{4.11}$$

The power spectra for displacement, velocity, and acceleration may be derived as:

$$S_z(n, \omega) = \omega^{2n} e^{-\frac{\omega^2}{g}z} S(\omega) \tag{4.12}$$

where $n = 0$ is used for displacement, $n = 1$ for velocity, and $n = 2$ for acceleration.
In the current study, $n = 2$ is used since the waves are modeled as disturbances in the accelerations.

4.2.3. Limitations of the study

Considering the most extreme environmental conditions in the southern North Sea, specifically along the Dutch coast, a significant wave height of 5 meters might be anticipated as the combined scenario. However, it's important to note that this scenario is not realistic, as current dredging operations typically do not occur under such extreme conditions. The authors of [29] indicate that the southern part of the North Sea reaches a maximum of 3m significant wave height. Taking as reference the former value, it is observed that the submarine cannot follow the reference signal. This discrepancy arises because the wave-induced heave force and pitch moment are substantial, exceeding the capabilities of the PID controllers currently in use. As detailed in [32], classical PID controllers demonstrate stability in CALM-RIPPLED wave conditions but face challenges in maintaining performance in SMOOTH-WAVELET waves. They become ineffective in SLIGHT wave conditions. The properties of the waves are given in 4.3.

Wave scale name	Wave height range	Description of sea surface
Calm-glassy	0 m	The sea surface is as smooth as a mirror, or there are only swells
Calm-rippled	0–0.1 m	Ripple and swell exist at the same time
Smooth-wavelet	0.1–0.5 m	The waves are very small, the crest begins to break, and the spray is not white but glassy
Slight	0.5–1.25 m	The crests of the waves are broken, and some of them form white spray
Moderate	1.25–2.50 m	Waves have distinct shapes and form white waves everywhere
Rough	2.50–4.0 m	There were big wave crests, the spray occupied a large area on the crest, and the wind began to cut off the spray on the crest
Very rough	4–6 m	The wave crests sometimes appear the long wave shape of storm wave
High	6–9 m	The crests of the waves were covered with spray
Very high	9–14 m	Dense spray covered the slope of the waves, and the sea turned white except in certain places within the trough
Phenomenal	>14 m	The whole sea surface is covered with dense spray layer, the air is full of water droplets, and the visibility is significantly reduced

Figure 4.3: International wave scale.

Consequently, a significant wave height of 3m which is classified as ROUGH according to the international wave scale cannot be handled by the PID controllers. For this reason, the significant wave height is set to 2m, and the simulation is performed. Remarkably, with proper tuning, as further analyzed in Chapter 6, the submarine successfully tracks the specified reference signal for depth and pitch control. Nevertheless, an issue arises as the submarine exhibits oscillations at the same frequency as the input disturbances, resulting in a maximum depth overshoot of 0.5 meters and a pitch overshoot of 0.5 degrees. Since the frequency of the disturbances is the same as the frequency of the submarine, this means that the PID fails to cancel out the former.

Another noteworthy limitation of this study is that the input disturbances are modeled for only one encounter frequency, neglecting the entire Jonswap spectrum. While the encounter frequency is pivotal

for controller design due to its high probability, incorporating the entire spectrum would provide a more accurate assessment of the energy required to compensate for these disturbances.

Given the PID controllers' ability to ensure submarine tracking, this model can be leveraged to evaluate a submarine's energy requirements in the early design phase. However, it's essential to address the submarine's oscillatory behavior, which also impacts the RPM of the vertical tunnel thrusters. To mitigate this challenge, a low-frequency filter is applied to provide a rough estimate of the necessary energy. It is worth noting that due to the complexity of the model, the resonance frequency of the model is not estimated. It is recognized as a limitation of this project and it is recommended to be studied in future research since it might be critical for the ALERD.

4.2.4. Low-frequency filter

According to [15] for sea states where the wave frequency motion is much higher than the bandwidth ω_b of the controller, a low-pass filter can be used to filter out the wave frequency motions if ω_b satisfies:

$$\omega_b \ll \omega_{ei} \tag{4.13}$$

where ω_{ei} is the encounter frequency. Then, the filter has to be designed using frequency ω_c which needs to meet the following requirement.

$$\omega_b < \omega_c < \omega_{ei} \tag{4.14}$$

Since the transfer function of this model is very complex and the control part of the study is out of the scope of this work, it is challenging to determine the ω_b of the system. Recognizing it as a limitation of this study, it needs to be mentioned that the cut-off frequency is designed following a trial and error approach. Using a step of 0.1 rad/s and considering that the encounter frequency is 0.5rad/s, the different outcomes after applying the low-pass filter are plotted, Figure A.3 in Appendix.. In order to select the optimum cut-off frequency for the approximation of the energy result, a result that converges to a value, and presents the lowest amplitude oscillation needs to be selected. After the iterative procedure with the different cut-off frequencies the ω_c is set to 0.2 which is lower than the encounter frequency. After this value, smaller frequencies such as 0.1rad/s give the same result.

To overcome this issue and estimate the energy, the low pass filter was designed as follows:

$$F(s) = \frac{\omega_c}{s + \omega_c} \tag{4.15}$$

Furthermore, first-, second-, and third-order low-pass filters are implemented to determine which one best fits the model and provide a more accurate estimate of the energy needed from the thrusters to compensate for environmental disturbances. These low-pass filters permit low frequencies to pass through while attenuating higher ones. Consequently, they smooth the thrust behavior, allowing it to converge to a stable value, which is then used to estimate the required energy. However, a challenge arises when applying these filters: they cut off the maximum values for RPM, which, in turn, affects thrust and power calculations for higher frequencies. This leads to an underestimation of power and results. To ensure a fair estimation of energy consumption and the maximum required output power for the thrusters, simulations are conducted in two stages. Initially, simulations are performed without any filters, enabling the calculation of the maximum power output of the thrusters. This value is crucial for determining the appropriate size of the thruster units.

Subsequently, the higher-order filters are incorporated into the simulation, allowing the estimation of the energy consumption more accurately while still considering the maximum required output power for the thrusters. This two-stage approach provides a comprehensive assessment of the system's energy needs and ensures that the thrusters are appropriately sized to meet the demands of the application.

4.2.5. Sanity Check

According to [15] the simulation of ocean current velocity and angle adopts a first-order Gauss-Markov process. Consequently, both the generated velocity and angle are expected to adhere to a Gaussian distribution. To confirm this, histograms displaying these values are generated and examined for both the generated velocity and angle in Figure A.1 and Figure A.2 respectively, given in the Appendix.

Evidently, the data exhibits adherence to a Gaussian distribution. The inclusion of the moving average block constrains the potential extreme values for both speed and angle. To specify this, it is

challenging for the submarine to precisely track the reference signal because when the white noise generates random values, abrupt changes occur, resulting in overshooting by the submarine. Using only PID controllers in such instances does not allow adequate time for the submarine to return to the reference signal, for this reason, the moving average is included.

Similar behavior is presented in A.5, Appendix, with the pitch due to the waves. The highest values are depicted when the ALERD is closer to the surface since the waves have greater influence. Again, the pitch moment remains constant when the submarine moves at the same depth, and as it descends towards the seabed, the influence of the waves and the created pitch moment reduces.

4.2.6. Discussion

Recognizing the importance of including wave effects in the model and comprehending their influence on submarines operating in shallow seas, it is clear that their contribution to energy consumption is certainly considerable. Waves shape the operational circumstances and energy needs of these underwater systems, making their proper evaluation critical for thorough study and design. The Matlab, Simulink model that is developed to model them provides a way to estimate and assess the energy that is required to compensate for the generated forces and moments. This model is a way to roughly estimate the required energy and define the size of the pumps/thrusters etc. in an early-stage design phase submarine that is about to operate in shallow water.

It is clear that the approach has some limitations and for the precise calculation of the required energy, further research has to be done. First of all, the inclusion of all the frequencies of the Jonswap spectrum needs to be taken into account. In this way, the result will be more realistic, and it might be more beneficial for the model. For the time being, only one encounter frequency is considered and this overestimates the energy that is needed since the remainder of the spectrum is not included. Moreover, the second-order forces which are of great importance as well, need to be modelled following the same procedure. In this way, more energy will be needed to compensate for these forces and moments since their contribution is higher than the first order. The components of the first-order forces are oscillatory and proportional with each wave component amplitude of the wave spectrum. It is important to filter out such disturbances and to identify the first-order wave-induced motions, in [33] an adaptive identification of lowpass filter cutoff frequency for online vessel model tuning is studied. As a result, future research can be carried out on that to smooth the result and eliminate the oscillatory behavior. The second-order forces (drift forces) are proportional to the square of wave components amplitude and have the effect of dragging the submarine to the sea surface. As the submarine approaches the sea surface, these suction forces increase exponentially and produce a destabilizing effect on the already marginally stable submarine.

As a result, the PID controllers will be not capable of dealing with these disturbances. In order to overcome this hurdle, an observer needs to be designed in order to predict the next step, or an adaptive controller [28] shall be integrated. It can be used in a feedback loop in order to cancel out the disturbances. Another possible solution to this issue might be the design of a wave filter [15].

4.3. Seabed and Surface Interaction

The influence of the seabed is significant to be defined for the modeling of submarines that operate near it in order to ensure accurate predictions of underwater vehicle motion and performance. The different forces acting on underwater vehicles in shallow water, including the drag force, lift force, and pitching moment are identified and will be applied to the submarine's model. Throughout the literature review, it was found that the surface has a significant contribution to the underwater vehicles creating the same forces as the seabed, with the difference that the lift force is towards the surface. For this reason and in order to estimate the energy that the submarine needs to counteract these forces, an accurate model needs to be developed to simulate the motions at different depths. Since the final dimensions of the submarine are unknown, the development of a numerical model that calculates these forces is expensive and time-consuming. Consequently, these forces can be estimated from similar studies that are carried out and incorporated into a model that can calculate the submarine motions and subsequently the energy consumption.

4.3.1. Seabed Interaction

One of the factors that significantly impact underwater vehicles' operation, which operate in shallow water is the seabed. The seabed is the bottom surface of the ocean floor, and submarines need to navigate and maneuver around it effectively. The seabed's topography, depth, and composition can affect the submarine's ability to operate and maintain a safe distance when it needs to operate close to it to perform tasks, for example, node placing or dredging. Thus, understanding the submarine-seabed interaction is crucial for the successful operation of these vessels. After a more thorough investigation in the literature review for the seabed interaction and its contribution to a submarine or an underwater vehicle, a drag force, a suction force towards the seabed, and a pitching moment appear to occur, [34], [35]. These forces are applied on the submarine and are developed due to the close operation near the seabed and as a result of the submarine's forward speed. The asymmetrical pressure distribution around the hull causes a heave force, that mainly acts on the aft of the vessel when at zero drift, resulting in the pitching moment [36]. Especially the heave force mentioned in [34], [37], [38], which is developed due to the approach of the seabed, is not applied at the centroid of the submarine, as a result, a pitching moment is created. In order to estimate the coefficients required to determine the aforementioned forces, most of the researchers use hydrodynamic software, running simulations. Due to the early or preliminary design phase of ALERD, the development of a model in any hydrodynamic software would be time-consuming and expensive. For this reason, a mathematical model can be used to simulate the problem. However, for the appraisal of the former, the results of the study from [34] were utilized.

Shallow water depth identification

Taking into account that the autonomous underwater vehicle will operate in the North Sea in shallow water, the depth of it should be defined. In order to determine whether shallow water conditions do apply within the operational area of the considered submarine the following method is considered:

$$\frac{d}{\lambda} \leq 0.05 \tag{4.16}$$

where d is the water depth and λ the wave length. According to [30], the wave power potential in the North Sea is compared with the resource of the West European coast near shore (< 30 km off the coast), and for the Dutch Coast and at a Sea State 5, the significant wave height is 4.5m and the energy period is 8.13s. The energy period T_e is a more generally accepted parameter for wave power calculations which represents the low frequencies better. A relation between T_e and $T_{m0,2}$ has been derived based on a Jonswap frequency spectrum with γ = 3.3. For peak periods between 3 and 15 s the ratio between T_e and $T_{m0,2}$ is approximately 1.162, according to [30]. To clarify the former, the equations for the mean wave period $T_{m0,2}$ and the energy period are presented below.

$$T_{m0,2} = \sqrt{\frac{m_0}{m_2}} \tag{4.17}$$

$$T_e = 1.162 T_{m0,2} \tag{4.18}$$

where m_n is the n-th moment of spectral density. Furthermore, the wavelength for shallow water is given by:

$$\lambda_s = T_e\sqrt{gd} \tag{4.19}$$

Using the equations 4.16 and 4.18, at Sea State 5 and in the North Sea, the depth up to 64m can be considered shallow water.

Nevertheless, in continuation of the project [39] and for coherence, the operational profile of ALERD is the same. An operational profile analysis made by C-Job is provided in [24], as a result the operational profile created by [39] is based on AIS data analyzed from conventional dredgers doing coastal replenishment along the Dutch coastline. During an operational cycle, the dredging, transit, and discharging modes are identified. Consequently, they were taken into account in order to build the operational profile of ALERD, where more information can be found in [24], [39] The maximum depth that is taken into account is 21m and in the current study, the dredging condition operational profile of ALERD takes place at 15m depth.

Seabed-induced Coefficients

In [34], the authors used computational models to simulate different distances to the sea bottom and angles of attack. The outcome demonstrates that while the drag coefficient increases with increasing attack angle, it decreases with decreasing distance. When UUV travels close to the seabed, there is an attraction force present, and the attraction force grows as the distance between the two objects decreases, [34]. Also, the angle of attack increases along with the lift coefficient. With a reduction in distance and an increase in attack angle, the pitching moment coefficient grows in absolute magnitude. Nevertheless, in the current model, the developed forces will change only with respect to depth and not with respect to the angle of attack for the simplification of the problem. In [34], the top surface of the domain was considered as a free slip wall and the UUV that was studied has a length of 1850 mm, its biggest diameter is 200 mm and the working conditions are 2 and 5knots. Furthermore, the coordinate system is placed at the seabed, so the closer to the seabed, the smaller the e value.

More specifically, the C_x, C_y and C_{mz} are extrapolated since the non-dimensional number $e = \frac{d}{D}$ needs to be adequately defined and the aforementioned variables need to be estimated. In figure 4.4 the C_x coefficient as a function of the non-dimensional variable e is presented. Plotting the fitting curve, the C_x values for $e \leq 1.5$ are estimated. In the current study, these values are essential since the underwater vehicle will operate in shallow water. The red circle indicates the depth from 0m to 48m, or in terms of the non-dimensional variable e, from 0 to 3. This approach is adopted with the anticipation that potential future enhancements to the operational profile of the ALERD might encompass a broader range of operational conditions, thus encompassing a greater spectrum of water depths.

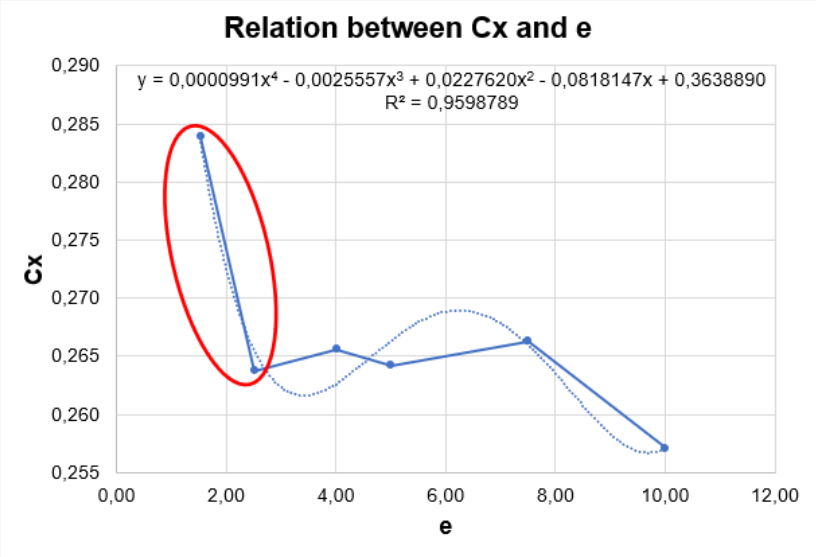

Figure 4.4: Relation between C_x and e for the reference study

Following the fitting curve, which is a 4-th order polynomial with $R^2 = 0.94$. the drag coefficients for ALERD, are presented in 1.1.

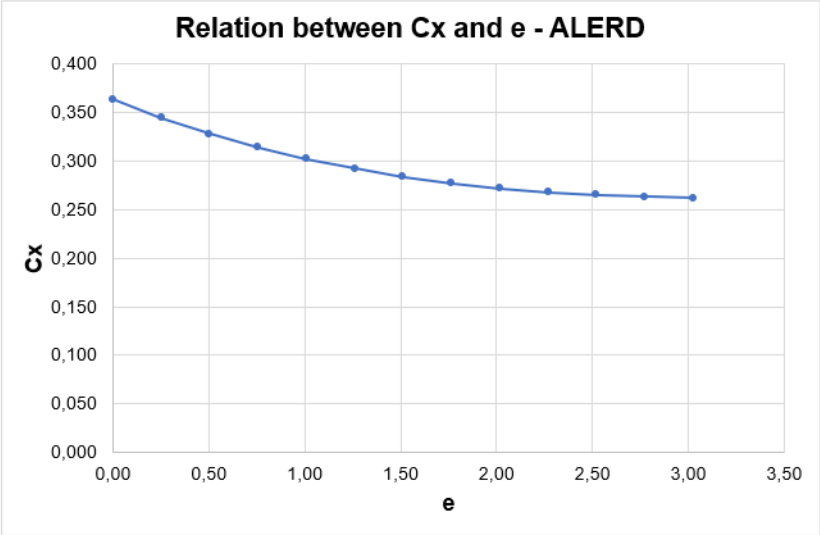

Figure 4.5: Relation between C_x and e for the ALERD

The resulting drag force is calculated by:

$$F_{drag} = \frac{1}{2}\rho C_x v_s^2 D^2 \tag{4.20}$$

Similarly, for the created suction force towards the seabed, the C_y values were obtained from [34], and extrapolated using a 4-th order polynomial with $R^2 = 0.997$, presented in Figure 4.6 (a).

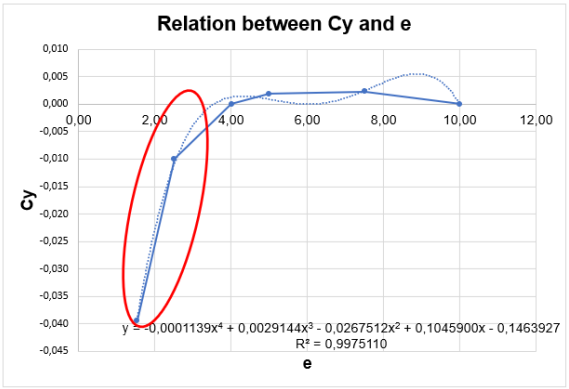

(a) Relation between C_y and e for the reference study

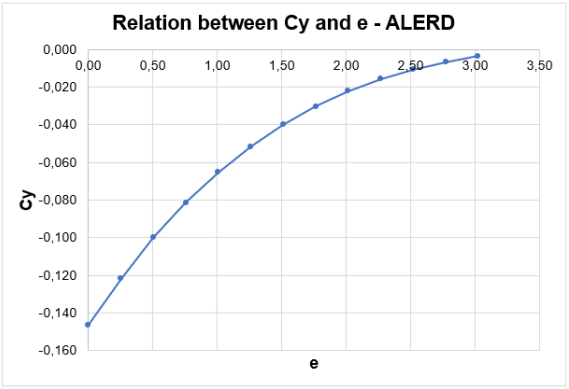

(b) Relation between C_y and e for the ALERD

Figure 4.6: Relation between C_y and e

Correspondingly to the study for C_x. the red circle indicates the operating zone. The scaled results for ALERD for C_y are depicted in 4.6 (b). The resulting suction force is calculated by:

$$F_{heave} = \frac{1}{2}\rho C_y v_s^2 D^2 \tag{4.21}$$

Apart from the drag force in the surge direction and the suction force in the heave direction, a pitch moment is created as the underwater vehicle approaches the seabed, due to the pressure difference. Equivalently, the C_{mz} coefficient from [34] needs to be scaled for $e \leq 1.5$ following the same procedure. As can be seen in Figure 4.7 (a), a 4-th order polynomial with $R^2 = 0.998$ is used to extrapolate the pitch coefficient, resulting in the values in 4.7 (b).

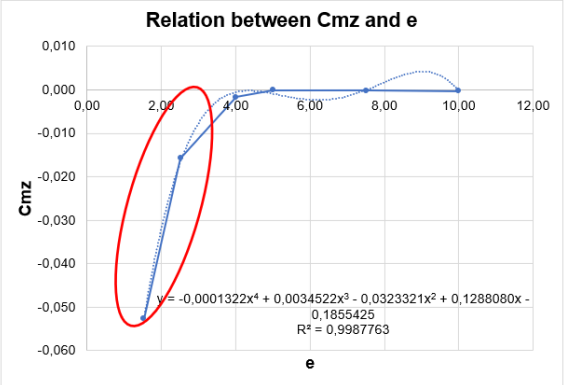

(a) Relation between C_{mz} and e for the reference study

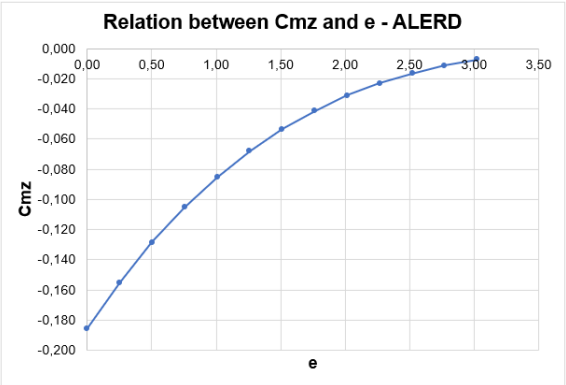

(b) Relation between C_{mz} and e for the ALERD

Figure 4.7: Relation between C_{mz} and e

The resulting pitch moment is calculated by:

$$M_{pitch} = \frac{1}{2}\rho C_{mz} v_s^2 D^2 L \tag{4.22}$$

As mentioned previously, although these coefficients alter with the different angles of attack, in this study they remain constant and are considered independent of the former for simplifying the problem.

4.3.2. Surface Interaction

From the literature review that was conducted, it can be stated that submarines are primarily designed to operate in deep waters, but as they approach the surface, they may encounter a phenomenon known as the free surface effect. This effect occurs when the submarine approaches the water's surface and the water begins to behave differently due to the air-water interface. However, the consequence of this effect on a submarine's performance heavily depends on the depth at which it operates. The free surface effect can have a significant impact on a submarine's maneuverability and stability capabilities in shallow waters. Thus, not only must the effective depth that affects the submarine's behavior be defined, but so must the created forces that act on the submarine. According to numerical methods which were carried out by [40] and [41], a lift force draws the submarine towards the free surface and uniform pressure distribution is observed at low Froude numbers. This pressure distribution creates a trimming moment that draws the bow towards the seabed and the aft towards the free surface. The authors of [42] investigate the hydrodynamic behavior of a shallowly submerged submarine under the free surface, which experiences large resistance force, lift force, and pitching moment varying periodically concerning the Froude number. Due to the primary design phase of ALERD, modeling in a hydrodynamic software is not preferable considering the time and the expenses However, for the appraisal of the coefficients of the developed forces and moments, the results of a previous study, [43] were utilized.

Surface-induced Coefficients

In [43], using Reynolds Averaging Navier Stokes (RANS) computational fluid dynamics (CFD) simulations, the authors present data at varying depths and speeds typical for a submarine operating near the free surface for the evolved DST Group/MARIN generic BB2 submarine at model scale. The submarine has a length of 1.692m and a diameter of 0.231m, operating in 2knots. Furthermore, the coordinate system is placed at the surface, so the closer to the surface, the smaller the non-dimensional e value. The study that has been conducted has taken into account the wave elevation for different Froude numbers since it affects the heave and surge forces developed by the surface, [43].

Similarly to the extrapolation of the seabed-induced coefficients, the operating area that is of the project's interest is for $e \leq 3$. For this reason, the drag and heave coefficients need to be extrapolated $e \leq 1.5$, where the results from [43] are not available.

In order to extrapolate the C_x values, a 2nd order polynomial is fitted at the study's data with $R^2 = 0.958$ as can be seen in figure 4.8a. As a result, the C_x values are extrapolated from 0m to 48m, or in terms of the non-dimensional variable e, from 0 to 3 4.8b.

The drag force induced by the surface is calculated by the equation given below:

$$F_{drag} = \frac{1}{2}\rho C_x v_s^2 L^2 \tag{4.23}$$

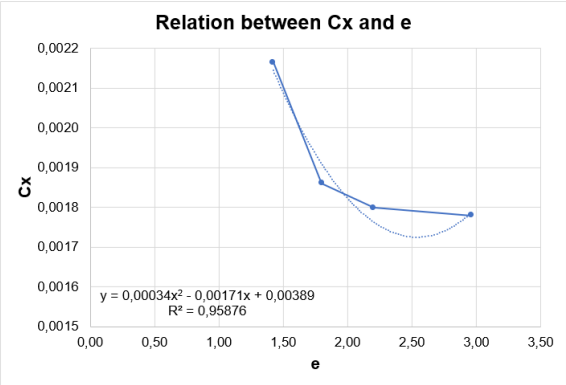

(a) Relation between C_x and e for the reference study

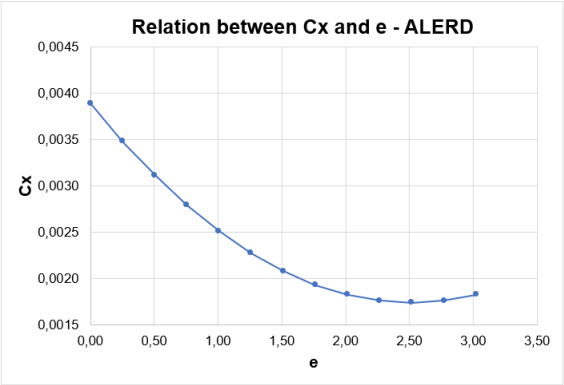

(b) Relation between C_x and e for the ALERD

Figure 4.8: Relation between C_x and e - Surface-induced coefficient

Similarly, for the created suction force towards the surface, the C_y values were obtained from [43], and extrapolated using a 2-nd order polynomial with $R^2 = 0.998$, presented in Figure 4.9a. As a result, the values for the ALERD are presented in Figure 4.9b.

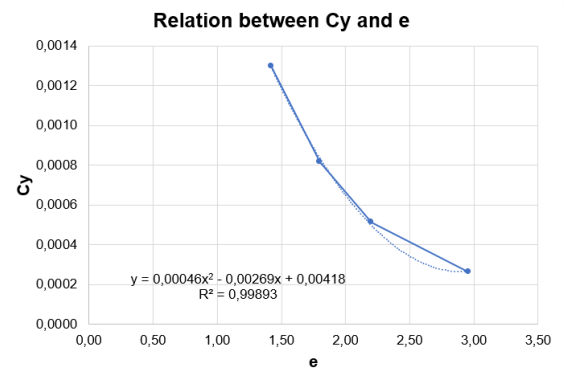

(a) Relation between C_y and e for the reference study

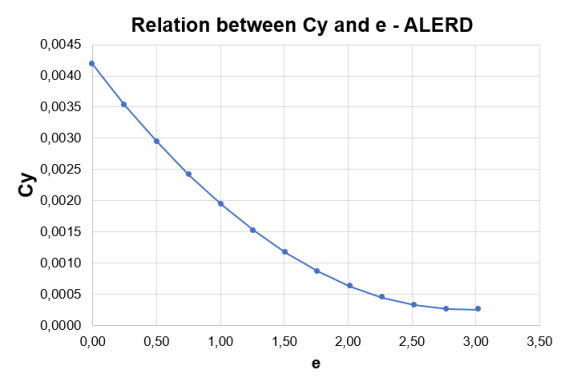

(b) Relation between C_y and e for the ALERD

Figure 4.9: Relation between C_y and e - surface-induced coefficient

The heave force induced by the surface is calculated by the equation given below:

$$F_{heave} = \frac{1}{2}\rho C_y v_s^2 L^2 \tag{4.24}$$

It is mentioned in [43] that the location in which the center of vertical force is acting will move and thus change the pitching moment at different velocities. Since this is a limitation in the [43] and it is recommended as a future study, there is no option to obtain the pitch coefficients for the current study. In order to determine them properly, a CFD analysis is needed, which is not in the scope of this work. It is recognized as a limitation of the current work as well since the results will be affected but when the model is finalized, hydrodynamic software will be used and the results for the developed forces and moments can be imported into the Matlab, Simulink model to obtain the actual behavior of the underwater vehicle.

4.3.3. Simulating Seabed Interaction: MATLAB Simulink Modeling and Analysis

The present investigation outlines the methodological framework employed in Simulink representation of surface and seabed interaction phenomena. The approach involves the utilization of scaled aforementioned coefficients, predicated on depth as well as non-dimensional parameter e. These coefficients are subsequently integrated into a lookup table, where they are paired with their corresponding depth values. The input in the seabed interaction block is the depth and the velocity of the ALERD. This configuration enables the application of equations 4.20, 4.21, 4.22 yielding the computation of resultant forces and moments.

4.3.4. Comparative Analysis of Forces Generated by Surface and Seabed Interactions

It has to be mentioned that all the forces and moments induced by the surface and the seabed are assumed to act on the center of buoyancy of the ALERD so they do not need to be transferred from inertial frame to body-fixed frame. In order to evaluate the results in terms of the magnitudes of forces and moments that are exerted on the ALERD, the aforementioned equations are utilized. The velocity that is used is the transit speed of ALERD which is 8.5 knots. With this approach, even though closer to the seabed, at the dredging condition, the transit speed is used in order to follow a conservative estimation of the developed forces and moments. In Figure 4.10 the drag forces created by approaching the surface and the seabed are depicted. Firstly, a common coordinate system was set at the surface and the forces can be compared. It is observed that, when operating near the seabed the drag force induced by it is tremendously higher. Furthermore, the surface interaction is not zero but is almost negligible compared to the seabed interaction. This is due to the fact that the submarine is quite big and operated in shallow water, so there is not enough depth for the seabed interaction to be eliminated or be considered negligible. In higher depths, this would happen. Approaching the seabed, the drag force induced by the surface decreases, while the drag force initiated by the floor increases.

As can be seen, at $e = 1.3$ both drag forces have the same contribution and from $e = 1.5$ onwards the

surface drag starts stabilizing. Similar behavior is observed for seabed drag from $e = 0$ to $e = 1.5$ due to the fact that the underwater vehicle is not so close to the surface and the interaction is minimal. This can be verified from [34] [43] where after $e = 1.5$ the coefficients tend to be constant and the underwater vehicle is close to operating under 'deep submerged' conditions or 'away from the free-surface.

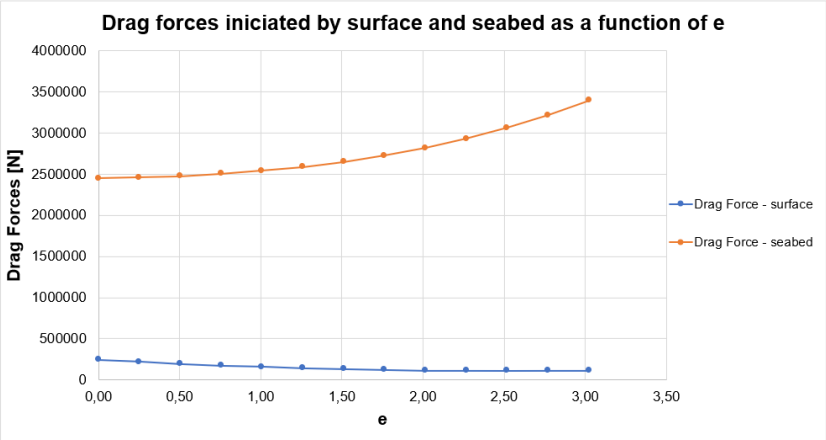

Figure 4.10: Surface and sea bottom drag induced forces - ALERD

The developed heave or suction force, if the studied case is the near-surface condition or near-seabed condition respectively, is observed in Figure 4.11.

It is observed in Figure 4.11 that when operating near the free-surface, the heave forces act on the underwater vehicle is almost 250kN and they decrease exponentially while approaching the seabed. Similar behavior is noted for the suction force created by the seabed interaction. The seabed contribution is again higher than the surface interaction. At $e = 3$ the former is almost 400kN towards the seabed. In the condition where the ALERD is at a distance $'h'$ from the free surface, the suction force towards the surface is lower than the suction force towards the seabed, in the condition where the ALERD operates at a distance $'h'$ from the seabed.

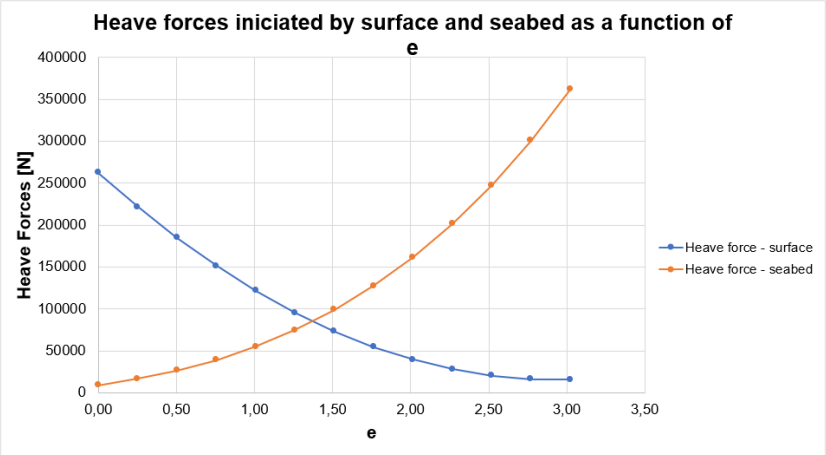

Figure 4.11: Surface and sea bottom heave induced forces - ALERD

Due to the limitation that there is regarding the data of the pitch moment induced by the surface, in Figure 4.12 only the pitch moment initiated by the seabed is depicted. As expected, approaching the seabed, the pitch moment is larger. The closer the ALERD is operating to the seabed, the lower the pressure in between the former is. As a result, the suction force that is created towards the sea floor does not act in the center of buoyancy and a pitch moment is developed.

The authors of [36] reveal that the hydrodynamic coefficients of the DARPA SUBOFF are influenced differently by the seabed and surface. More specifically, it is stated that the contribution of the surface is higher than the one of the seabed when the submarine is located at a distance h from the surface,

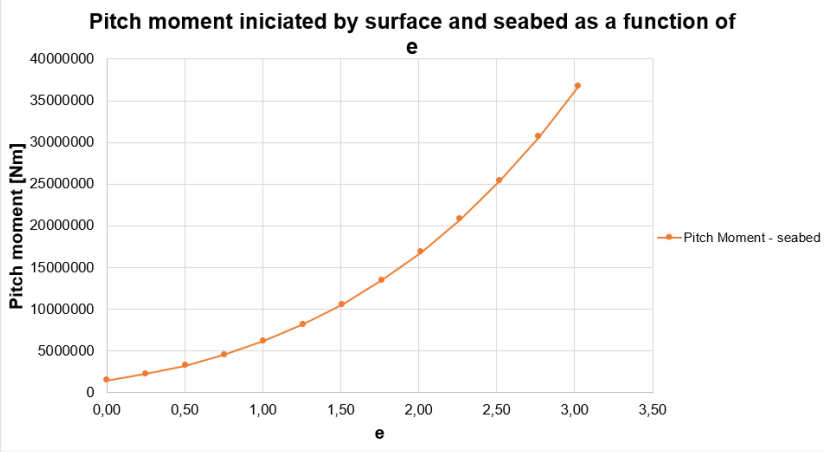

Figure 4.12: Seabed pitch induced moment - ALERD

and at the same distance h from the seabed respectively. As a result, the outcomes diverge from those presented in [36]. This variance arises due to the adoption of disparate methodologies in evaluating drag, heave, and pitch coefficients for interactions with both the water's surface and the seabed. These coefficients originate from distinct investigations, wherein the authors opt for varying approaches in computing the Froude number and employing diverse formulas to approximate the resultant forces. Consequently, the sequence of coefficients differs, leading to incomparable force assessments.

To prevent the potential underestimation of the energy required to counterbalance these forces, it becomes imperative to carefully identify and investigate the most pivotal condition. It has to be taken into consideration that for the surface contribution, the pitch moment is a limitation and constrains the accuracy of the model. This study aims to elucidate the extent of the seabed's influence on the forces acting on underwater vehicles and ascertain the corresponding energy necessary for compensation. Hence, the emphasis within this study is placed on seabed interactions as they hold greater significance, excluding the surface interaction from the analysis and recognizing it as a limitation.

4.3.5. Sanity Check

To ensure the accuracy of the analysis, a sanity check using a case study the ALERD was conducted. This involved utilizing its dimensions and parameters, as outlined in Table 2.1, to define the force and moment exerted on the ALERD. As previously discussed, these force and moment values vary with depth and speed.

As mentioned previously, the generated drag force, suction force, and pitch moment by the seabed are all influenced by the relative velocity of the submarine and the depth. The operational profile which is illustrated in 6.2 is used as well as the velocity profile of ALERD Fig. 6.1, which are both described in Chapter 6.

It is observed that the created drag force in Figure A.6 in the Appendix, due to seabed, is maximum when the submarine operates in transit mode since the influence of the speed is taken into account in the calculation of the force and it is squared. Although one would expect that the drag force would be higher near the seabed, the relative speed is 1.7knots, and compared to the transit one very low. This means that the influence of the seabed when operating in dredging conditions is low.

In Figure A.7, Appendix, a similar trend to the drag force behavior is observed. It might seem intuitive that the suction force would be higher when operating near the seabed and lower when near the surface. However, the relative speed, which is squared to estimate the force, plays a critical role in this behavior.

Additionally, a noteworthy peak in the suction force is observed when the submarine descends to 15 meters and then ascends back to 8 meters at around 7000 seconds. This behavior can be attributed to the tuning of the depth PID controller, which results in a minor overshoot at 200 seconds and at 7000s. However, the suction force stabilizes quickly and since it lasts only a couple of seconds it does not affect the energy consumption.

When tuning the various controllers for different environmental conditions separately, it becomes

evident that different gain values work better under different conditions. While the implementation of an adaptive PID controller could address this issue, this study does not cover that aspect. Consequently, the selected PID gains are those that yield the desired submarine behavior, encompassing all environmental conditions within the combined scenario. However, this means that when taking into account only the influence from the seabed the gains are not the most suitable ones, leading to the forces that are depicted in the Figures A.6 A.7,A.8. In this situation, a trade-off exists, and the chosen gains are optimized for the combined scenario, even if they lead to the observed peak in the suction force and pitch moment. Nevertheless, both of these deviations can be managed by the PID controllers, with an overshoot of only 0.1 meters, ensuring overall system stability.

4.3.6. Discussion

It is critical to be able to predict how the developed forces change with varying speeds and depths to ensure the trim tanks and control surfaces that are typically utilized in this condition are effective. According to the literature review that was conducted, when operating near the surface and near the seabed, a drag force, a heave force and a pitching moment in each case act on the underwater vehicle. Since obtaining the exact coefficients for the aforementioned forces and moments was not in the scope of this study, an estimation was used.

The omission of surface interaction from the present study results from the absence of the pitch moment coefficient. Additionally, the decision to exclude it stems from the observation in [43] that coefficient calculations employ the characteristic length for Froude number determination, unlike [34] which employs the characteristic diameter. This yields results that are not comparable and the integration of both surface and seabed interaction will lead to unrealistic outcomes. Thus, to ensure the validity of findings and align with the primary research objective of seabed investigation, the study exclusively focuses on seabed interaction dynamics.

Recognizing the limitations of the current model's approach, it needs to be stated that for future improvements, the relation between the angle of attack and the developed forces and moments has to be studied. Furthermore, the surface interaction significantly contributes to the total forces and moments vector which leads to underestimation of the required power. Thus, it is recommended to be investigated and added to the model for a more precise estimation of the power. In essence, the modeling of seabed interaction serves as an initial approximation, aimed at providing a preliminary assessment of the energy required to counteract the resultant forces and moments.

4.4. Draghead Force and moment

Since the ALERD is used as a case study and it is a dredger submarine, an extra resistance force that also causes a trimming moment needs to be introduced, the draghead resistance. During the dredging condition, this extra resistance force and moment need to be compensated by the actuators mentioned previously. According to [39], the total resistance force that acts on the negative x direction is due to the suction tubes and the dragheads. The resistance of both is dependent on the forward speed and the current and is equal to 260 kN. Taking into account that the moment arm is 3.5m and the hull-seafloor clearance is 2m, a positive created moment due to the resistance is created. The resistance force is depicted in Figure 4.13 and is applied in the τ vector of the main function.

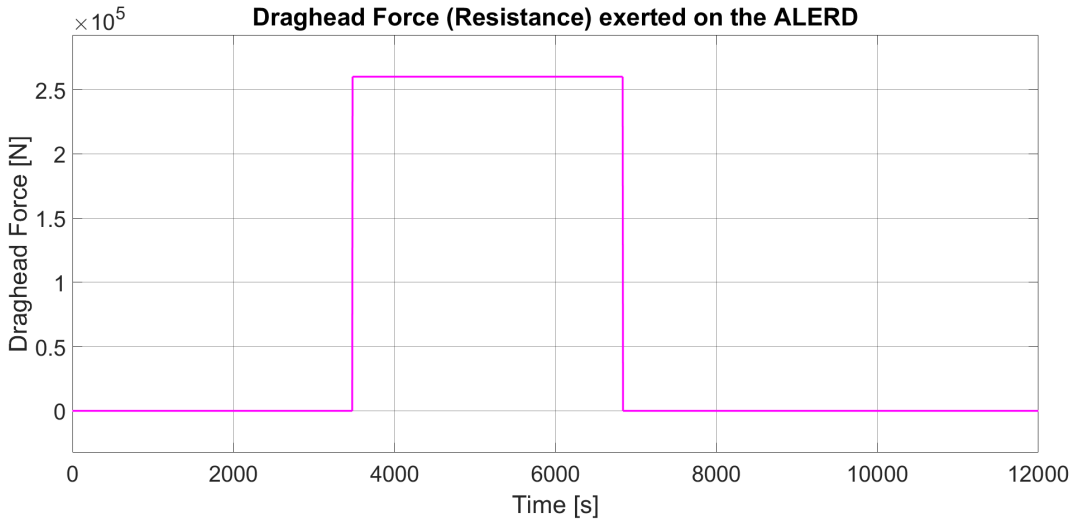

Figure 4.13: Draghead resistance

4.5. Conclusions

In summary, this chapter provides a comprehensive overview of ocean current modeling, emphasizing the stochastic technique advocated by Fossen [15]. This approach, employing the first-order Gauss-Markov process to simulate ocean current velocity and angle, allows for the incorporation of real-world randomness and variability into current patterns. This stochastic modeling technique has proven effective in generating realistic current data for various maritime applications, as demonstrated through the simulations.

To address challenges related to overshoot during operations, the inclusion of additional control mechanisms, such as the moving average block, has been instrumental as a temporary solution. However, future research opportunities lie in the development of adaptive PID controllers capable of efficiently responding to abrupt changes.

Recognizing the significant impact of wave effects on submarines operating in shallow seas, particularly in terms of energy consumption, a Matlab and Simulink model has been developed to estimate and assess the energy required to counteract forces and moments generated by waves. This model serves as a preliminary tool for sizing pumps and thrusters during the early design phase of shallow-water submarines.

However, certain limitations persist. Future research should consider incorporating all frequencies of the Jonswap spectrum to provide more accurate results. Additionally, second-order forces, which contribute significantly, need to be modeled in a similar manner. Techniques to filter out disturbances and eliminate oscillatory behavior should also be explored. The integration of observers, adaptive controllers, or wave filters may be necessary to mitigate the destabilizing effects of second-order forces.

Furthermore, understanding the relationship between the angle of attack and developed forces and moments is essential for future improvements. Surface interaction, particularly the impact of surface forces on total forces and moments, should also be investigated and integrated into the model for a more precise energy estimation.

This modeling approach serves as an initial approximation, offering a preliminary assessment of the energy required to counteract forces and moments, with an acknowledgment of its limitations. Additionally, for dredging submarines like the ALERD, the introduction of draghead resistance as an extra force necessitates further consideration in future studies.

5

Actuators

As it is known, underwater vehicles need to be equipped with actuators amongst others in order to control motions and stabilize the vessel. One of the critical components of the former is their propulsion system, which allows them to move and maintain depth. These actuators can be ballast tanks, horizontal thrusters, vertical thrusters, or control planes which can be modeled as actuators.

In the current study, as mentioned in Chapter 3, for the specific case study of the ALERD, the τ vector contains the control forces from the vertical tunnel thrusters that control the heave motions and the generated moments from the trim tanks capable of controlling the pitch. Furthermore, the ALERD is equipped with two ducted thrusters that control the speed in the surge direction. These forces are included in the τ vector as well. It needs to be mentioned that there are more means to control the generated forces as the depth control tanks and the control planes but they are not in the scope of this project.

5.1. Forward Thrusters

To counteract the forces exerted on the underwater vehicles in the x-direction and provide the necessary thrust to follow the operational profile, underwater vehicles are equipped with forward thrusters.

5.1.1. Modelling of Forward Thrusters in Matlab, Simulink

Using the ALERD as a case study to check the developed model and the results it provides, the forward thrusters that are equipped, need to be modeled. In order to model the thrust force provided by the forward thrusters, the equation below is used.

$$T_{FT} = \frac{1}{2} \cdot \rho \cdot D^4 \cdot KT \cdot n^2 \tag{5.1}$$

It is worth noting that the $\frac{1}{2}$ is set because the ALERD is equipped with two forward thrusters. The total thrust force is included in the τ vector. Based on findings from prior studies [3], the obtained propeller characteristics are presented in Table 5.1, which are crucial for calculating propeller thrust. Initially, the simulation model incorporates two propellers. It's important to note that the torque generated by the propellers can potentially produce a rolling moment. However, given that two counter-rotating propellers are employed, it is reasonable to assume that the resulting moment is negligible.

The characteristics of the propeller of the forward thruster are given in Table 5.1 :

B-Series SRP 490	
D_{VTT}	$2.8m$
KT	0.207
n_{max}	$660rpm$

Table 5.1: Forward Thruster's propeller characteristics

5.1.2. Physical Limitations

Constraints are implemented into the speed controller to ensure the development of a realistic and time-varying speed. The PID controller's speed output, which reflects the propeller speed n, is subject to upper and lower restrictions. Based on the propeller's properties, it is anticipated that the maximum allowed propeller speed is $660rpm$ in this context. The minimum propeller speed is set at $-660rpm$. It should be noted that a thorough explanation and derivation of these propeller restrictions is beyond the scope of this study. More information about the selected propeller can be found in [44]. As a result, restrictions relating to the physical systems responsible for propeller speed, such as electrical engines, or the losses and the efficiency are not taken into account in this study.

5.2. Vertical Tunnel Thrusters

It is widely known that submarines primarily rely on ballast tanks and control planes for their descent and ascent. However, recent research has been dedicated to submarines equipped with vertical tunnel thrusters. This shift in focus is driven by several compelling reasons. One important aspect is the decreased efficiency of typical control planes at low speeds in producing the necessary forces to counteract disturbances. Vertical tunnel thrusters, on the other hand, excel in such scenarios, particularly when precise hovering capabilities are required.

Another advantage of vertical tunnel thrusters is their ability to make rapid adjustments in RPM, making them invaluable for compensating for high-frequency disturbances like waves. In contrast, relying solely on ballast tanks to control these same disturbances would prove more challenging due to physical limitations such as pump pipe velocity and diameter. This approach would also be more time-consuming.

Vertical tunnel thrusters have been beneficial in allowing survey-style submarines to function efficiently at lower speeds. By equipping these vehicles with vertical through-body tunnel thrusters, they have transformed into hover-capable, flight-style Autonomous Underwater Vehicles (AUVs), as exemplified in research presented in [45]. Furthermore, research, as outlined in [46], has indicated that vertical tunnel thrusters have the potential to eliminate the need for control surfaces in maneuvering for low speeds. This not only reduces the vehicle's drag but also improves the flow dynamics around the propeller by providing an axisymmetric profile. In summary, the integration of vertical tunnel thrusters in submarine design represents a significant advancement, addressing challenges associated with low-speed control, rapid response to disturbances, and improving overall vehicle performance in various underwater applications.

5.2.1. Modelling of Vertical Tunnel Thrusters in Matlab, Simulink

In order to make use of the generated Matlab, Simulink model and draw results, the ALERD is used as a case study. This underwater vehicle is at a very early design stage. As a result, there are no vertical tunnel thrusters or a relevant design study for the former, to be utilized for the control of the heave motion. Given the freedom to design, vertical tunnel thrusters have been strategically placed at distances $x = 32m$ and $x = -32m$ from the center of buoyancy to maintain symmetry with respect to the center of buoyancy and avoid introducing any additional pitch moment, Figure 5.1.

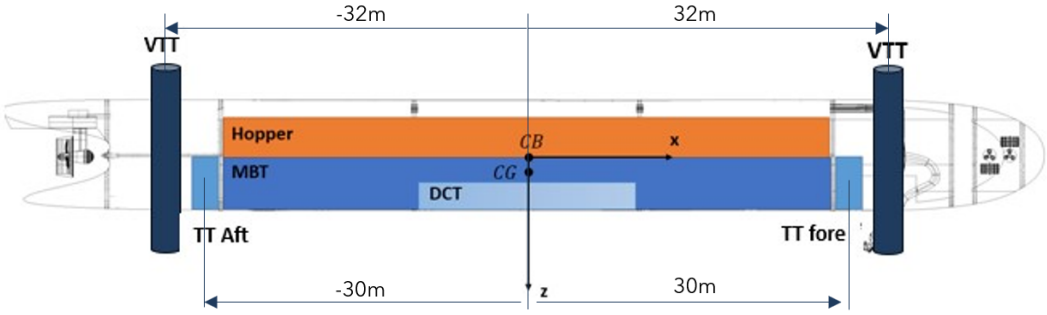

Figure 5.1: ALERD's internal layout

Initially, a decision was made for the vertical tunnel thrusters to operate at the same number of

RPM, solely providing a vertical force to the underwater vehicle without generating any extra pitch moment. This simplification was chosen to streamline the problem, as it allows for the use of a single PID controller for heave motion control. The equation to model the forces that come from the vertical tunnel thrusters is given by the equation:

$$T_{VTT} = \rho \cdot D^4 \cdot KT \cdot n^2 \tag{5.2}$$

where the diameter and the required RPM were determined by an iterative procedure. The aforementioned force is included in the τ vector. First, the diameter is set to $D = 0.7m$ and the maximum value for the RPM is defined by the equation below in order to avoid the cavitation region.

$$n = \frac{V_{tip} \cdot 60}{\pi \cdot D} \tag{5.3}$$

where $V_{tip} = 30m/s$ a value provided by C-Job. This value is valid for common surface vessels whereas ALERD is operational at larger depth and higher pressure so this value is expected to be a bit higher but further research needs to be performed to define it.

With these values, it is observed that the underwater vehicle cannot follow the desired reference operational profile signal and cannot compensate for the exerted forces and moments on it. Furthermore, it has to be mentioned that the RPM of the vertical tunnel thrusters was maximum. Upon analysis, it was determined that the power output from the vertical tunnel thrusters was insufficient to effectively compensate for the environmental disturbances. As a result, a decision was made to opt for larger thruster diameters. Taking into account the combined scenario which is when the underwater vehicle operates under the presence of heading current, and waves and including the seabed interaction to the model, the required power by the vertical tunnel thrusters is estimated.

This iterative process led to the determination of an optimal thruster diameter, which was found to be $D = 1.3m$. Furthermore, to prevent cavitation, the maximum recommended RPM for this diameter was set at $n = 441rpm$.

The characteristics of the propeller of the vertical tunnel thruster are an assumption and they are given in Table 5.2:

Wageningen B3-65 nozzle 19A	
D_{VTT}	$1.3m$
KT	0.604
n_{max}	$441rpm$

Table 5.2: Vertical Tunnel Thruster's propeller characteristics

5.2.2. Physical Limitations

Similar physical limitations to the forward thrusters are applied to the vertical tunnel thrusters related to the rpm. The tuned PID controller gives the desired signal which is used as an input to the main function in order to calculate the desired thrust but without applying the limitations the final output of the PID is not realistic. A physical limitation for the propeller of the vertical tunnel thrusters is the maximum and minimum values for the rpm. In this case, and in order to avoid the cavitation the maximum value is set to $441rpm$ and the minimum to $-441rpm$.

Furthermore, a delay, modeled as a low-pass filter is included in order to make the simulation more realistic. Although the controllers give an instant input signal to change the rpm in order to minimize the error, these changes are abrupt and not realistic. In reality, there is a delay of a few seconds between the moment that the signal is produced and the response of the system. In the current study, determining the correct time delay was not the goal so further research needs to be done to simulate a more precise behaviour.

5.3. Trim Tanks

Main ballast tanks (MBTs), depth control tanks (DCT), and trim tanks (TTs) are critical components of a submarine's buoyancy control system. They collaborate to assist the submarine in submerging, surfacing, and maintaining its depth while navigating underwater. Especially, trim tanks are smaller

tanks located within the submarines that are used to adjust their pitch and roll. The trim tank system is usually a closed system and thus the weight and buoyancy do not change using these tanks. This closed system includes a pump that pumps the water from one tank to the other. Changing the water mass, a pitch moment is created in order to compensate for the developed angle in pitch direction from internal or external disturbances. For this particular study, these are only environmental disturbances.

5.3.1. Modelling of Trim Tanks in Matlab, Simulink

In the specific case study of ALERD, it's assumed that two tanks are positioned 30 meters both fore and aft concerning the center of origin (CO) along the longitudinal direction, denoted as $x_{TT,fore}$ and $x_{TT,aft}$, Figure 5.1. Due to the symmetrical placement of these tanks, no additional trimming moments are generated in either the pitch or roll directions.

The trim tanks play a crucial role in creating the necessary restoring moments to maintain zero pitch at all times. To control the pitch angle, the motion controllers utilize the variable $\delta_{tm,fore}$, which represents the mass that must be added to or removed from the forward trim tank. This adjustment is translated into a trimming moment, subsequently incorporated as input into the forces and moments vector τ.

Since the trim tank system is closed, this means that the amount of water mass that is removed from one tank is added to the other one. Consequently, the total amount of water in the trim tank system remains constant and it is denoted as $m_{TT,tot}$. The generated moments are modeled as:

$$M_{TT,fore} = -g \cdot x_{TT,fore} \cdot (\frac{m_{TT,tot}}{2} + \delta_{tm,fore}) \tag{5.4}$$

$$M_{TT,aft} = -g \cdot x_{TT,aft} \cdot (\frac{m_{TT,tot}}{2} - \delta_{tm,fore}) \tag{5.5}$$

Moreover, it needs to be mentioned that when the submarine is at a pitch angle the tanks are relocated in this angle as well. As a result, their distance is modeled and expressed as:

$$x_{TT,fore} = 30 \cdot \cos(\theta) \tag{5.6}$$

$$x_{TT,aft} = -30 \cdot \cos(-\theta) \tag{5.7}$$

The total mass of the trim tanks was initially chosen arbitrarily based on data from [9], and it was set at $m_{TT,tot} = 10.000kg$. However, as the impact of all environmental disturbances was considered, it became evident that the trim tanks have a limited capacity. Consequently, the total water mass required for proper control was determined to be $m_{TT,tot} = 13.000kg$.

It is important to note that while this value was adjusted as the total mass in the simulation, it didn't alter the total mass of ALERD itself. This limitation is acknowledged within this work, and it underscores the need for further research to accurately define both the required water mass and the dimensions of the trim tanks to ensure optimal control and performance.

5.3.2. Physical Limitations

In the context of the pitch controller, physical constraints are established based on the physical limitations of pipe-flow systems and pumps, which are the actual systems being utilized. Pumps and pipe-flow systems come with several inherent limitations, including constraints on the maximum volume flow rate that a pump can handle and restrictions on the maximum allowable flow velocity in pipelines.

For the purposes of this study, it is assumed that the velocity of water in the pipelines serves as the limiting factor. This assumption is made based on the fact that centrifugal pumps are capable of delivering high-volume flows. These constraints are essential for creating a simulation model that accurately reflects the real-world behavior of the underwater vehicle and its associated systems. C-Job provided the maximum and reference velocities in the pipes for pumps. The maximum velocity though is determined to be 2m/s. Setting the maximum velocity in pipes to 2m/s, the maximum mass flow, that is the output from the pitch controller, is defined in Table 5.3.

Performing the simulations for the combined scenario which included all the environmental disturbances, it is defined that a pipe of $D = 0.2m$ diameter is required. In the model, a rate limiter is included which limits the maximum and minimum mass flow that comes from the PID. The maximum and minimum values for it were set to $64kg/s$ and $-64kg/s$ respectively. The minus sign means that mass is transferred from the fore tank to the aft.

Diameter [m]	Volume Flow [m^3/s]	Mass Flow [kg/s]
0.1	0.0157	16
0.2	0.0628	64
0.3	0.1414	145
0.4	0.2513	258

Table 5.3: Pipes' physical constraints

To enhance the realism of the simulations, a low-pass filter is incorporated to introduce a delay. This delay is introduced in a manner similar to the vertical tunnel thrusters. Unlike a direct translation of the signal from the PID controller into the main function, a time delay is introduced to better emulate real-world dynamics.

5.3.3. Determination of the diameter of the pipe in the Trim Tank System

In the context of performing a sanity check for the trim tanks and since there are no available data for the ALERD, [39] was used to verify the results.

Taking into account the same environmental conditions, which were no current, no waves, and no seabed interaction, it was observed that the same mass profile was needed in order to compensate for the generated trim. Furthermore, as mentioned previously, the diameter of the pipes was first set to D=0.4m in order to compare the results. Nevertheless, the total consumed energy in kWh was different. In Figure 5.2 and Figure 5.3 the total consumed energy is presented for Bakker's [39] project and the current project respectively.

Since the deviation of the total consumed energy is very high, to elaborate this, Bakker's is almost 0.4kWh while for the current study is 0.001kWh, this needs to be examined in detail.

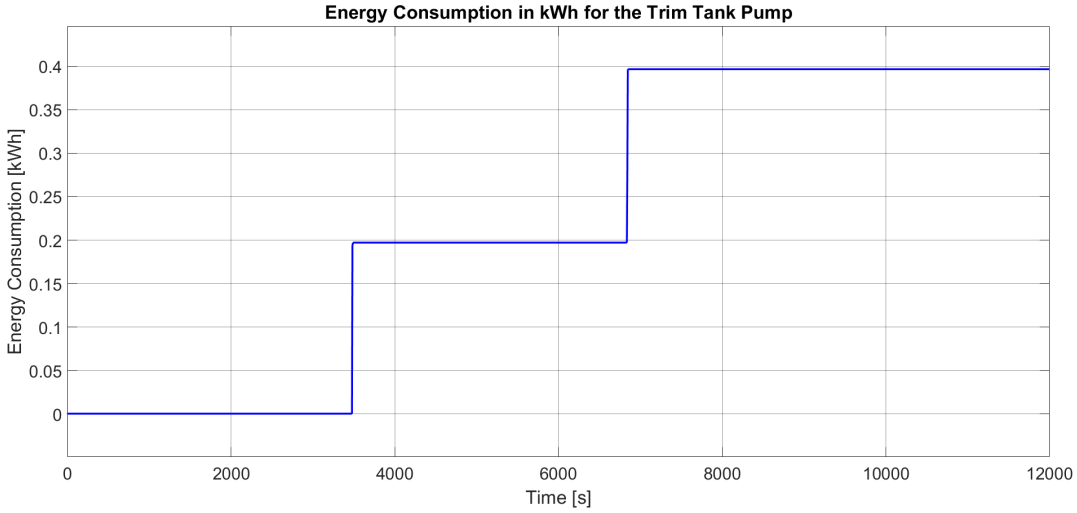

Figure 5.2: Energy Consumption for the Trim Tank Pump Bakker's - $D = 0.4m$

First of all, the depth and trim behavior of Bakker's is not finely tuned. As a result, the PID controllers are more aggressive in handling the depth changes and trim changes. Since the profile of the mass distribution is the same in both projects this deviation is completely due to the aggressive behavior of the PID.

In order to prove this, the volume flow is presented for both projects in Figure 5.4, Bakker's and 5.5, the current project. It is noticed that the maximum volume flow is $0.4m^3/s$ and lasts for 3 seconds. This ends up with a high velocity in the pipes, Figure 5.4 which is more than 3m/s and in a very high pump power, Figure 5.6. This velocity in the pipes exceeds the limit of 2-2.5m/s that is provided by C-Job.

On the other hand, performing the simulation for the current project, given the pipe diameter of $D = 0.4m$ the velocity in the pipes is very low, up to $0.16m/s$, presented in Figure A.10. The corresponding power for the pump is 0.03kW. Slow flow rates result in a reduced volume of water passing through the pipe per unit of time. This can be problematic in applications like ALERD, where a certain amount

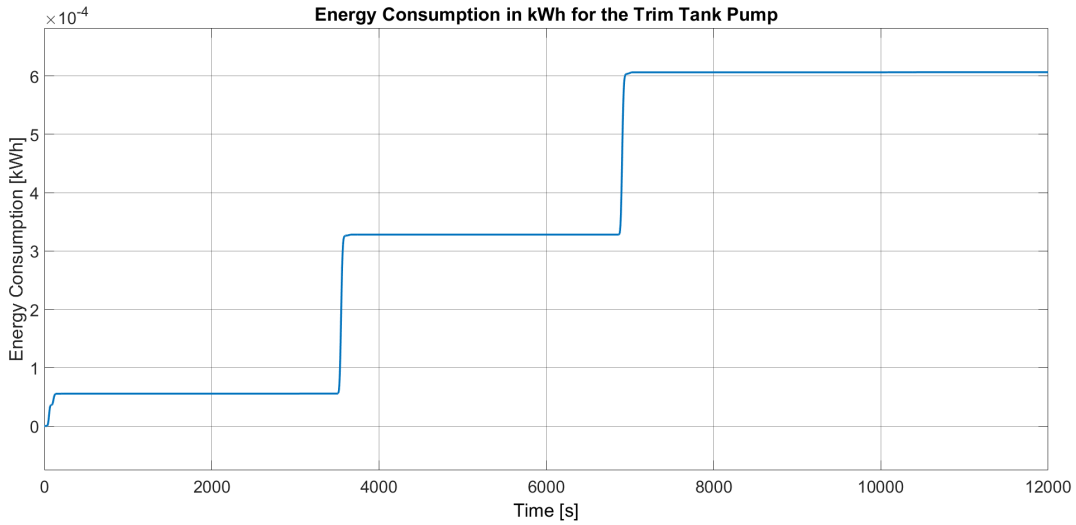

Figure 5.3: Energy Consumption for the Trim Tank Pump - $D = 0.4m$

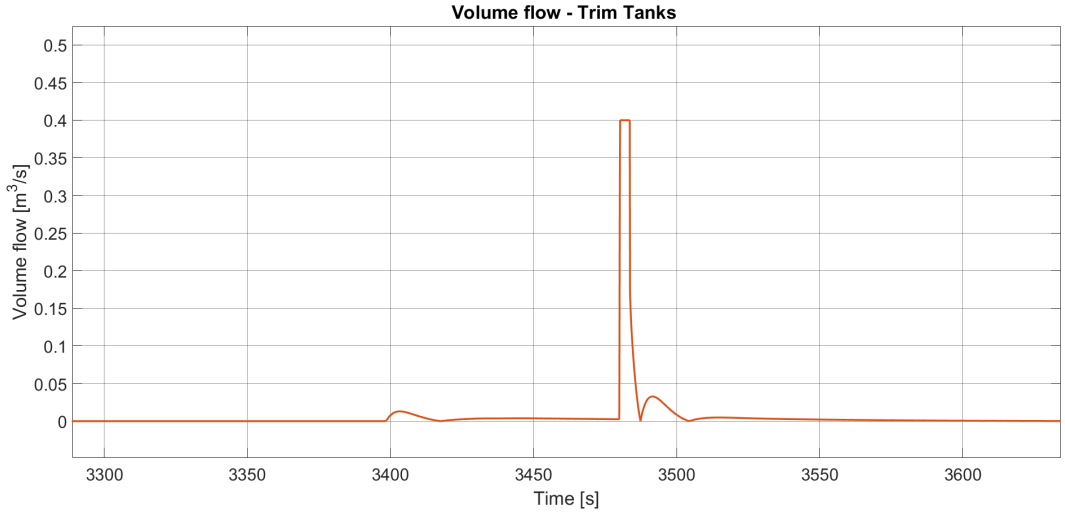

Figure 5.4: Peak volume flow - Trim Tanks Bakker's

of water is needed within a specific time frame to compensate quickly for the trim. In cases where pumps are used to move water through the pipe, operating at a slow flow rate can increase energy costs. Pumps may need to work harder to maintain the desired flow rate, leading to higher electricity consumption. Nonetheless, as can be seen, the flow lasts more seconds and the same amount of mass is provided. Since this value is not acceptable according to C-Job, the diameter should change.

Following an iterative procedure where the diameter was altered, the physical constraints of the maximum allowable speed in the pipes and the maximum volume flow were examined. Considering a diameter of $0.1m$ and the combined scenario, ended up with a velocity in the pipes that exceeded the value of $3.5m/s$. As a result, the diameter of the pipe was changed again and set to $0.2m$. The maximum velocity for the same environmental conditions is $0.6m/s$ which is acceptable and can be seen in Figure 5.7

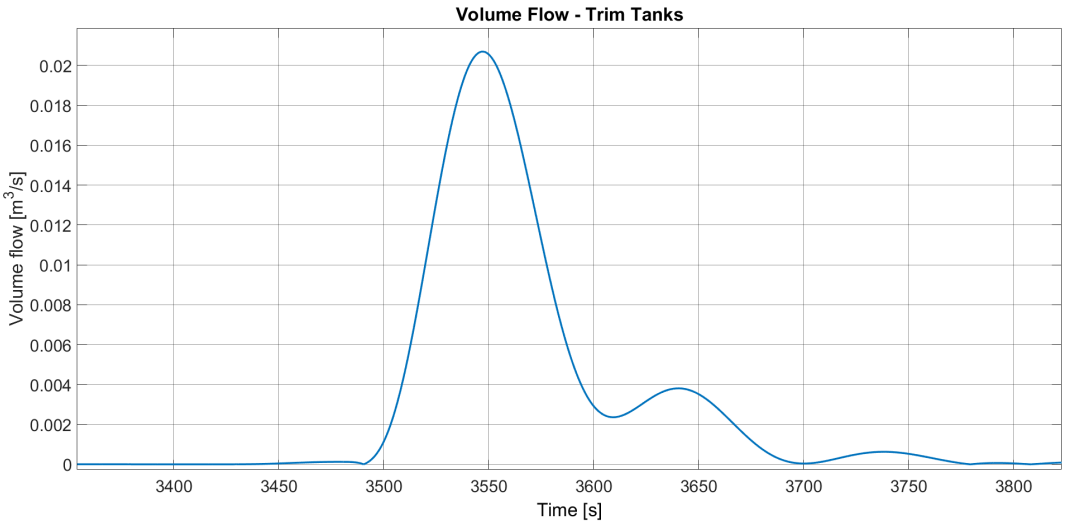

Figure 5.5: Peak volume flow - Trim Tanks

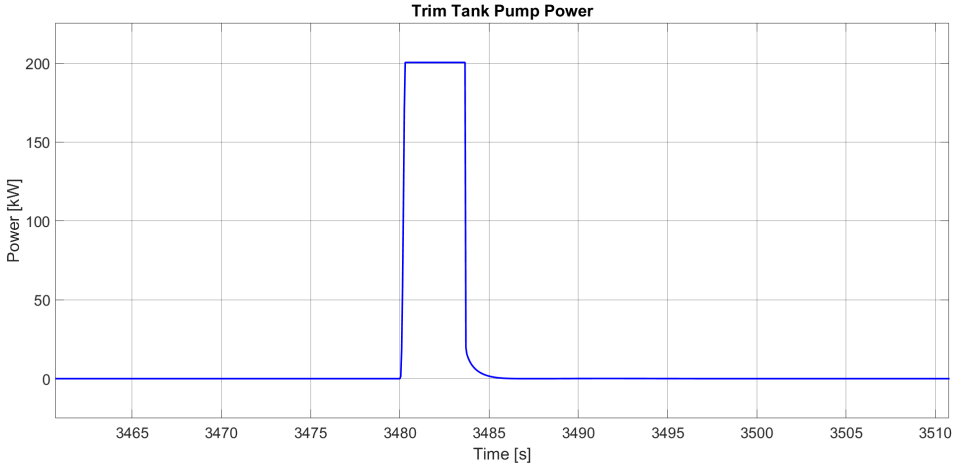

Figure 5.6: Maximum pump power - Trim Tanks Bakker's

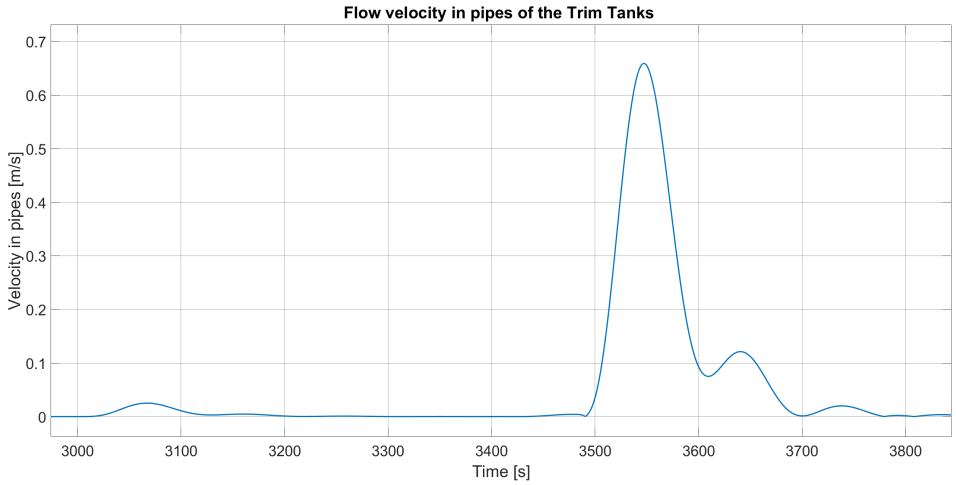

Figure 5.7: Peak velocity in pipes - Trim Tanks $D = 0.2m$

5.4. Discussion

Taking into account the importance of actuators, such as forward thrusters, vertical thrusters, and trim tanks, in controlling the motions and therefore stabilizing the vessel, modeling, and simulations are important to demonstrate the behavior of the submarines that are equipped with the former. A numerical simulation has been executed to investigate the ability of a submarine that is armed with forward thrusters, vertical thrusters, and trim tanks, to maintain control in the vertical plane at transit speeds and at low speeds.

The components of the propulsion and maneuvering used on an underwater vehicle were reviewed and the key factors influencing their performance were identified. As mentioned previously, there are a lot of physical constraints for each actuator that need to be defined in the Simulink model in order to achieve a realistic simulation. Tuning the PID controllers in surge, heave, and pitch ensures a stabilized behavior of the underwater vehicle given a desirable reference profile for tracking not only forward speed but also depth and pitch. In order to simulate a more realistic scenario, low-pass filters are integrated into the model, reproducing the time delays that there are in real life. Nevertheless, since this is not the main goal of this thesis project, these delays can be optimized and chosen properly in order to achieve a more precise result. Furthermore, extended separate design studies have to be executed for the selection of both the forward and the vertical tunnel thrusters. Similarly, a prolonged study on the simulated delays should be performed.

For the simplification of the project, it has been assumed that the two vertical tunnel thrusters in the case study of ALERD, operate with the same revolutions per minute (rpm). Thus, further research needs to be carried out to include different rpm for the thrusters. In this way, a pitch moment will be induced in the model, and different control strategies need to be applied. Additionally, a combined experimental and CFD analysis to characterize in great detail the inflow and outflow from a propeller-based thruster and to develop an analytical model of these flows and how they interact would be something that needs to be examined. Considering the trim tanks, an extended investigation of their capacity and subsequently their dimensions and placement needs to be done in order to obtain a model that can handle the combined scenario environmental conditions.

6

Model Overview and Energy Analysis

In the following Chapter, the reference signals that are used in the Matlab, Simulink model are mentioned explicitly. Moreover, a general overview and explanation of how the model works is presented, as well as the manual tuning of the PID controllers. The energy analysis is introduced, as well as the assumptions that have been made for the calculations of the required energy.

6.1. Reference signals and Simulink Overview

6.1.1. Overview reference signals

In order to create a realistic operational profile for the ALERD, it is essential to introduce a speed profile into the model, as illustrated in Figure 6.1. This addition will account for variations in the vehicle's speed during its mission.

In this particular case study of the ALERD, two distinct speed regimes are considered. The transit speed, set at 8.5 knots, represents the velocity at which the ALERD moves efficiently between locations or when it needs to cover large distances quickly. On the other hand, the dredging speed is set at 1.7 knots, indicating a slower operational speed that the ALERD may employ during dredging. By incorporating this speed profile into the model, it becomes more representative of the ALERD's real-world behavior, accounting for the varying speeds it may operate at during different phases of its missions. This speed profile and the duration of each of the operations phases have been determined in previous studies [24].

It is worth noting that the speed operational profile is based on three different operational modes, transit, dredging, and discharging. According to [24], an optimal transit speed for the ALERD is calculated to be 8.5knots and a dredging speed of 1.7knots. During the discharging operation, 10300 seconds onwards, the speed is 0.2knots and it minimizes to 0knots at the end of the dredging cycle. This value is determined based on the time duration and the rate of change in cargo weight inside the hopper, which needs to be compensated by the main ballast tanks.

The depth profile is visually represented in Figure 6.2. In this representation, positive values indicate that the positive axis of the z-coordinate is directed from the water surface towards the seabed. This convention helps provide a clear understanding of the ALERD's vertical positioning with respect to the ocean floor, ensuring that positive values signify a descent or movement closer to the seabed. The authors in [24] indicate that the depth for each operational mode is used to generate a reference depth signal. The ALERD is assumed to be at the surface, it dives to 8m and it is in transit mode up to 3400s. Then it descends up to 15m in order to initiate the dredging mode for 3360s, ascends to 8m (transit mode) again, and at 4m depth, it starts the discharging procedure. This happens at almost 10300s when the speed is 0.2knots and it is zero when the ALERD has completed the dredging cycle and is assumed to be at the surface again.

The pitch input signal is intentionally set to a constant value of 0 $^{\circ}$, as presented in Figure 6.3. This choice reflects the desired behavior for the submarine, which is to maintain a pitch angle of 0 $^{\circ}$ and hold its position steadily. This configuration is likely chosen to ensure that the submarine remains level and avoids any pitch deviations during its operations, especially when dredging. Due to the length

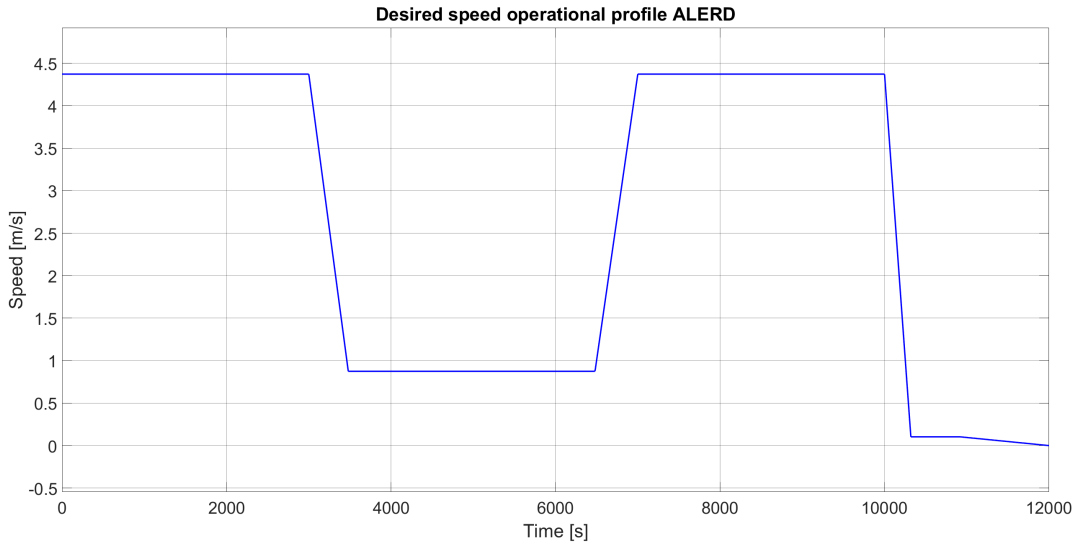

Figure 6.1: ALERD's Desired speed operational profile

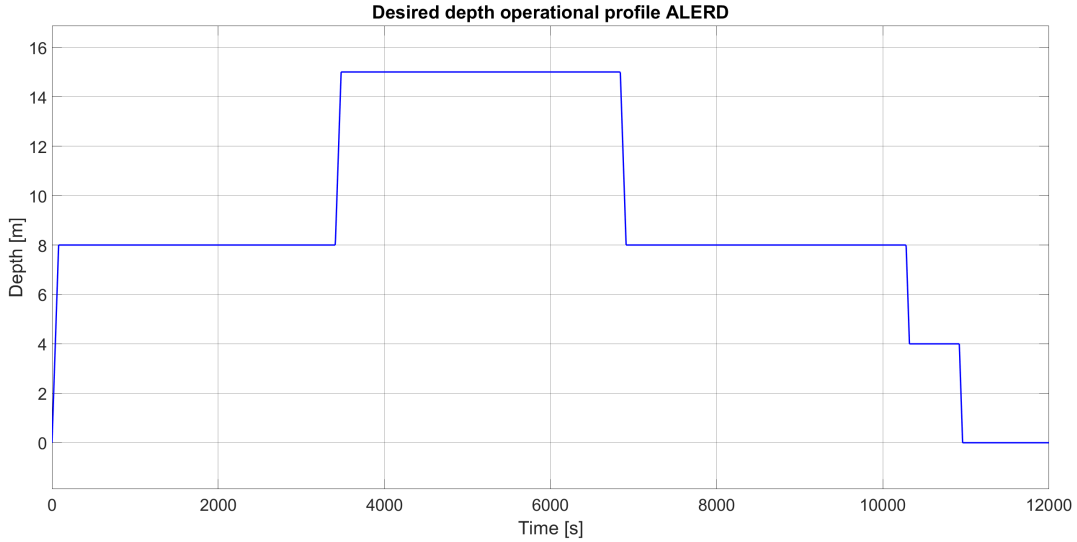

Figure 6.2: ALERD's Desired depth operational profile

of ALERD, minimum pitch angles already cause a significant additional draught which might cause grounding in shallow waters.

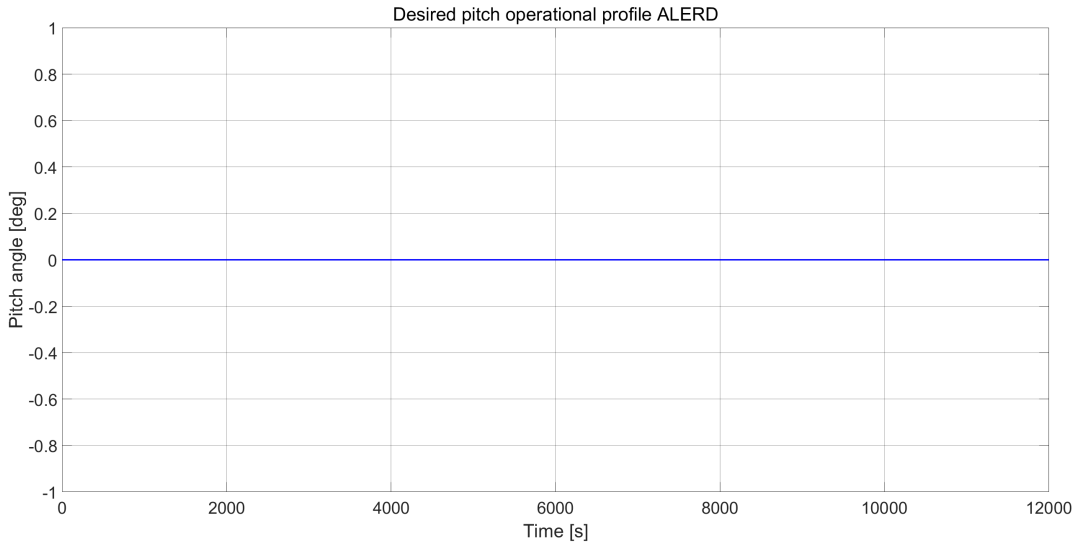

Figure 6.3: ALERD's Desired pitch operational profile

6.1.2. General Overview

For a comprehensive understanding of the model's structure and the interactions among its components, Figure 6.4 provides a general overview. The previously mentioned reference signals, such as the speed, depth, and pitch profiles, serve as inputs to the controllers, specifying the desired positions and operational parameters for the ALERD.

The output of each controller is specific to the actuator it manages. For instance, the speed controller determines the required RPM for the forward thrusters, while the heave controller calculates the RPM for the vertical tunnel thrusters. In the case of pitch control, the controller computes the mass that needs to be transferred between trim tanks to maintain the desired pitch angle.

These controlled values, generated by the controllers, play a crucial role not only in assessing energy requirements but also in calculating the forces needed to counteract environmental disturbances. Furthermore, the model incorporates the actual position of the submarine into a feedback loop. This real-time feedback information is utilized before the controller stage to compute the error between the desired and actual positioning. This error signal serves as a critical input to the controllers, enabling them to make precise adjustments to achieve the desired positioning and maintain stable operation. In this way, the model integrates inputs, controllers, feedback, and actuator outputs to create a dynamic and responsive system that effectively manages the ALERD's positioning and energy consumption in various operational scenarios.

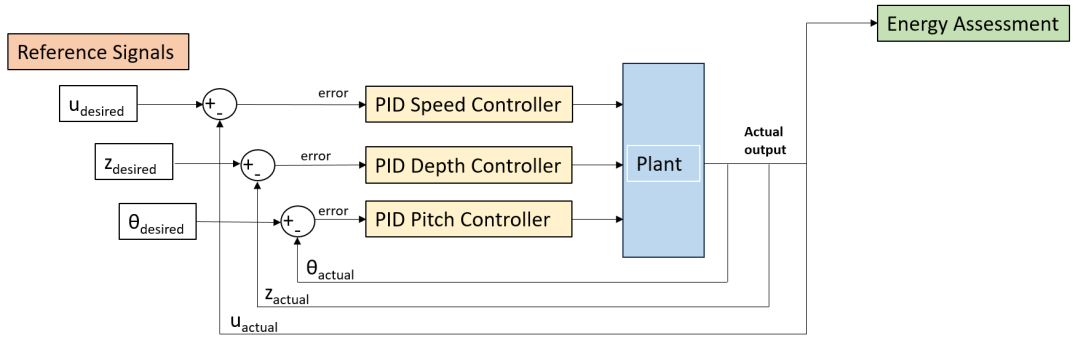

Figure 6.4: General Overview Simulink Model

6.1.3. Proportional-Integral-Derivative (PID) Control

According to the literature review that preceded, PID control is a widely used control algorithm characterized by its robust performance and simple functionality. It consists of three components: proportional, integral, and derivative gains, which can be adjusted to optimize control performance. The proportional gain determines the output response based on the error signal, the integral gain reduces the steady-state error, and the derivative gain improves the transient response [47]. Tuning the three gains allows control over rise time, overshoot, settling time, steady-state error, and stability.

Manual Tuning

The primary objective in fine-tuning PID controllers is to minimize overshoot, reduce settling time, and minimize oscillations. In the initial attempt, the automatic tuning function was applied, revealing that the preconfigured gains failed to yield the desired performance for the underwater vehicle. Consequently, a manual tuning was chosen, which ultimately enabled the underwater vehicle to effectively track reference signals.

In this subsection, the procedure of tuning that was followed is described. To commence, a simulation was initiated with a basic input reference signal, such as a step function, and all gains, except for the proportional gain K_p, were set to zero. Subsequently, the response of the underwater vehicle was observed. The proportional gain K_P was incrementally increased until the control loop exhibited continuous oscillations at a consistent amplitude. Following this, the integral gain K_I was introduced gradually, with the aim of correcting any deviation from the desired setpoint within an acceptable timeframe, while avoiding excessive values that could lead to instability.

Finally, the derivative gain (K_D) was introduced incrementally, with the objective of achieving a sufficiently rapid response in returning to the reference signal after encountering a load disturbance.

It is worth noting that increasing K_D causes excessive response and overshoot and also the rpm which is the output of the controllers oscillating continuously between the maximum and minimum limits that were set. Since this is not an acceptable response and there was a trade-off with a higher K_D gain, there was better tracking of the reference signal and there was a quick response from the system but it caused high oscillations, which was not a realistic scenario. In Figure 6.5 the effect on the rpm output for the vertical tunnel thrusters is depicted, increasing K_D.

As a result, the proper gains were chosen based on the desired behavior of the ALERD and the minimum energy requirement.

PID Performance Assessment

In order to evaluate the PID performance there are indices that calculate the error. The most commonly used are the Integral Squared Error, the Integral Absolute Error, and the Integral Time-weighted Absolute Error. Integral Squared Error (ISE) involves the accumulation of error squares over time. It gives greater weight to significant errors due to the squaring operation, which causes larger errors to contribute substantially more. Systems aiming to minimize ISE will prioritize the rapid elimination of substantial errors, even if minor errors persist for an extended duration. This approach often results in swift responses, accompanied by notable yet minor oscillations.

Integral Absolute Error (IAE) encompasses the integration of absolute errors across time. It treats all errors uniformly without assigning varying weights to them. Control systems designed to minimize IAE will generally exhibit a more gradual response compared to those optimized for ISE, while also yielding reduced and less persistent oscillations. The Integral Time-weighted Absolute Error (ITAE) performance index has the advantage of producing smaller overshoots and oscillations than the IAE or the ISE performance indices. In addition, it is the most sensitive of the three. In the current project, in order to evaluate the performance of the PID controllers for speed, depth, and pitch, the IAE will be assessed.

Following an iterative procedure and changing the gains for the PID controllers, the response of the underwater vehicle was tested. The KPIs in order to select the most suitable gains are the overshoot and the IAE. As mentioned previously, the IAE integrates the absolute errors across time uniformly, as a result, the less the IAE, the smaller the error. The settling time is another KPI that cannot be precisely mentioned due to the oscillating behavior of the ALERD but it was observed from the generated figures. An example of the procedure that was followed is presented in Table 6.1. Furthermore, another KPI is the rpm which is the output of the PID. The more the K_D increases, the more oscillations from the maximum to the minimum rpm are observed. So this is a trade-off for the gains of the PID controllers,

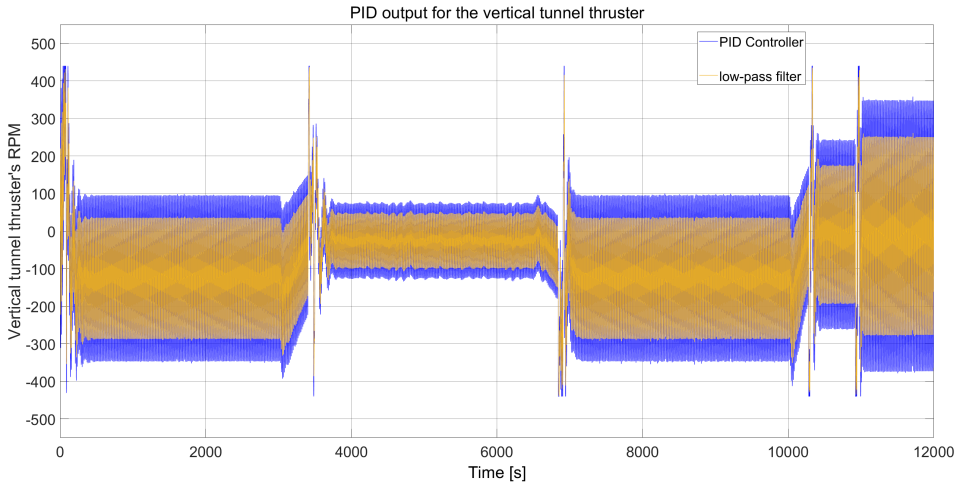

(a) Vertical Tunnel Thruster's rpm - $K_D = 5000$

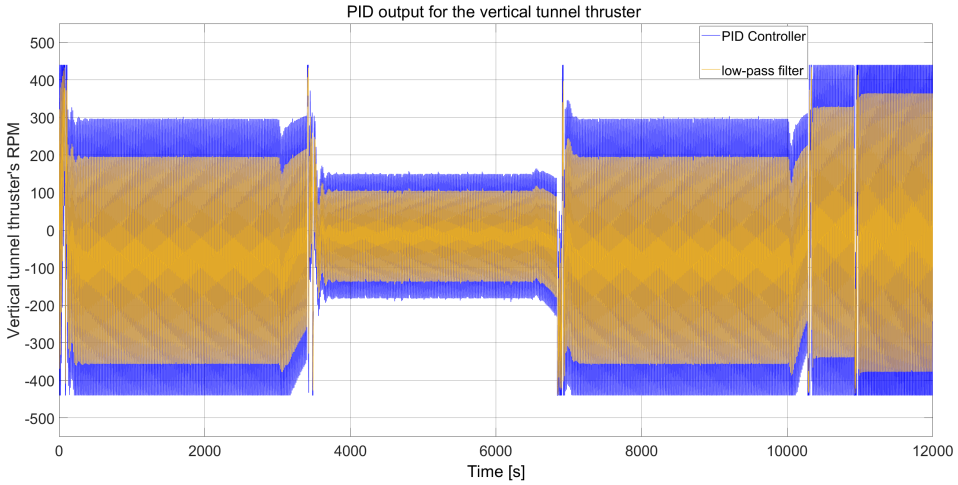

(b) Vertical Tunnel Thruster's rpm - $K_D = 8000$

Figure 6.5: Influence of K_D gain to the PRM response on the vertical tunnel thrusters

since the overshoot decreases but the rpm response is not favorable. The gains that are selected as the most suitable ones, lead to an acceptable overshoot, a preferable settling time, and an rpm behavior that more or less converges to a specific value and does not oscillate between the extreme values.

Another aspect that needs to be taken into consideration is the required energy and the relation with the PID gains. Performing the simulations and changing the PID gains to tune the controllers and to obtain the desired behavior, it was noticed that the resultant energy alters. Subsequently, the overshoot of the submarine and the energy that it requires to compensate for the environmental disturbances and the seabed interaction is a trade-off. More detailed information and an example of how the PID gains affect the required energy is given in Chapter 7.

K_P	K_I	K_D	$Overshoot$	$IAE\ (\cdot 10^3)$
400	7	20000	0.80	1.44
400	7	10000	0.60	1.19
400	**7**	**8000**	**0.50**	**1.13**
400	7	5000	0.60	1.09
400	7	4000	0.80	1.12

Table 6.1: PID gains for depth controller and KPIs

The same procedure was followed per controller for pitch and speed as well. Consequently, the most appropriate gains were chosen, depicted in Table 6.2.

	P	I	D
Speed Controller	500000	10	2000000
Depth Controller	400	7	8000
Pitch Controller	10	1000	2000

Table 6.2: PID gains used in the developed model

6.1.4. Controller Constraints

While tuning the PID controllers in order to obtain the best response from the underwater vehicle, some design objectives needed to be established. For instance, dredging condition is critical since in case the ALERD has a large overshoot, the clearance is reduced and the ALERD may be grounded. Also, the settling time has to be in between logical time spans since if not, it will take too long to descend and the operations will not be carried out sufficiently. Having no available data for the ALERD in order to define and validate the results, the acceptable settling time is defined to be 300 seconds (5 minutes). Taking into consideration that the clearance is 2m since the grounding is not foreseen, the overshoot is considered acceptable. These hard constraints are based on safety and operational considerations but they are chosen arbitrarily. Simultaneously, the tuning of the controllers aims to safe operations for the entire operational profile and close reference tracking on the desired signals.

6.1.5. Discussion

Due to their simplicity and suitable performance in many applications, PID controllers are widely used. The problem emerges when new conditions are imported, such as ocean currents, or wave disturbances. In this case, the set of gains needs to be re-tuned with respect to the new conditions. The previous statement is verified at [48]. In [32] the difficulty in controlling the motion when sailing near the surface is highlighted. So, as it can be verified from the literature review that was performed, the PID controllers usually have limited capabilities when the waves and the near seabed and surface operation are induced.

More specifically, executing the simulations without any environmental disturbances involved, the ALERD which was a case study, was perfectly following the desired tracking with minimum overshoot and short settling time. When inducing the current, the gains for the PID needed to be altered, in order to have a more favorable behavior regarding less overshoot and settling time. Similar behavior is observed when the seabed interaction is induced. Using the same gains for the PID controllers, the follow tracking is achieved but a higher overshoot is noticed and a higher pitch angle deviation. Consequently, the PID gains need to be altered again. In the final stage, when the waves are included in the model, the PID cannot handle the wave disturbances. To specify this, the ALERD follows the reference signals regarding the depth and pitch but with high oscillating behavior. This means that it oscillates with the same frequency as the first-order modeled waves and an absolute deviation of 0.1m is noticed (oscillating amplitude). Apart from that, the maximum overshoot is 0.5m. Similar to the positioning, although the desirable pitch angle is 0°, the ALERD oscillates around 0° but with an absolute deviation of 0.5°. Also, the output of the depth controller, PID, which is the rpm for the vertical tunnel thrusters, has an oscillating behavior around for instance, -100 rpm.

This is not realistic, since such behavior would cause damage to the motor of the thrusters, and subsequently, the PID controller fails to handle the wave disturbances. Since changing a control strategy was out of the scope of this project, the solution that is recommended in order to estimate the energy that the vertical tunnel thrusters consume, a low-pass filter is applied. This allows the low frequency to pass cutting off the higher ones and in this way, the output rpm converges in one specific value. For the improvement of the behavior of the underwater vehicle but also for a more precise calculation of the energy consumption another control strategy is recommended. According to [49], the Fuzzy controller assists in selecting appropriate gains for the PID controller for different paths and different environmental conditions as needed. Furthermore, [18] proposes the design of a PID controller with a wave filter that predicts the disturbance and allows a smoother behavior of the underwater vehicle. In [50], a state observer (SO) based control solution has been proposed to estimate and compensate for unknown environmental forces in real-time. The effectiveness of this approach has been demonstrated through a simulation study, comparing the performance of the proposed SO-based controller with a traditional PID controller on an offshore supply vessel indicating [50].

6.2. Energy Analysis

The operation of the submarine involves the constant adjustment of its position and orientation to counteract environmental disturbances and external forces. These modifications are made possible by the operation of numerous actuators, which need energy. To model and assess energy consumption in this context, the speed profile, operational profile (depth), and pitch profile must be defined within the established Matlab and Simulink model. This model employs three PID controllers, each dedicated to a specific degree of freedom: surge, heave, and pitch.

Specifically, this chapter focuses on the case study of the ALERD which is equipped with two forward thrusters responsible for controlling surge speed, two vertical tunnel thrusters to manage heave motions, and a closed system of trim tanks for pitch control. During its operation, these actuators actively work to compensate for environmental disturbances, and as a result, they consume energy.

The primary objective of this chapter is to calculate and quantify the energy consumed by these actuators, thereby establishing the total energy consumption for the ALERD's operational scenarios. This energy analysis is crucial for understanding the vehicle's power requirements and optimizing its energy efficiency during missions.

6.2.1. Speed Control

The forward speed of the ALERD is controlled by the forward thrusters with the aid of the PID controller in the surge direction. In order to estimate the required power from them the equation below is used:

$$P = T \cdot v_A \tag{6.1}$$

where T is the thrust in N provided by the propeller and v_A the propeller speed given by:

$$v_A = (1 - w) \cdot v \tag{6.2}$$

It needs to be mentioned that for ships with one propeller, the wake fraction coefficient w is normally in the range of 0.20 to 0.45, but due to the lack of data, in the specific case study of ALERD, it is an assumption and is taken equal to 0.45. This assumption is based on the fact that the bigger the block coefficient for a ship, the bigger the wake fraction. Although this applies to ships, a similar relation should be for the submarines. In the specific case study of the ALERD, the block coefficient is expected to be large and that is why the highest value for the wake fraction is used. Nevertheless, future research has to be executed to properly define the former. Also, v is the velocity of the vehicle.

The total thrust for both the forward thrusters is calculated using the equation:

$$T_{FT} = 2 \cdot \rho \cdot D^4 \cdot KT \cdot n^2 \tag{6.3}$$

To elaborate more, the output of the PID in the surge direction is the rpm for the forward thrusters. Using this rpm n, the required thrust from equation 6.3 is estimated, and then, with the aid of equation 6.1 the power is calculated. It is worth noting that the provided power is the thrust power but the brake power should be a bit higher since the involved efficiencies were not taken into account since it is out of the scope of this project.

6.2.2. Depth control

As mentioned previously, the vertical movement of ALERD is controlled by two vertical thrusters that operate with the same number of rpm to simplify the model. In order to calculate the required power from the generated forces from the vertical tunnel thrusters the equation 6.5 can be used to estimate them.

$$P = 2 \cdot \pi \cdot n \cdot v \cdot Q = \frac{T \cdot U}{\eta} \tag{6.4}$$

where n is the rotational speed in s^-1. Q is the torque in Nm, T is the thrust force in N, U is the velocity in m/s and η is the efficiency. Hence, an approximation of the power denoted as P becomes feasible upon determination of the requisite thrust denoted as T, with the presumption of an appropriate efficiency η.

Challenges emerge when the vehicle necessitates sustaining its position and upholding a state of rest. In this scenario, the velocity U reaches zero, consequently driving the efficiency of the thruster to

zero, using standard definitions, despite a thrust force is still produced. To overcome this problem, a momentum theory-based relationship can be used to estimate the required power.

$$P = T \cdot \sqrt{\frac{1}{2}} \cdot \sqrt{\frac{T}{\rho \cdot A}} \tag{6.5}$$

According to [51] this formulation gives an ideal value and in reality the constant $\sqrt{\frac{1}{2}}$ will be much larger. By the equation 6.5, the estimate of the power requirement once the thrust is known, is feasible.

Momentum theory

In order to apply the momentum theory a simplified representation of the propeller of the vertical tunnel thrusters was considered. Furthermore, a propeller is considered a disk that impacts a uniform acceleration to the fluid passing through it. A representation is depicted in Figure 6.6 where the generated thrust is given by 6.6.

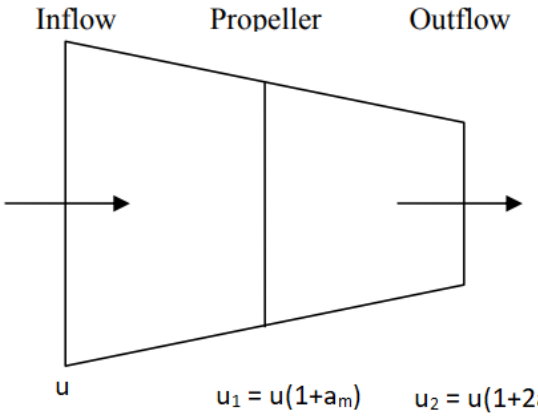

Figure 6.6: Momentum theory representation of a propeller of a vertical tunnel thruster

$$T = \dot{m} \cdot (\Delta u) = \rho \cdot A \cdot u_1 \cdot (u_2 - u) = \rho \cdot A \cdot u^2 \cdot (1 + a_m) \cdot 2a_m \tag{6.6}$$

The velocity increases compared to the speed of advance, so a slip ratio s is defined.

$$s = \frac{2 \cdot a_m \cdot u}{u} = 2a_m \tag{6.7}$$

Considering the ideal efficiency of the propeller in terms of the slip ratio gives:

$$\eta_{IDEAL} = \frac{\text{Useful Work}}{\text{Work Done}} = \frac{T \cdot u}{T \cdot u_1} = \frac{1}{1 + a_m} = \frac{2}{2 + s} \tag{6.8}$$

Integrating the slip ratio into the generated thrust yields:

$$T = \rho \cdot A \cdot u^2 \cdot (1 + \frac{s}{2}) \cdot s \tag{6.9}$$

The thrust coefficient C_T in terms of the slip ratio is defined in the equation below.

$$C_T = \frac{T}{1/2 \cdot \rho \cdot A \cdot u^2} = s \cdot (2 + s) \tag{6.10}$$

And now rearranging the equation 6.10, the slip ratio in terms of the thrust coefficient is:

$$s = \sqrt{C_T + 1} - 1 \tag{6.11}$$

Assuming low speed $C_T \gg 1$ the ideal efficiency is:

$$\eta_{IDEAL} = \frac{2}{C_T^{1/2}} \tag{6.12}$$

Consequently, the power required by the propeller is given by:

$$P = \frac{T \cdot u}{\eta_{IDEAL}} = \frac{T \cdot u \cdot {C_T}^{1/2}}{2} = \frac{T \cdot u}{2} \cdot \sqrt{\frac{T}{0.5 \cdot \rho \cdot A \cdot u^2}} = T \cdot \sqrt{\frac{1}{2}} \cdot \sqrt{\frac{T}{\rho \cdot A}} \tag{6.13}$$

Rearranging this gives the ideal power per unit thrust required to develop a given thrust from a propeller of a given area:

$$\frac{P}{T} = \sqrt{\frac{1}{2}} \cdot \sqrt{\frac{T}{\rho \cdot A}} \tag{6.14}$$

It has to be noted that sometimes the term $\sqrt{\frac{1}{2}}$ is neglected by some authors in terms of convenience. The required energy by the thrusters is calculated numerically by integrating the power drawn over the time period. To take into account the performance of the thruster the equation 6.5 is modified to:

$$P = \frac{T^{3/2}}{2 \cdot \tau^{3/2} \cdot \sqrt{\rho \cdot A}} \tag{6.15}$$

where τ is a measure of the performance of the thruster, compared to an ideal one. In the current study, this is taken to be 0.55 considering the available commercial thruster performance and surface vessel bow thruster data [52].

6.2.3. Pitch Control

Regarding the pitch control, the trim tanks are used to correct and control the pitch angle created by the environmental disturbances. The output of the PID controller is the mass m that is required to be transferred from one tank to another in order to fix the angle and stabilize the underwater vehicle.

For the energy calculation, the mass is differentiated to obtain the mass flow $\dot{m}$ in kg/s. This mass flow is used as an input in the function named pump.m. In this function, the volume flow $\dot{V}$ is considered and used as an input to determine the velocity of the flow in the pipes. This is executed by the equation:

$$v_{pipes} = \frac{\dot{V}}{D_{pipe}^2 \cdot \pi/4} \tag{6.16}$$

The required power from the tanks is defined by the equation:

$$P_{TT} = \frac{\dot{V} \cdot \Delta P}{\eta_{pump}} \tag{6.17}$$

where ΔP are the dissipative losses determined by:

$$\Delta P = 0.5 \cdot \zeta \cdot rho \cdot v_{pipes}^2 \tag{6.18}$$

It is worth noting that ζ , which is the local loss coefficient, specific for the geometry, in which the pressure loss takes place, is normally in the range of 10 to 100 and in this project is assumed to be 70. Moreover, the efficiency of the pump that transfers the water from one tank to another is assumed to be $\eta_{pump} = 0.725$.

6.2.4. Discussion

In this chapter, an analysis of the energy requirements for the submarines, especially for the case study of ALERD, has been presented. Detailed equations and explanations have been provided to estimate the power needed to operate the vehicle's thrusters and trim tanks. One significant conclusion from this analysis is the importance of proper power estimation for the vehicle's successful operation. Understanding the power needs of each control component is critical for optimizing energy consumption, guaranteeing efficient operation throughout long operational profiles, and meeting the goals that are defined for every condition, for example, transit or dredging. Overall, a thorough understanding of energy requirements is critical not only for the proper functioning of the ALERD but also for designing energy-efficient underwater vehicles in general.

To advance the understanding of energy dynamics in underwater operations, future research endeavors could explore the potential positive influence of complete or deep submersion on the efficiency of both forward and vertical tunnel thrusters. Investigation into these scenarios may reveal opportunities for improved energy efficiency and operational performance in fully submerged conditions. Additionally, optimization of propeller selection presents a compelling area for future exploration, with the potential to significantly reduce energy consumption. While these research directions extend beyond the scope of the current study, they offer promising avenues for enhancing the overall efficiency and sustainability of underwater autonomous vehicles.

7

Results

For the verification of the model, the case study of ALERD will be employed, which is going to be the first autonomous underwater unmanned replenishment dredger, developed by C-Job Naval Architects. The reduction of energy requirements for a dredger compared to current dredgers is the goal of the design of ALERD, so this study aims to the assessment of the energy that the former needs in order to compensate for the environmental forces and the seabed interaction. Overall, the following Chapter is focused on the ALERD and the estimation of the energy requirements when it operates in shallow water.

7.1. PID Gains - Corresponding Response

Implementing the gains that are selected as the ones providing the best simulation results, the desired and actual depth is depicted in Figure 7.1. As can be seen, the maximum overshoot is observed when the ALERD is at 8m, where the underwater vehicle reaches 8.5m, Figure 7.3. Moreover, the ALERD is oscillating around the desired depth signal but with a maximum amplitude of 0.1m as can be seen in Figure 7.2.

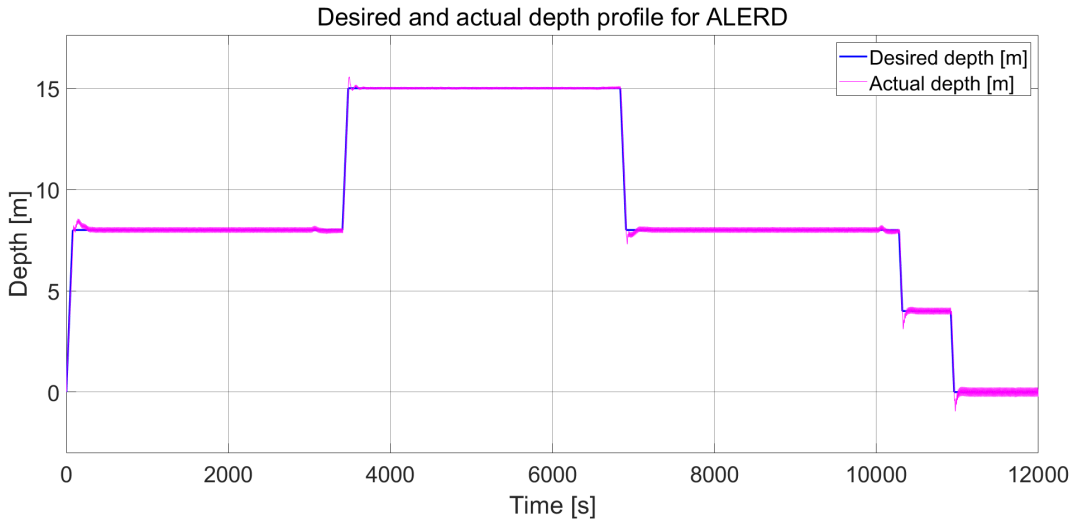

Figure 7.1: Desired and actual depth profile for ALERD

The most critical condition is the dredging condition, where the ALERD operates near the sea bottom and a risk of hitting the seabed exists. Nevertheless, as noticed in Figure 7.2 the maximum amplitude of these oscillations is 0.1m, and the overshoot is around 0.5m which is acceptable since grounding is not foreseen.

The maximum overshoot is observed at 8m, 6.25% overshoot, which is not such a critical condition since the submarine is not at dredging but in transit condition and not so close to the seabed. Although

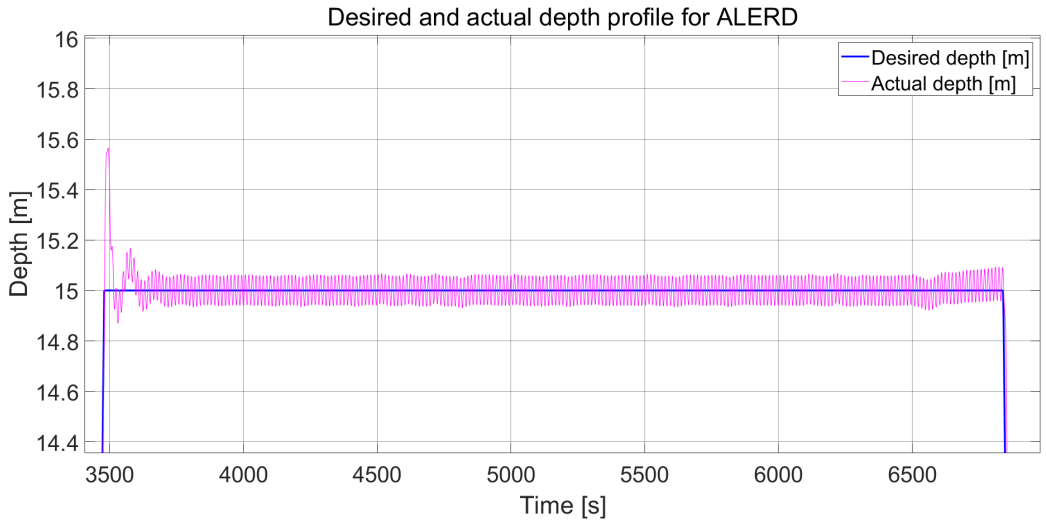

Figure 7.2: Desired and actual depth profile for ALERD at dredging condition

the settling time is not clear to read, it is worth noting that the ALERD returns fast to the desired position, around 150-200s.

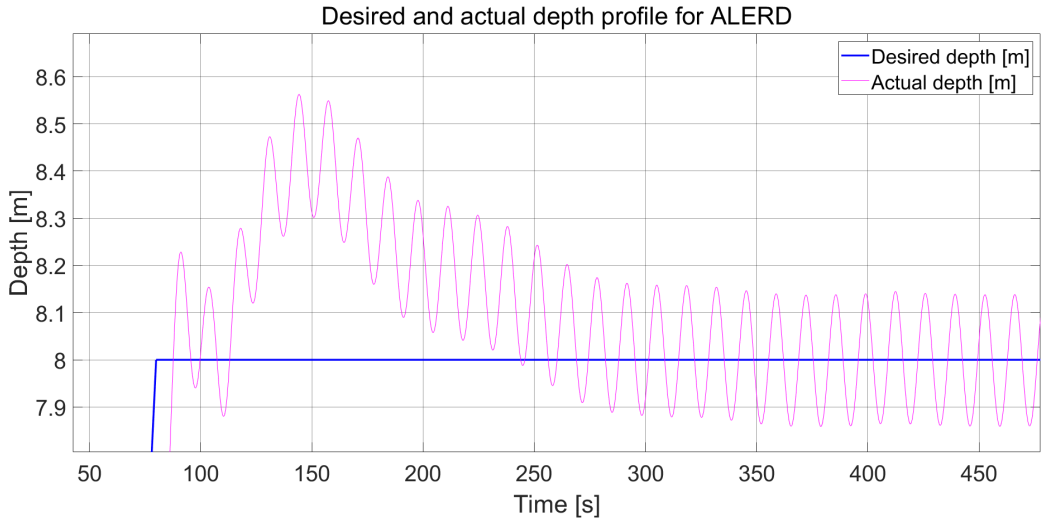

Figure 7.3: Maximum overshoot for depth profile

Regarding the pitch, in Figure 7.4 the corresponding behavior of the ALERD is depicted. It is noticed that due to the waves, the ALERD oscillates around 0° with the frequency of the first-order wave disturbances. The amplitude of these oscillations is 0.2° and the maximum pitch is presented in Figure 7.5 to be 1.2°. This is translated into a deviation of 0.84m extra draft which is not favorable, but from a safety point of view, it is acceptable since it does not exceed the clearance of the 2m. After 400s the ALERD returns to the initial position and it oscillates around 0° which is not the desired behavior but it is still within the safety limits. In order to improve this response, a different control strategy needs to be applied.

Considering the mass that needs to be transferred from one trim tank to another, a smooth response is observed from Figure 7.4.

Primarily, when the ALERD descends to a depth of 15m in order to start the dredging operation, the draghead moments in combination with the suction forces generated by the seabed, contribute to the formation of a maximum pitch angle of less than 1°. Furthermore, at 10000s, when the ALERD starts ascending, the pitch angle is almost 2° which is due to the higher value of the suction force. The ALERD operates in transit mode, so its speed is 8.5knots and its contribution in the suction force and

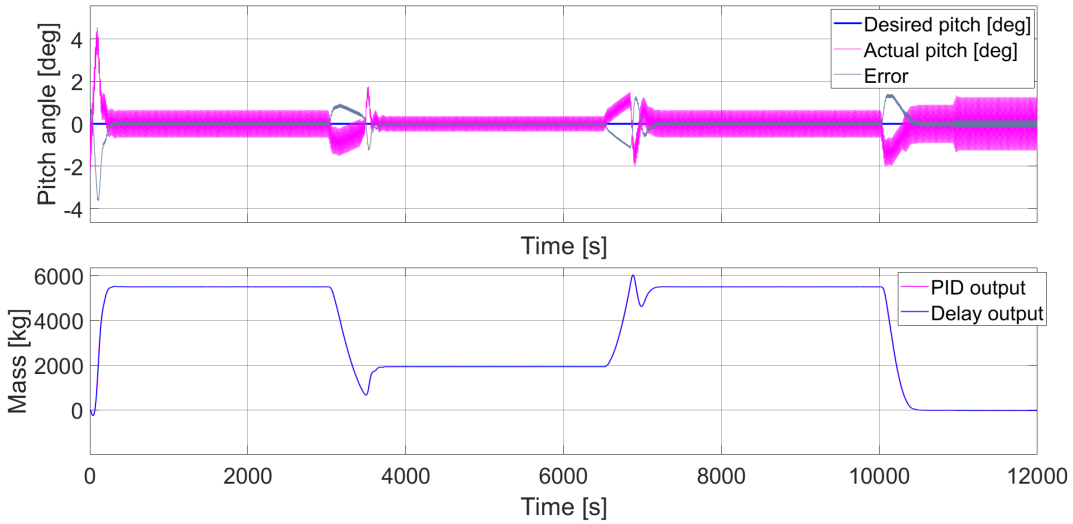

Figure 7.4: Desired and actual pitch angle for ALERD - Required mass to be transferred in the trim tanks

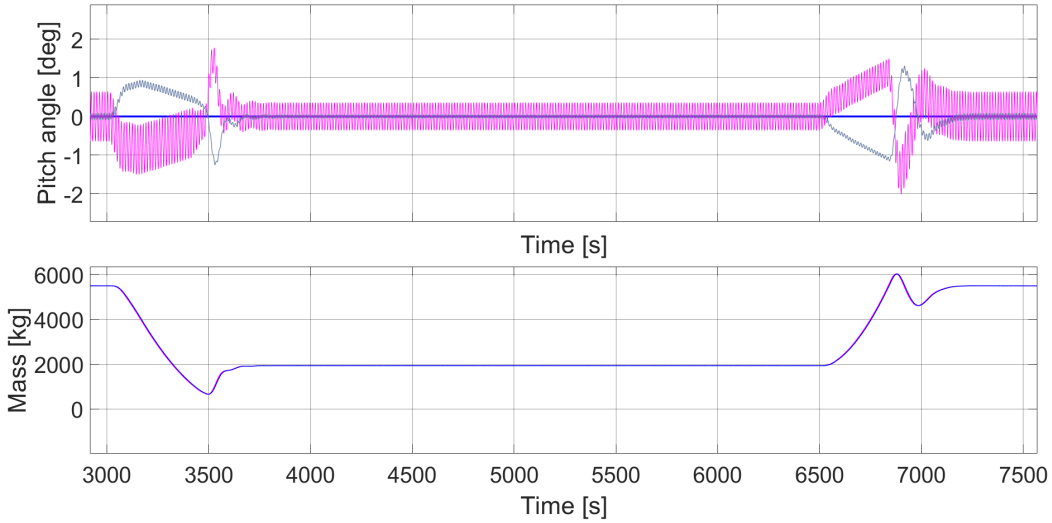

Figure 7.5: Desired and actual pitch profile for ALERD at dredging condition

the pitch moment generated by the seabed is squared. This is not such a critical condition since the ALERD is at a depth of 8m, but to eliminate it a different control strategy needs to be applied.

It is worth noting that taking into consideration the overshoot of the depth controller and the overshoot in the pitch, it is necessary to plot the combined maximum draught of the ALERD.

As it can be seen in Figure 7.6 and during the dredging condition, the combined maximum overshoot is up to 1.1m, with the ALERD descending to 16.1m instead of 15m. It needs to be mentioned that in Figure 7.6 the maximum overshoot is provided, which means that when the submarine has a specific pitch angle, the point that is closer to the seabed is depicted, either bow or aft. In this way, the worst-case scenario is presented in order to verify that there will be no grounding. Nevertheless, since the clearance is 2m, grounding is not foreseen, and the ALERD operates safely. In order to improve this oscillating behavior and the overshoot, a new control strategy needs to be examined.

7.2. Combined Scenario - Description

To estimate the energy consumption of the ALERD, it is imperative to consider a scenario that is as close to reality as it can be, involving environmental conditions. Naturally, the ALERD will exhibit increased energy consumption when it operates in heading seas due to the opposing horizontal component of the current, necessitating counteraction. Regarding the waves, the Combined scenario is when the

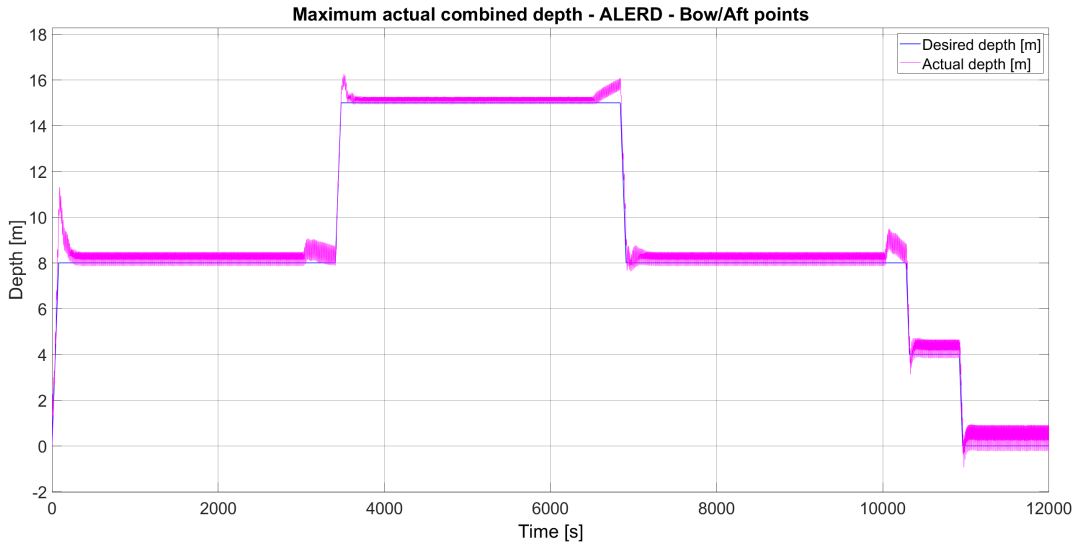

Figure 7.6: Maximum actual combined depth - ALERD

significant wave height is set to the highest that the PID controllers can handle, so, as was mentioned previously, $H_s = 2m$ and the relative angle between the ALERD and the waves is zero. This scenario accounts for the maximum challenge posed by wave conditions. The draghead forces and moments created by the dragheads and the pipes are incorporated into the model as well, to simulate a more realistic response. The resistance and suction forces, as well as the pitch moment induced by the seabed, are included in the model. Consequently, the considered scenario is a comprehensive one, where all the aforementioned forces and moments are factored into the model in order to define their interaction and the required energy consumption.

In this Chapter, the energy consumption will be presented per actuator and for different cases. Given the project's focus on assessing the energy requirements for underwater vehicles when operating near the seabed, every case will be taken into account separately in order to present the contribution of every disturbance. In Table 7.1 the induced disturbances, in different cases, are mentioned to achieve coherence and understand what the figures are in the x-axis of the following figures. Specifically, the simulation was performed multiple times, starting with only track-following, when the operational profile for depth and pitch as well as for speed was provided and the energy consumption was calculated per actuator. Then, the draghead forces are induced in the model, and the energy consumption is estimated. Following the same procedure, the current and later the waves are incorporated into the model separately, and the consumed energy is assessed. Seabed interaction was later included in the model to calculate the energy required to compensate for induced forces and moments. In Case 6, the simulation is executed without the draghead forces and moments, so all the environmental disturbances that act on an underwater vehicle that operates near the seabed are taken into account. Finally, Case 7 represents the Combined scenario, which includes the draghead forces and moments tailored to the specific case study of the ALERD.

It needs to be mentioned that Case 7 was decided to be called the Combined Scenario due to the fact that all the environmental disturbances and the seabed interaction are applied to the model, consequently, overall, more energy is consumed to counteract these disturbances. It is observed though that in Case 4, the pump of the trim tank system needs slightly more energy to compensate for the seabed than when all the aforementioned disturbances are applied. Nevertheless, case 7 remains the Combined scenario since regarding the rest of the actuators, it requires more energy to compensate for the disturbances.

7.3. Actuator Results

7.3.1. Forward Thrusters

In Figure 7.7 the total consumed energy for the two forward thrusters that ALERD is equipped with is presented. As expected, when the ALERD performs only track-following, the least energy consumption

Case 1	Operational profile
Case 2	Draghead Forces
Case 3	Ocean Current
Case 4	Seabed Interaction
Case 5	Ocean Waves
Case 6	Combined Scenario without Draghead Forces
Case 7	Combined Scenario

Table 7.1: Cascading integration of the different cases - description per case

is required, 544kWh per forward thruster, since it does not need to compensate for any environmental forces and moments, or for the draghead forces. The energy consumed when the dragheads are included is a bit higher and equal to 611kWh, indicating that their incorporation has a contribution in the surge direction since an extra resistance is included. In Case 3, when the heading current is incorporated into the model, slightly more forward power (632kWh) is needed in order to compensate for the components of the current disturbance. This is expected since the component in the x-direction opposes the motion of ALERD.

In Case 4, the consumed energy for the seabed interaction only is depicted. It is worth noting, that almost 2000kWh of energy is required per forward thruster, to compensate for the generated forces and moments due to the seabed, which is almost 3.5 times higher than the track-following condition only.

In Case 5 where the wave disturbance was included, the forward thrusters demand the same amount of energy as for track-following. Considering the modeling of the disturbances which is only in heave and pitch direction, this is a logical result, since there is no force in the surge direction. Cases 6 and 7 require almost the same amount of energy since the only difference that they have is the additional draghead forces/moments where they have a small contribution to the forward thruster's consumed energy. Nevertheless, the total energy consumption from both the forward thrusters is 4192 kWh, which is required to compensate for all the environmental disturbances and the draghead forces.

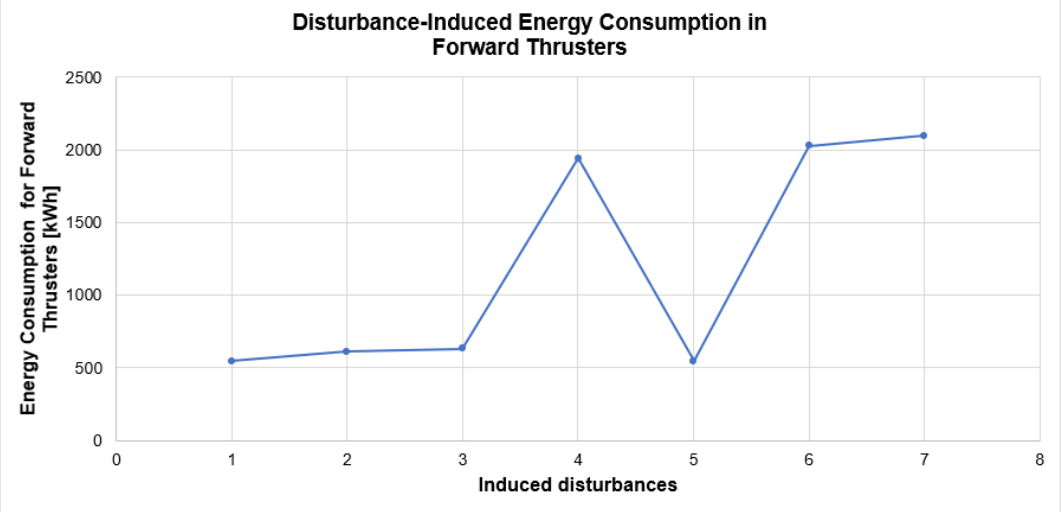

Figure 7.7: Disturbance-induced energy consumption per forward thruster

The required power to time, per forward thruster is depicted in Figure 7.9 for the combined scenario. The required power per actuator for every different studied case is plotted separately in Appendix A.4. As can be seen, there is a peak of almost 1400kW in the first seconds and then an oscillating behavior up to 150s. This is due to the fact that the ALERD is still and then it is asked to reach a velocity of 8.5knots. Due to the inertia forces and the tuning of the PID controller in the surge direction, it takes some time for the ALERD to settle in the desired speed. The required forward thrust follows the horizontal velocity profile since the former is directly used for the estimation of the thrust. Although there is no observed overshoot in the velocity profile in Figure 7.8, the calculated thrust has a peak

due to the coupling with the vertical velocity. Consequently, the peak is due to the overshoot that is presented in the depth operational profile and the corresponding vertical velocity.

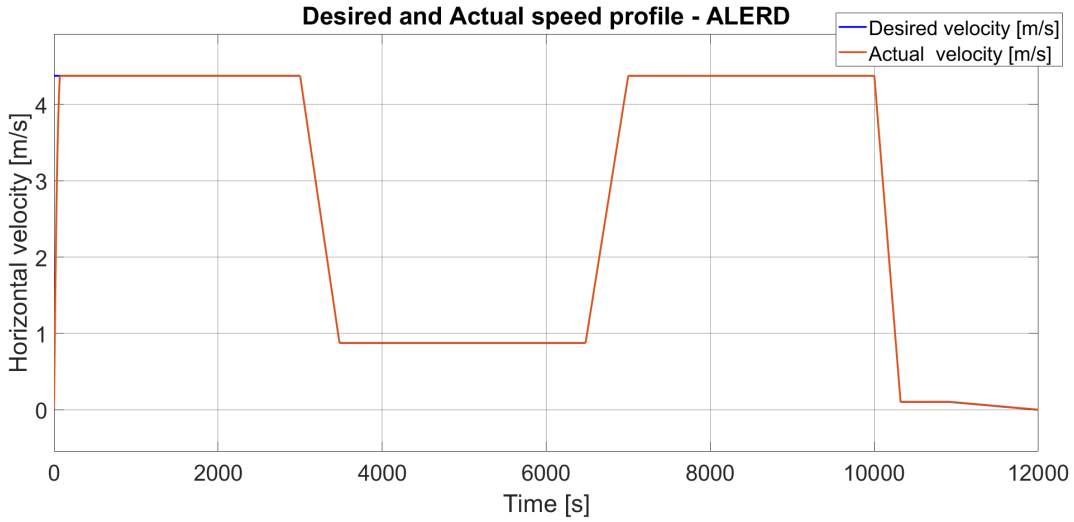

Figure 7.8: Desired and actual speed profile for ALERD

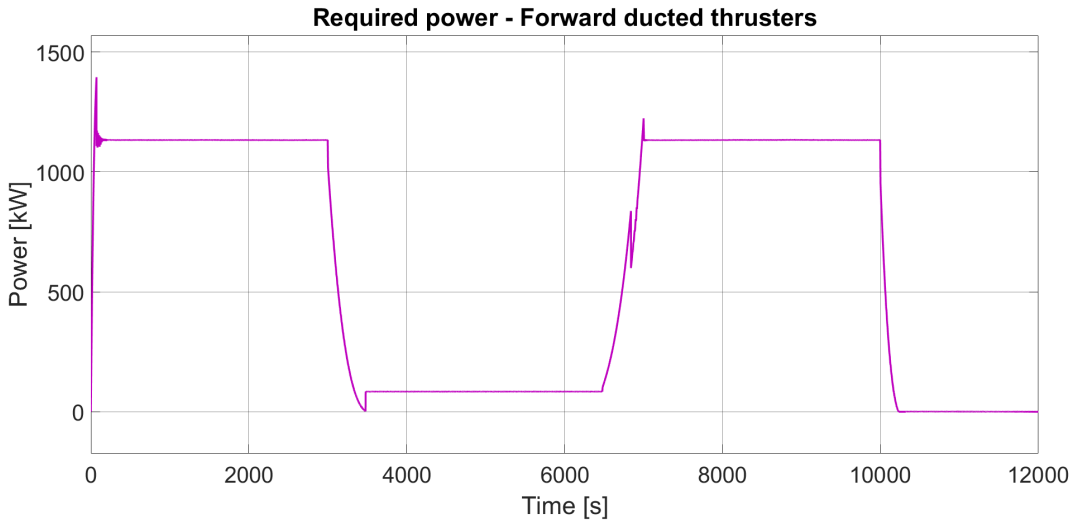

Figure 7.9: Required thrust per forward ducted thruster

7.3.2. Vertical Tunnel Thrusters

In Figure 7.11 the energy consumption in kWh for the vertical tunnel thrusters is presented per each induced-disturbance. As described previously for the forward thrusters, the same procedure was followed in order to take into account the contribution of each environmental condition separately. Overall, regarding the energy consumption of the vertical tunnel thrusters, an ascending behavior is observed. This is the expected result since each of the environmental disturbances has a component in the heave direction that needs to be compensated. The bigger the magnitude of the forces, the more the required energy to compensate for them. Due to the fact that the generated forces in the z-direction from the waves, Case 5, are bigger than the ones in the same direction by the seabed, the more required energy is observed. The issue that was evoked with the incorporation of the waves in the model was the oscillating behavior of the rpm and subsequently of the ALERD. As explained earlier, the PID controller is not able to handle the first-order wave disturbances without a filter or an observer. In order to overcome this hurdle, a low-pass filter was used, as mentioned in Chapter 4.2. Nevertheless, in order to decide which order filter has to be used, a lot of simulations were executed using first, second, and third-order filters.

As can be seen from Fig. 7.11, when there is no filter in the rpm for the vertical tunnel thrusters, the model shows very high energy consumption and this is not a realistic scenario since the output rpm are oscillating between the extreme values. Similar behavior is observed for the required thrust of the vertical tunnel thrusters, Figure 7.10.

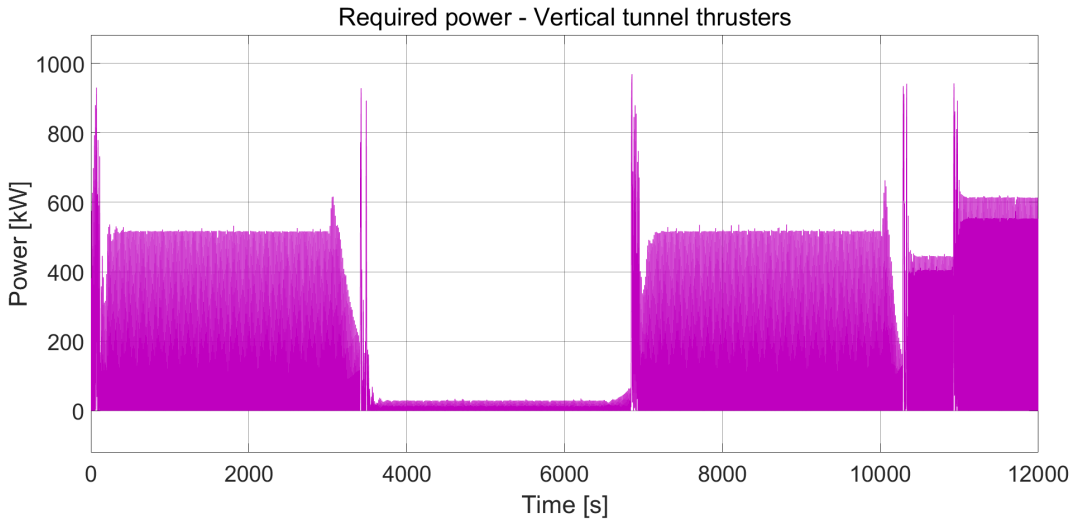

Figure 7.10: Required thrust per vertical tunnel thruster

Nonetheless, the no-filter simulation is considered in order to estimate the maximum power in kW of the vertical tunnel thrusters, Figure 7.12, and choose the motor that provides such power. This is because, after applying the low-pass filters the maximum frequencies are cut off and the result regarding the maximum power is underestimated. From Figure 7.12 is noticed that the maximum power that is demanded is 970kW and it is observed in Case 7, when the combined scenario is implemented.

Considering the waves, the required power per vertical tunnel thruster is 964kW. The filters are used in order to smooth the generated oscillating rpm signal and provide a rough estimation of the required energy. As a result, in evaluating the maximum power of the vertical tunnel thrusters without the utilization of the low-pass filter, a conservative and no realistic approach is followed.

From Figure 7.11 it can be concluded that the 3rd order filter cannot be used either because is noticed that for Case 5, which represents the ocean waves, less energy is needed compared to Case 1, track-following, which is not realistic. This means that the 3-order filter underestimates the energy that is required to compensate for the forces and moments.

In a similar vein, the exclusion of the 2nd-order filter can be justified due to its marginally higher energy consumption in kilowatt-hours (kWh) when compared to the 3rd-order filter. This choice is driven by the need to counteract the substantial forces and moments generated by ocean waves.

As a result, the decision has been made to utilize the 1st-order filter for the purpose of estimating

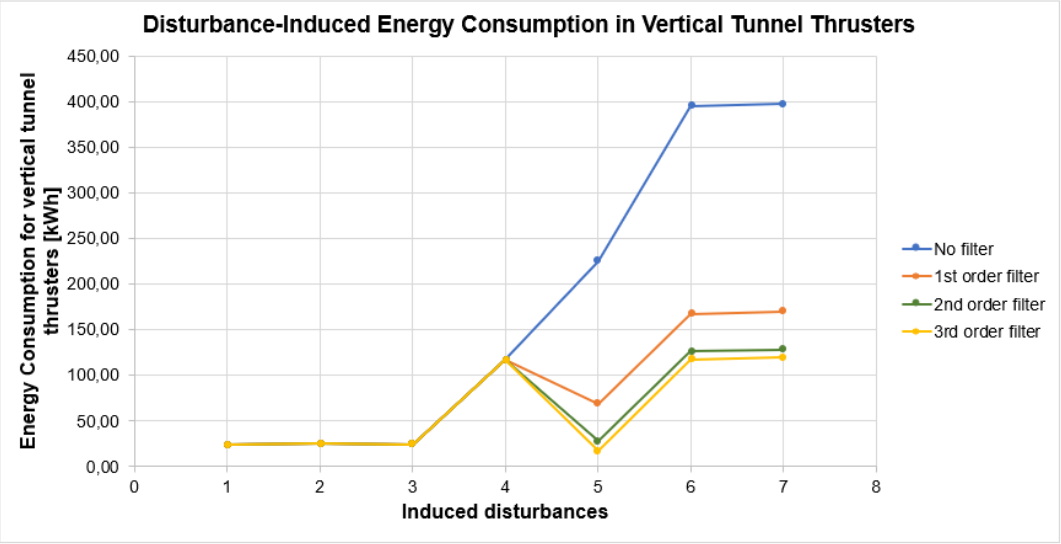

Figure 7.11: Disturbance-induced energy consumption in vertical tunnel thrusters

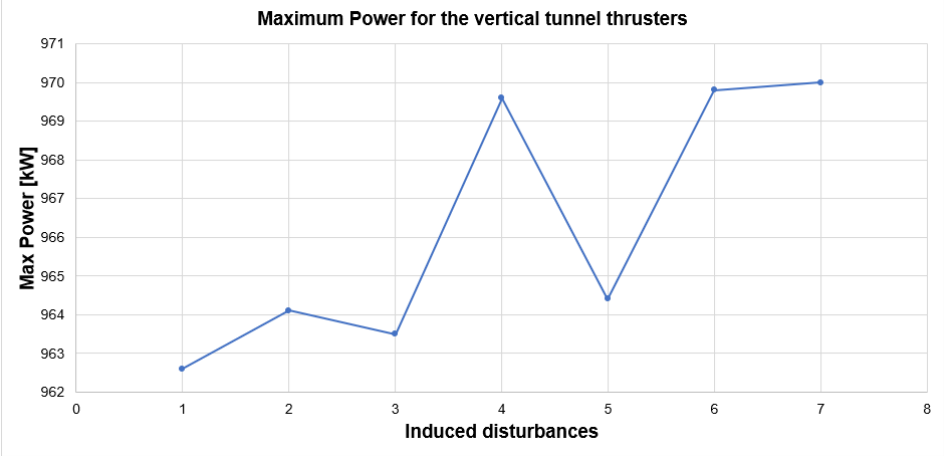

Figure 7.12: Maximum power for the vertical tunnel thrusters per case

energy consumption, as it offers a conservative approach. It is acknowledged that this estimation is rough, but it remains suitable for assessing the energy requirements during this early design phase.

7.3.3. Trim Tanks

The energy consumption for the pump of the trim tanks is presented in Figure A.11 in Appendix. It is concluded that the total energy consumption of the trim tank in the Combined Scenario is 0,19kWh and a pump of at least 12.30kW is needed. The pump capacity is defined from the compensation of the seabed interaction since more energy is needed to counteract the developed forces and moments. The same approach that was followed for the forward thrusters and the vertical tunnel thrusters is applied to the pump. Every environmental disturbance is implemented separately in the model in order to observe the contribution of each. Cases 1, 3, and 5 are observed to consume almost 0 kWh, but in reality, the pump consumes around 0.001 kWh. This is because the pitch angle does not deviate a lot from the desired angle, which is 0°, for instance, in Figure 7.13 only the current is applied in the model. When the ALERD descends to a certain desired depth, such as from 8 to 15m and vice versa, a small pitch angle is observed, but it is quickly fixed. Initiating the simulation, for the first few seconds of the simulation, a higher pitch angle is noticed, but this is due to the fact that the ALERD is first still. Due to inertia, the ALERD tends to remain still, but then it responds as it should.

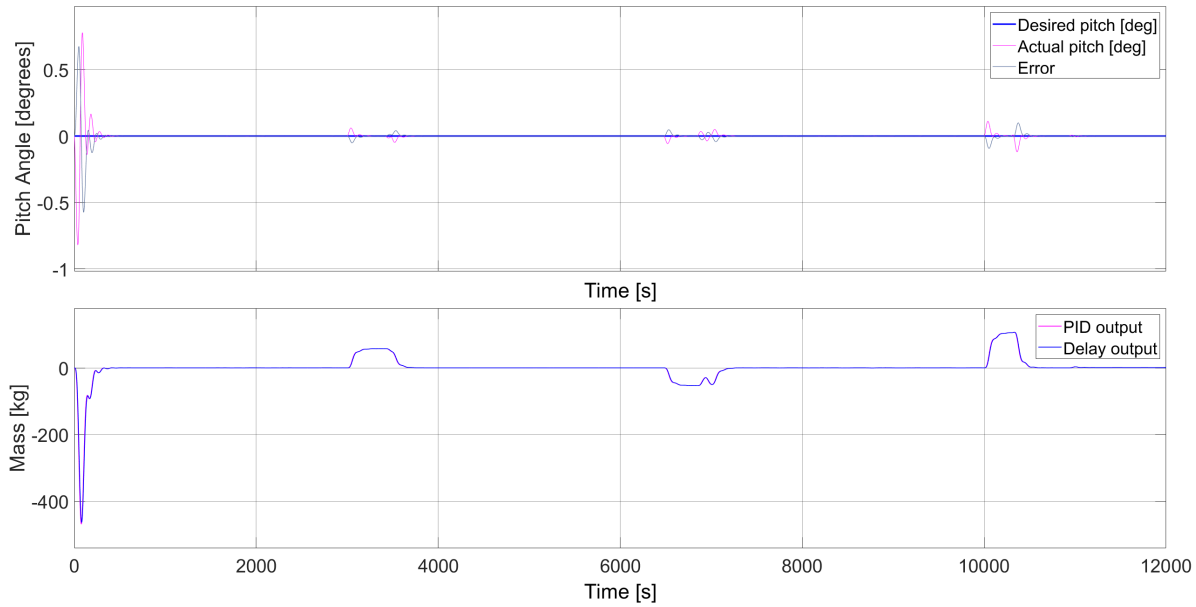

Figure 7.13: Desired and actual pitch angle when only heading current is present - Required transferred mass in the trim tanks

In Case 4, during the seabed interaction, the pump power is the highest, and at least a pump of 12.30 kW, Figure 7.14 is necessitated for the ALERD.

In order to elaborate on this, Figure 7.15 and Figure 7.16 are provided. In Figure 7.15 the total mass distribution in the trim tanks is presented. To compensate for the generated pitch 7000kg needs to be transferred from one tank to the other, due to the descending following track and the generated forces. For instance, for the first 300 seconds, the ALERD needs to descend to 8m and stabilize itself there. In order to achieve this goal, a mass of 7000kg needs to be transferred from one tank to the other in order to compensate for the pitch that is developed.

Since one of the limitations is the flow velocity in the pipes, which cannot exceed 2m/s, the mass is transferred at an allowable rate. In Figure 7.16, the volume flow for the first 400 seconds is presented. With the maximum volume flow of $0.058m^3/s$ the maximum velocity in the pipes does not reach the $2m/s$.

A notable disparity in energy consumption was observed concerning the trim tank pump's operation. Specifically, when the seabed interaction was activated within the model, the pump consumed 0.20 kWh, while in the Combined scenario encompassing all disturbances, it consumed 0.19 kWh. To elucidate this discrepancy, a systematic approach was pursued. An investigation was initially done to determine the particular time frame during which the pump's power usage peaked, finding a key interval lasting from 100 to 150 seconds. Following that, thorough observations were made regarding the trim angle at this point, as well as the mass being moved in each case. Further analysis involved the multiplication of the time duration (50 seconds, calculated as the difference between 150 and 100 seconds)

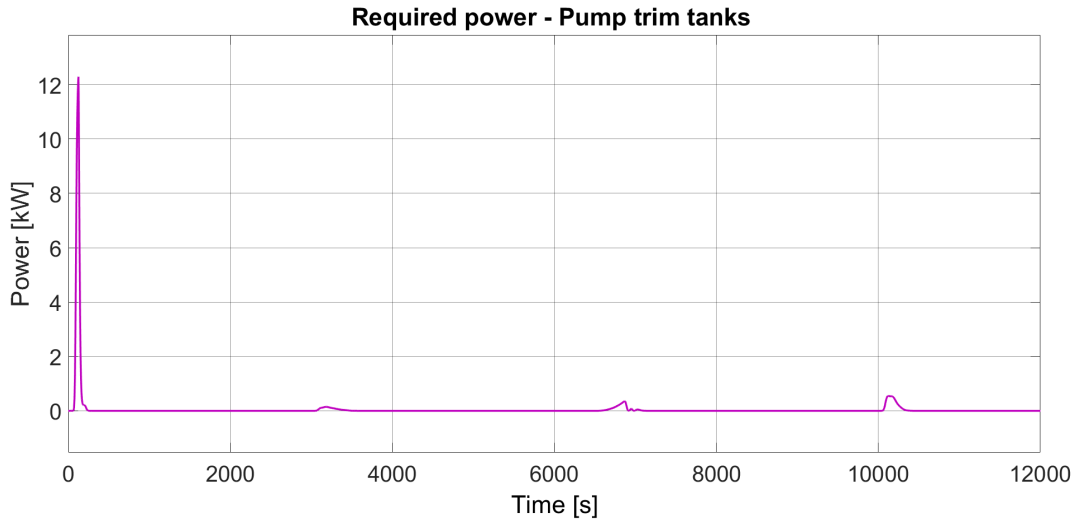

Figure 7.14: Required power - Pump trim tanks

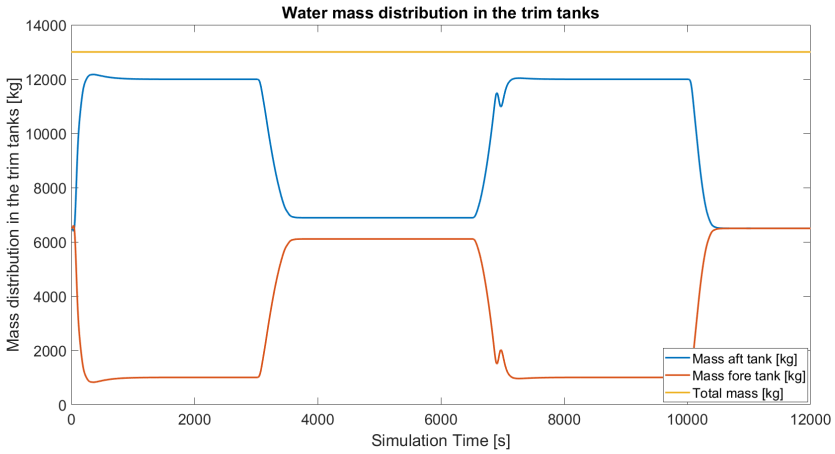

Figure 7.15: Mass distribution in the trim tanks - Case 4

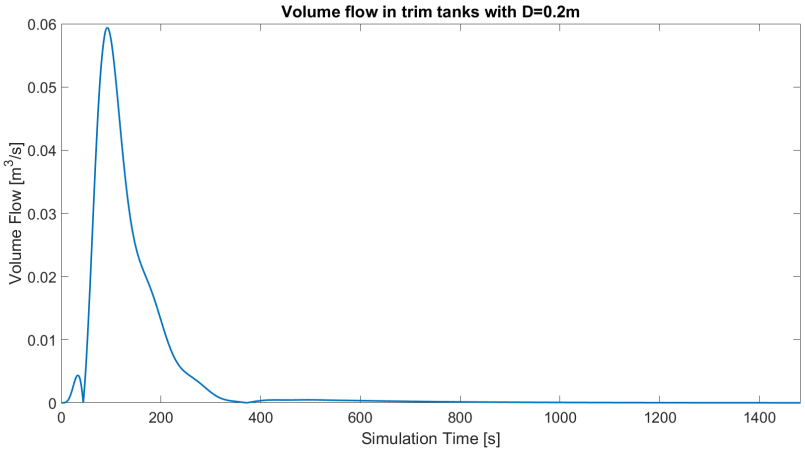

Figure 7.16: Volume flow in the pipes of the trim tank system - Case 4

by the mass, yielding a rough approximation of the interaction between the mass and the x-axis(time). This examination unveiled a distinctive pattern: while all disturbances resulted in mass transfer from

the fore to the aft, the seabed interaction stood out as an exception, leading to a significantly higher mass transfer in the opposite direction.

The summing of the mass-time products, each with its own sign, was the final stage of these trials. The overall result was favorable, necessitating a comparison analysis with the combined scenario determined from simulation data. This analysis revealed an apparent variance of 35,000 kilograms, though it should be noted that this estimate is an approximation intended to validate the hypothesis that all other disturbances, such as current, waves, and draghead, exert beneficial forces acting in the opposite direction to the seabed interaction. Finally, these data highlighted the energy usage discrepancy, with the combined scenario needing 0.19 kWh and the seafloor interaction requiring 0.20 kWh to power the trim tank pump.

7.4. Energy Consumption Overview

To sum up, from the results that were drawn above, the estimated consumed energy per actuator is presented in Table 7.2 for a simulation time of 12000s, a full dredging cycle. It needs to be mentioned that the aforementioned results regarding the forward thrusters, and vertical tunnel thrusters are only per thruster, while ALERD is equipped with two in each case. The simulation results for one vertical tunnel thruster and the thrust it provides with and without filters are given in Figure A.12 in the Appendix. Consequently, the total consumed energy per actuator is multiplied by two and presented in Table 7.2.

	Total Consumed Energy [kWh]	**Max Power [kW]**
Forward Thrusters	4192	1450
Vertical Tunnel Thrusters	340	970
Trim Tank Pump	0.2	12.30

Table 7.2: Total Energy Consumption and maximum power per actuator

In the third column of Table 7.2 the maximum power is presented per actuator. It needs to be mentioned that when the thrusters and the pump are chosen, these values will be multiplied by a safety factor in order to be able to provide more power. This is out of the scope of this project, so it is not studied.

Furthermore, a more detailed estimation of the required energy is presented for the vertical tunnel thrusters in Table 7.17. Comparing cases 6 and 7 is observed that the Combined scenario consumes the maximum energy, which is expected since all the disturbances are included. Moreover, the red value for Case 5 (waves) and for the 3rd filter means that the demanded energy is less than the one that the ALERD consumes for track-following. This means that the 3rd order filter underestimates the required energy. The first-order filter is chosen for the reasons mentioned previously as a more precise and conservative approach for the estimation of the energy. Last but not least, in the last column the max power for the vertical tunnel thruster is presented per induced-disturbance.

	Power VTT [kWh]				
	no filter	1st order	2nd order	3rd order	Max Power [kW]
Operational profile	24	24	24	24	963
Draghead Forces	25	25	25	25	964
Ocean Current	24	24	24	24	964
Seabed Interaction	117	117	117	117	970
Ocean Waves	226	69	28	17	964
Combined Scenario wt Draghead Forces	395	168	126	117	970
Combined Scenario	398	**170**	128	119	970

Figure 7.17: Calculated energy per case with and without low-pass filters per VTT

Similar results can be drawn for the pump of the trim tank and the forward thrusters in Table 7.18. The values regarding the total energy consumption for both the pump and the forward thrusters represent the maximum consumed energy in kWh in a dredging cycle of 12000s. The water distribution in the trim tanks for the Combined scenario is presented in Figure A.13.

	Trim Tank Pump		Forward Thrusters	
	Consumption [kWh]	Max Power [kW]	Consumption [kWh]	Max Power [kW]
Operational profile	0,001	0,05	1088	1393
Draghead Forces	0,009	0,45	1222	1393
Ocean Current	0,001	0,05	1263	1395
Seabed Interaction	0,204	12,30	3881	1395
Ocean Waves	0,001	0,03	1088	1395
Combined Scenario wt Draghead Forces	0,186	9,95	4058	1395
Combined Scenario	0,190	9,95	4192	1395

Figure 7.18: Total Calculated energy per case - Maximum power per actuator and per case

7.5. Contribution of tuning to the energy requirements

As mentioned in Chapter 6, the tuning of the PID not only affect the behavior of the ALERD with respect to positioning but also the calculated energy requirements.

The same procedure that was mentioned in Chapter 6 for the tuning of the PID controllers was followed in this case as well, but now also the calculated energy was considered. So, instead of using the gains that are mentioned in Chapter 6 and with an iterative procedure changing the PID gains the energy was estimated. An example of the altered PID values for the depth controllers is provided. The new PID gains for the depth controller are provided in Table 7.3.

P	I	D
400	5	9000

Table 7.3: Example PID gains for depth controller

In Figure 7.19 the energy consumption for one vertical tunnel thruster is calculated. Comparing the results of this simulation with the results from the previous one, Figure 7.17 observed a difference in the calculated energy. It can be concluded that without the proper tuning, the simulation can end up with results that overestimate the energy consumption. It needs to be mentioned that all the aforementioned parameters regarding the allowable overshoot and the settling time were taken into account.

	Power VTT [kWh]				
	no filter	1st order	2nd order	3rd order	Max Power [kW]
Operational profile	24	24	24	24	963
Draghead Forces	25	25	25	25	964
Ocean Current	24	24	24	24	963
Seabed Interaction	117	117	117	117	968
Ocea Waves	323	96	33	18	965
Combined Scenario wt Draghead Forces	476	182	128	117	968
Combined Scenario	478	**184**	130	119	970

Figure 7.19: Calculated energy per case with and without low-pass filters, different PID gains

Similar results are observed for the forward thrusters and the pump of the trim tanks. In both cases, the energy requirement is higher with the altered PID values.

	Trim Tank Pump		Forward Thrusters	
	Consumption [kWh]	Max Power [kW]	Consumption [kWh]	Max Power [kW]
Operational profile	0,001	0,05	1088	1393
Draghead Forces	0,009	0,45	1222	1393
Ocean Current	0,001	0,05	1263	1395
Seabed Interaction	0,202	12,26	3881	1395
Ocean Waves	0,001	0,03	1088	1395
Combined Scenario wt Draghead Forces	0,182	9,68	4058	1395
Combined Scenario	0,186	9,68	4192	1395

Figure 7.20: Calculated energy per case - Maximum power per actuator and per case, different PID gains

Overall, the tuning of the PID controllers needs to be executed cautiously and all the parameters that are critical for the model, need to be considered. Furthermore, special attention should be given to the physical constraints of the actuators, but also to the overshoot when the submarine operates near the seabed.

7.6. Discussion

In this chapter, a comprehensive analysis of the results obtained from the case study of ALERD was undertaken. It was focused on estimating the energy requirements of the ALERD when operating in shallow waters under various environmental conditions and disturbances. The current study's major goal was to calculate the amount of energy required to compensate for the complicated interplay of environmental disturbances and seabed interaction experienced during transit and dredging operations.

The Combined scenario encompassed a multitude of factors, including heading seas, significant wave heights, draghead moments, seabed interactions, and ocean currents. By meticulously examining each of these elements individually, their distinct contributions to the overall energy consumption of the ALERD were calculated. To compensate for the aforementioned disturbances, three pivotal actuator components were used: forward thrusters, vertical tunnel thrusters, and trim tank pumps. These components were scrutinized to determine their energy consumption under varying environmental disturbances, and their energy demands under different operational conditions.

In the case of forward thrusters, the findings revealed that the lowest energy consumption occurred during track-following, where no compensation for environmental forces or draghead moments was required. Conversely, the Combined scenario, encompassing all environmental disturbances and draghead forces and moments, led to the highest energy demands for the forward thrusters. Turning to the vertical tunnel thrusters, a consistent increase in energy consumption was observed with the introduction of environmental disturbances. Notably, the choice of a low-pass filter played a pivotal role in accurately estimating energy requirements, as it addressed the oscillatory behavior in the thruster's RPM.

For the trim tank pumps, minimal energy consumption was identified during cases where the ALERD closely adhered to the desired pitch angle. However, when seabed interactions were considered, the pump's power demand surged significantly, necessitating a pump capable of delivering 12.30 kW for effective compensation.

The consolidated overview of total energy consumption for each actuator and their corresponding maximum power requirements, as presented in Table 7.2, provides a comprehensive view of the energy demands of the ALERD in shallow waters.

Furthermore, the influence of PID controller tuning on the energy requirements was examined. The current analysis revealed that improper tuning could result in overestimations of energy consumption. Therefore, meticulous attention to critical parameters and the physical constraints of actuators, particularly when operating near the seabed, is imperative during PID controller tuning. In summary, this study has offered valuable insights into the intricate energy demands of the ALERD during operations in shallow waters. It has shed light on the unique contributions of various environmental disturbances and underscored the significance of precise PID controller tuning. Nevertheless, since there is always space for improvement, in order to eliminate the oscillating behavior of the ALERD and the contribution of the waves, a PID controller in combination with an observer needs to be implemented. Then, a more precise result regarding the energy can be obtained. Furthermore, CFD analysis should be performed in order to define properly the drag coefficients from the seabed interaction, since ALERD needs a lot of energy to compensate for them. Last but not least, design studies for the actuators have to be performed separately in order to define their characteristics because they significantly contribute to the calculation of energy consumption.

8

Conclusion and Future Recommendations

In this Chapter, the key findings and insights drawn from the preceding chapters are presented. The aim of the research will be demonstrated as successfully achieved, with comprehensive answers provided to the research questions introduced in Chapter 1. Furthermore, recommendations for prospective research endeavors will be presented.

8.1. Conclusions

The primary objective of this research was to develop a model that determines the energy required to compensate for environmental forces and seabed effects on a submarine operating in shallow water. This will contribute to a better understanding of the energy requirements of submarines and enable the development of more energy-efficient solutions.

After the development of the model and the execution of the simulations, the research questions that were set during the literature review can be answered.

What are the main environmental forces that affect submarine operations in shallow waters, both in transit as well as in dredging conditions?

In both conditions, the submarines that operate in shallow water are affected by the ocean currents, the ocean waves, the seabed interaction, as well as the surface interaction. Regarding the ocean waves, the deeper the submarine descends, the less the contribution of the waves is, since with the increasing depth the energy is dissipated. The wave forces depend on the displacement and the main characteristics of the submarine, as well as on the depth at which it operates. The seabed contributes to the submarine's behavior as well. Based on the geometrical characteristics of the former, the speed and the distance from the seabed it operates, a resistance force in the surge direction, a suction force in the heave direction, and a pitch moment are induced. During the execution of the literature review, it was figured out that similar forces and moments are generated by the surface interaction when operating close to it, and there is a significant contribution of them in the model. Since it was not part of this project and due to the limited time, this part was excluded.

How can the environmental forces be included in the mathematical model?

Regarding the ocean current, there are two ways to include it in the developed model. Following the deterministic approach, the velocity of the current and the angle of it remains constant and the relative velocity of the underwater vehicle is estimated and integrated into the state-space model. In this project, the stochastic approach is chosen in order to include randomness in the model. The mean

values of the current's speed and angle are selected and following Fossen's approach, [15], the components of the velocity are estimated and included in the state-space equations. The waves are modeled as one sinusoidal force exerted on the underwater vehicle and one sinusoidal moment. These forces and moments are translated into disturbance accelerations and are added to the state-space equation.

How does the seabed contribute to the overall forces on a submarine in shallow waters? How can the effect on resistance and surge, pitch and heave by the seabed be included in the mathematical model?

As mentioned previously, the seabed interaction generates a resistance force in the x-direction, a heave force in the z-direction, and a pitch moment. Using as inputs the actual speed and position (depth) of the underwater vehicle, the developed forces can be calculated and they are added to the τ vector. In order to precisely calculate the contribution of the seabed to the overall forces on a submarine, CFD analysis is required in order to estimate the drag coefficients that are used for the generated forces. In this project, these coefficients are taken from another performed study and are an assumption in order to develop a model that will estimate the energy consumption of the submarine.

How many DOF should be included in the model? What is the most significant direction in terms of the impact on the submarine of the seabed effect?

The aforementioned environmental disturbances and seabed interaction are modeled with forces or velocity and acceleration components in surge, heave, and pitch direction. Consequently, these 3DOF are the most important that need to be included in the developed model. The submarine requires more power to compensate for these forces and moments in these specific directions. Considering the seabed interaction, the generated forces are of great importance but the induced pitch moment affects more the model since the magnitude is bigger than the forces.

What are the best control strategies that can be implemented in the mathematical model considering energy requirements and operability?

It is concluded that the PID controller itself cannot handle the wave disturbances. Nevertheless, following the approach that was proposed including the low-pass filter, the energy requirements can be estimated. The tuning of the PID controller is always a trade-off between the generated overshoot of the submarine and the consumed energy. Different gains for the PID end up with different results and the decision of them is at the user's discretion and the constraints of the problem. Ideally, the PID should be used in combination with a wave filter, or an observer in order to predict the wave disturbances and cancel them out, smoothing the output behavior.

A case study will be performed for the application within ALERD, determining the energy requirements.

Considering the case study of ALERD, and taking into account that it is equipped with two forward ducted thrusters, two vertical tunnel thrusters, and a closed trim tank system, energy consumption is defined. For accomplishing a full dredging cycle, in the surge direction, the forward thrusters consume 4192kWh, while in the heave direction, the vertical tunnel thrusters consume 340kWh. As regards the pitch direction, the pump of the trim tank system consumes 0.2kWh. It needs to be mentioned that the aforementioned power consumption is calculated for the combined scenario which will be representative of the reality.

8.2. Future Recommendations

In order to improve the simulation model, and obtain more precise and realistic results, the following research is recommended.

- Implement an Adaptive PID controller for achieving better behavior of the submarine. By changing the gains of the PIDs per operating condition, the minimization of the overshoot can be accomplished.
- Develop an observer in order to eliminate the oscillating behavior of the submarine, coming from the first-order wave terms.
- Regarding the waves, it is recommended to include the whole Jonswap spectrum and higher wave heights, as well as the second-order terms to obtain more precise results.
- Include the surface interaction in the Matlab, Simulink model for more accurate energy consumption estimation.
- Performing a CFD analysis and calculating the drag coefficients for the seabed interactions would help improve the accuracy of the model, but also the hydrodynamic coefficients for the submarine itself.
- Implementation of other actuators, like planes and verification of the most optimal one per operating condition.

References

[1] E. Brand, G. Ramaekers, and Q. Lodder, "Dutch experience with sand nourishments for dynamic coastline conservation – An operational overview," *Ocean and Coastal Management*, vol. 217, Feb. 2022, ISSN: 09645691. DOI: 10.1016/j.ocecoaman.2021.106008.

[2] M. of Infrastructure, A. the Environment Ministry of Economic Affairs, and Innovation, *Delta Programme 2012: Working on the delta. Acting today, preparing for tomorrow*. The Hague, Netherlands: Ministry of Infrastructure and the Environment, 2011, pp. 76–77.

[3] R. M. J. Hijdra and S. Van Der Harst, "Design of an Autonomous Underwater Maintenance Dredger A teaser to the maritime industry," Tech. Rep.

[4] J. Kalwa, R. Stach, A. Stavenhagen, N. Richter, T. Voß, and W. H. Wehner, "Large Modifiable Underwater Mothership-MUM Operational and Technical Concepts for Complex Unmanned Tasks," Tech. Rep., 2019. [Online]. Available: https://www.researchgate.net/publication/341312461.

[5] Y. Xing, O. Gaidai, Y. Ma, A. Naess, and F. Wang, "A novel design approach for estimation of extreme responses of a subsea shuttle tanker hovering in ocean current considering aft thruster failure," *Applied Ocean Research*, vol. 123, Jun. 2022, ISSN: 01411187. DOI: 10.1016/j.apor.2022.103179.

[6] W. Hoekwater, W. De Jonge, M. Kuntz, and T. De Vlieger, "Dredging slurry storage for the autonomous underwater maintenance dredger," Tech. Rep.

[7] I. Bačkalov, M. Vidić, and S. Rudaković, "Lessons learned from accidents on some major European inland waterways," *Ocean Engineering*, vol. 273, Apr. 2023, ISSN: 00298018. DOI: 10.1016/j.oceaneng.2023.113918.

[8] J. Estrela Da Silva, B. Terra, R. Martins, and J. Borges De Sousa, "Modeling and Simulation of the LAUV Autonomous Underwater Vehicle," Tech. Rep.

[9] M. Bakker, "A Model Predictive Control Approach Towards the Energy Efficiency of Autonomous Sub-merged Dredging," Ph.D. dissertation. [Online]. Available: http://repository.tudelft.nl/..

[10] J. L. A. Hofstede, R. Zijlstra, J. L. A. Hofstede, T. Piontkowitz, and F. Thorenz, "Coastal risk management Wadden Sea Quality Status Report Coastal risk management," Tech. Rep. [Online]. Available: https://www.researchgate.net/publication/359423790.

[11] M. v. I. e. Waterstaat, "Innovaties in De Kustlijnzorg," *Rijkswaterstaat*, Jan. 2023.

[12] S. Haugen, A. Barros, C. v. Gulijk, T. Kongsvik, and J. E. Vinnem, *Safety and reliability : safe societies in a changing world : proceedings of the 28th international European Safety and Reliability Conference (ESREL 2018), Trondheim, Norway, 17-21 June 2018*, p. 3201, ISBN: 9780815386827.

[13] S. C. Mallam, S. Nazir, and A. Sharma, "The human element in future Maritime Operations–perceived impact of autonomous shipping," *Ergonomics*, vol. 63, no. 3, pp. 334–345, Mar. 2020, ISSN: 13665847. DOI: 10.1080/00140139.2019.1659995.

[14] J. de Vos, R. G. Hekkenberg, and O. A. Valdez Banda, "The Impact of Autonomous Ships on Safety at Sea – A Statistical Analysis," *Reliability Engineering and System Safety*, vol. 210, Jun. 2021, ISSN: 09518320. DOI: 10.1016/j.ress.2021.107558.

[15] T. I. Fossen, *Handbook of marine craft hydrodynamics and motion control*. Wiley, 2011, p. 596, ISBN: 9781119991496.

[16] Y. Valeriano-Medina and A. Martinez, ""Dynamic model for an autonomous underwater vehicle based on experimental data," ISSN: 13873954. DOI: 10.1080/13873954.2012.717226.

[17] M. Moonesun, K. Y. Mikhailovich, D. Tahvildarzade, and M. Javadi, “Practical scaling method for underwater hydrodynamic model test of submarine,” *Journal of the Korean Society of Marine Engineering*, vol. 38, no. 10, pp. 1217–1224, Dec. 2014, ISSN: 2234-7925. DOI: 10.5916/jkosme.2014.38.10.1217.

[18] T. I. Fossen, *Handbook of Marine Craft Hydrodynamics and Motion Control*. Apr. 2011, ISBN: 9781119991496. DOI: 10.1002/9781119994138.

[19] M. Moonesun, M. Javadi, P. Charmdooz, and K. U. Mikhailovich, “Evaluation of submarine model test in towing tank and comparison with CFD and experimental formulas for fully submerged resistance,” Tech. Rep. 8, 2013, pp. 1049–1056. [Online]. Available: https://www.researchgate.net/publication/265336511.

[20] D. Norske Veritas, “RECOMMENDED PRACTICE ENVIRONMENTAL CONDITIONS AND ENVIRONMENTAL LOADS,” Tech. Rep., 2010. [Online]. Available: http://www.dnv.com.

[21] H. Vindenes, K. A. Orvik, H. Søiland, and H. Wehde, “Analysis of tidal currents in the North Sea from shipboard acoustic Doppler current profiler data,” *Continental Shelf Research*, vol. 162, pp. 1–12, Jun. 2018, ISSN: 18736955. DOI: 10.1016/j.csr.2018.04.001.

[22] S. Groeskamp and J. Kjellsson, “The northern european enclosure dam for if climate change mitigation fails,” *Bulletin of the American Meteorological Society*, vol. 101, no. 7, E1174–E1189, Jul. 2020, ISSN: 00030007. DOI: 10.1175/BAMS-D-19-0145.1.

[23] K. Bruserud and S. Haver, “Uncertainties in current measurements in the northern North Sea,” *Journal of Atmospheric and Oceanic Technology*, vol. 34, no. 4, pp. 855–876, Apr. 2017, ISSN: 15200426. DOI: 10.1175/JTECH-D-16-0192.1.

[24] R. Hijdra, “AUTONOMOUS LOW ENERGY REPLENISHMENT DREDGER (ALERD) Operation-eel Profiel Analyse.,” 2021.

[25] M. Jeon, H. K. Yoon, J. Park, and Y. You, “Analysis of maneuverability of X-rudder submarine considering environmental disturbance and jamming situations,” *Applied Ocean Research*, vol. 121, Apr. 2022, ISSN: 01411187. DOI: 10.1016/j.apor.2022.103079.

[26] J. S. Riedel, “NAVAL POSTGRADUATE SCHOOL MONTEREY, CALIFORNIA DISSERTATION SEAWAY LEARNING AND MOTION COMPENSATION IN SHALLOW WATERS FOR SMALL AUVS,” Tech. Rep., 1999.

[27] R. J. Richards and D. P. Stoten, “DEPTH CONTROL OF A SUBMERSIBLE VEHICLE,” pp. 30–39, 1981. DOI: 10.3233/ISP-1981-2831802.

[28] E. Liceaga-Castro and G. M. Van Der Molen, “Submarine H m Depth Control Under Wave Disturbances,” *IEEE TRANSACTIONS ON CONTROL SYSTEMS TECHNOLOGY*, vol. 3, no. 3, 1995.

[29] J. Schloen, E. V. Stanev, and S. Grashorn, “Wave-current interactions in the southern North Sea: The impact on salinity,” *Ocean Modelling*, vol. 111, pp. 19–37, Mar. 2017, ISSN: 14635003. DOI: 10.1016/j.ocemod.2017.01.003.

[30] C. Beels, J. C. C. Henriques, J. De Rouck, M. T. Pontes, G. De Backer, and H. Verhaeghe, “Wave energy resource in the North Sea,” Tech. Rep.

[31] L. Moreira and C. G. Soares, “Autonomous underwater vehicle control in presence of waves,” in *Proceedings of the International Conference on Offshore Mechanics and Arctic Engineering - OMAE*, vol. 6, American Society of Mechanical Engineers (ASME), 2008, pp. 549–560, ISBN: 9780791848234. DOI: 10.1115/OMAE2008-57927.

[32] D. Lyu, H. Su, Y. Li, Z. Zhang, H. Long, and J. Zhao, “An Embedded Linear Model Three-Dimensional Fuzzy PID Control System for a Bionic AUV under Wave Disturbance,” *Mathematical Problems in Engineering*, vol. 2022, 2022, ISSN: 15635147. DOI: 10.1155/2022/4126595.

[33] X. Han, Z. Ren, B. J. Leira, and S. Sævik, “Adaptive identification of lowpass filter cutoff frequency for online vessel model tuning,” *Ocean Engineering*, vol. 236, Sep. 2021, ISSN: 00298018. DOI: 10.1016/j.oceaneng.2021.109483.

[34] X. x. Du, H. Wang, C. z. Hao, and X. l. Li, “Analysis of hydrodynamic characteristics of unmanned underwater vehicle moving close to the sea bottom,” *Defence Technology*, vol. 10, no. 1, pp. 76–81, Mar. 2014, ISSN: 22149147. DOI: 10.1016/j.dt.2014.01.007.

[35] A. Ursolov, M. Moonesun, Y. M. Korol, N. Valeri, A. Brazhko, and A. Ursolov, “Bottom effect on the submarine moving close to the sea bottom,” *Journal of Scientific and Engineering Research*, vol. 3, no. 1, pp. 106–113, 2016, ISSN: 2394-2630. [Online]. Available: https://www.researchgate.net/publication/331001062.

[36] X. Ling, Z. Q. Leong, C. Chin, M. Woodward, and J. Duffy, *Comparisons between seabed and free surface effects on underwater vehicle hydrodynamics*, Jan. 2022. DOI: 10.1016/j.ijnaoe.2022.100482.

[37] Institute of Electrical and Electronics Engineers, *OCEANS 2019 MTS/IEEE SEATTLE*, ISBN: 9781728114507.

[38] M. A. Jahangir, I. Mahmood, N. Raza, S. Bilal, and M. Rafique, “Study on effect of Sea Bottom distance on an Underwater Body,” Tech. Rep.

[39] M. Bakker, “A Model Predictive Control Approach Towards the Energy Efficiency of Submerged Dredging,” Ph.D. dissertation, Delft University of Technology, 2022.

[40] L. J. Doctors and R. F. Beck, “CONVERGENCE PROPERTIES OF THE NEUMANN-KELVIN PROBLEM FOR A SUBMERGED BODY.,” *Journal of Ship Research*, vol. 31, no. 4, pp. 227–234, Dec. 1987, ISSN: 00224502. DOI: 10.5957/jsr.1987.31.4.227.

[41] b. P. Thomas Crook, “E LEcTE f7 AN INITIAL ASSESSMENT OF FREE SURFACE EFFECTS ON SUBMERGED BODIES,” Tech. Rep., 1994.

[42] M. M. Amiri, P. T. Esperança, M. A. Vitola, and S. H. Sphaier, “How does the free surface affect the hydrodynamics of a shallowly submerged submarine?” *Applied Ocean Research*, vol. 76, pp. 34–50, Jul. 2018, ISSN: 01411187. DOI: 10.1016/j.apor.2018.04.008.

[43] A. S. T. Conway, F. Valentinis, and G. Seil, “Characterisation of suction effects on a submarine body operating near the free surface,” Tech. Rep.

[44] “Hydra is an extra service from SCHOTTEL-YOUR PROPULSION EXPERTS,” Tech. Rep., 2023.

[45] L. V. Steenson, A. B. Phillips, M. E. Furlong, E. Rogers, and S. R. Turnock, “The Performance of Vertical Tunnel Thrusters on an Autonomous Underwater Vehicle Operating Near the Free Surface in Waves,” Tech. Rep., 2011.

[46] A. R. Palmer, “Analysis of the Propulsion and Manoeuvring Characteristics of Survey-Style AUVs and the Development of a Multi-Purpose AUV,” Tech. Rep., 2009.

[47] A. O’dwyer, “A SUMMARY OF PI AND PID CONTROLLER TUNING RULES FOR PROCESSES WITH TIME DELAY. PART 1: PI CONTROLLER TUNING RULES,” Tech. Rep.

[48] Z. Xu, M. Haroutunian, A. J. Murphy, J. Neasham, and R. Norman, “A comparison of functional control strategies for underwater vehicles: Theories, simulations and experiments,” *Ocean Engineering*, vol. 215, Nov. 2020, ISSN: 00298018. DOI: 10.1016/j.oceaneng.2020.107822.

[49] A. Sahoo, S. K. Dwivedy, and P. S. Robi, “Adaptive Fuzzy PID Controller for A Compact Autonomous Underwater Vehicle,” in *2020 Global Oceans 2020: Singapore - U.S. Gulf Coast*, Institute of Electrical and Electronics Engineers Inc., Oct. 2020, ISBN: 9781728154466. DOI: 10.1109/IEEECONF38699.2020.9389483.

[50] X. Han, W. Yu, and H. Xu, “Research of Station Keeping Controller of Dynamic Positioning Vessel in Varying Sea States Based on State Observer,” Tech. Rep. DOI: 10.1109/IMCCC.2018.00137.

[51] J S Carlton, “Marine Propellers and Propulsion,” Tech. Rep.

[52] J. L. Beveridge, “UNCLASSIFIED SecuhtvClaMificjtioji DOCUMENT CONTROL DATA-R&D iSeriMltr clmwtilirmlion mi till; botr of mb»tm€l mnd indeming mmotmlitm mu*l b€ wifwrf mh-t lfc» ovmrmlt fport im cl*»»iH*d) l ORICIN&TINC AC TI vi TV (Cotponl* muOtor) DESIGN AND PERFORMANCE OF BOW THRUSTERS 4. DESCRIPTIVE MO’ff (Trp* ol rmportand inclutire drntrm) Final Report s AUTHORISI (Fitpt nnw. midtttm inlllml. 1**1 n*m*) DD ””*’ 1473 Security Classification,” Tech. Rep., 1971.

A

Appendix

A.1. Sanity Check

A.1.1. Ocean Current

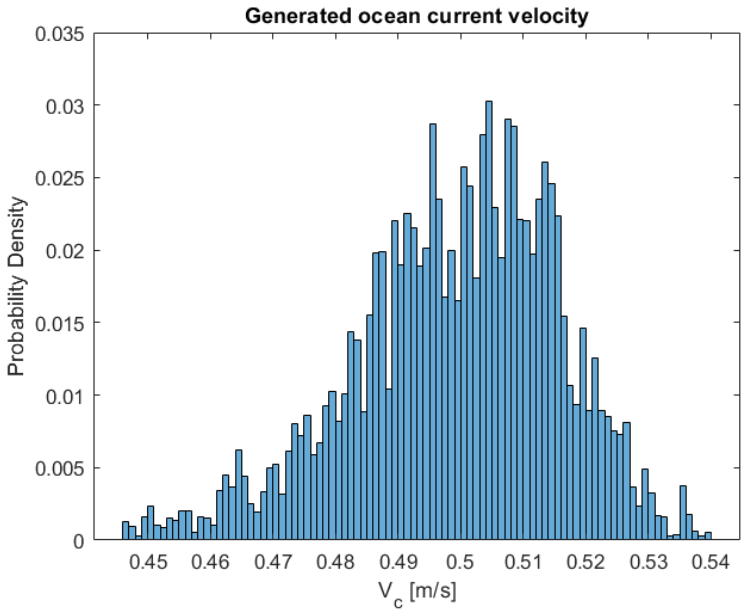

Figure A.1: Ocean current velocity distribution

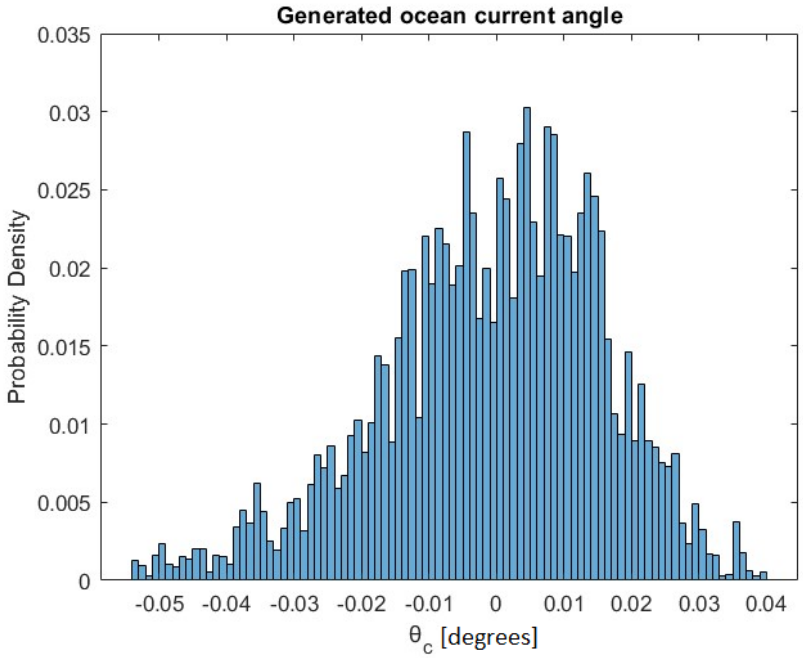

Figure A.2: Ocean current angle distribution

A.1.2. Ocean Waves

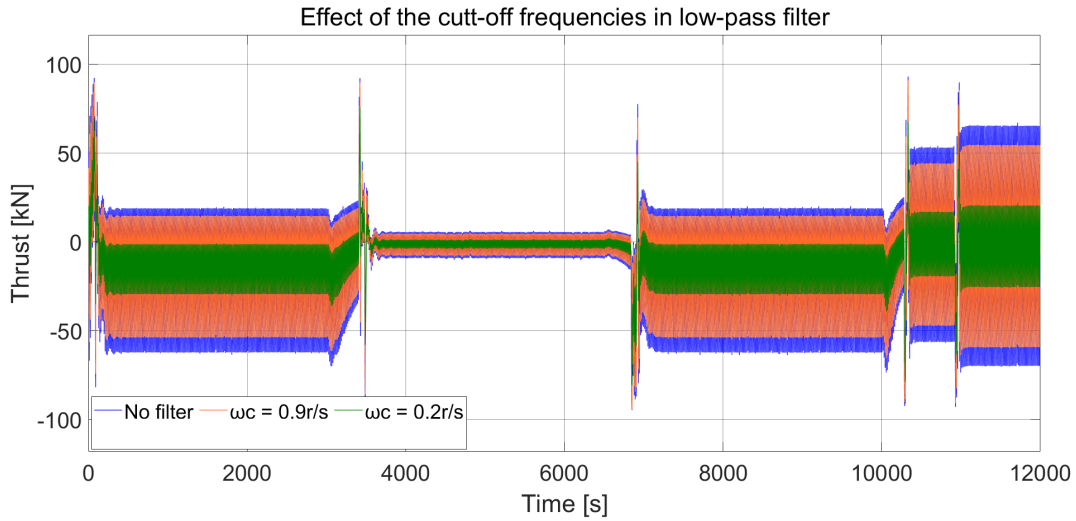

Figure A.3: Effect of cut-off frequency on the thrust outcome

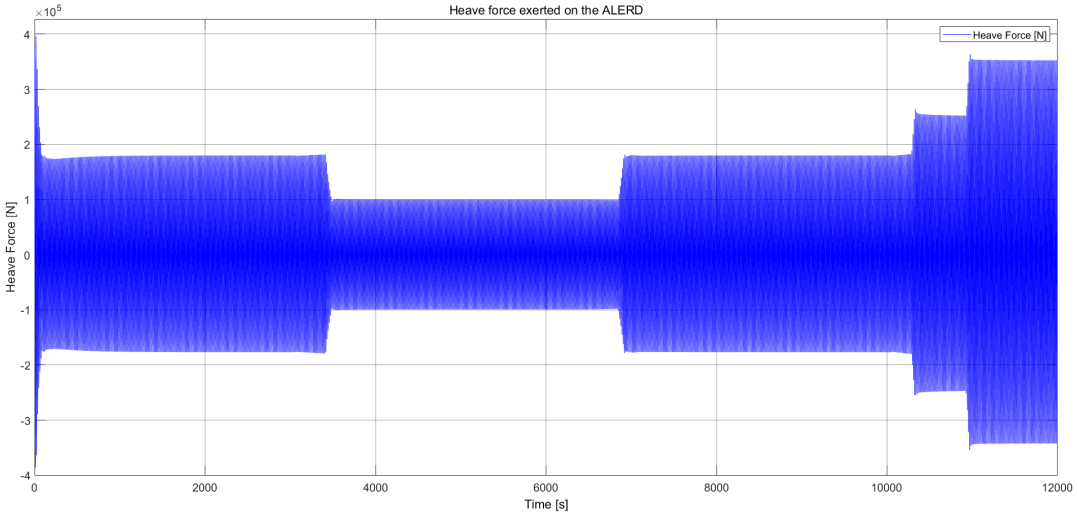

Figure A.4: Heave force exerted on ALERD created by the waves

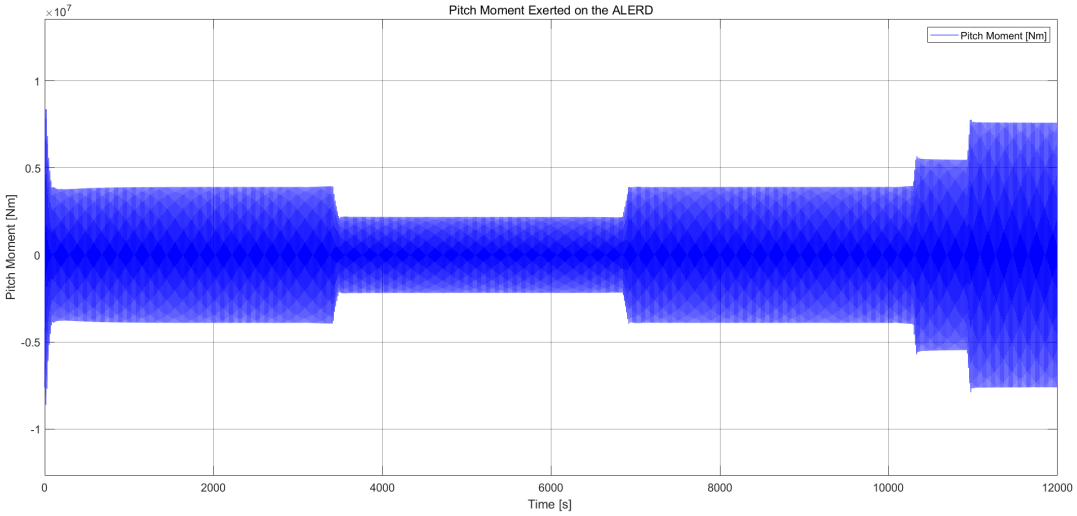

Figure A.5: Pitch moment exerted on ALERD created by the waves

A.1.3. Seabed Interaction

Identical behavior is illustrated in Figure A.8, Appendix, for the created pitch moment by the seabed.

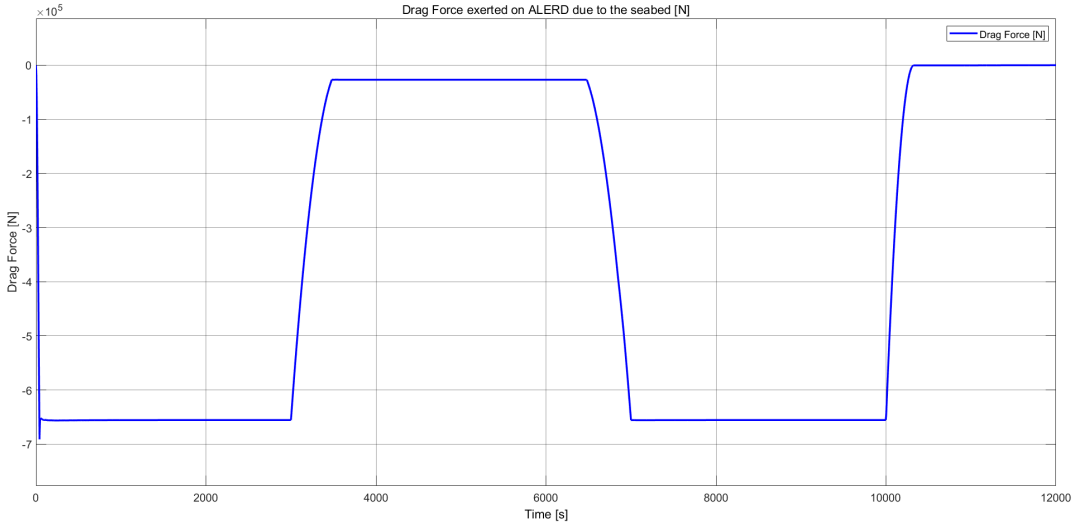

Figure A.6: Drag force created due to seabed exerted on the ALERD

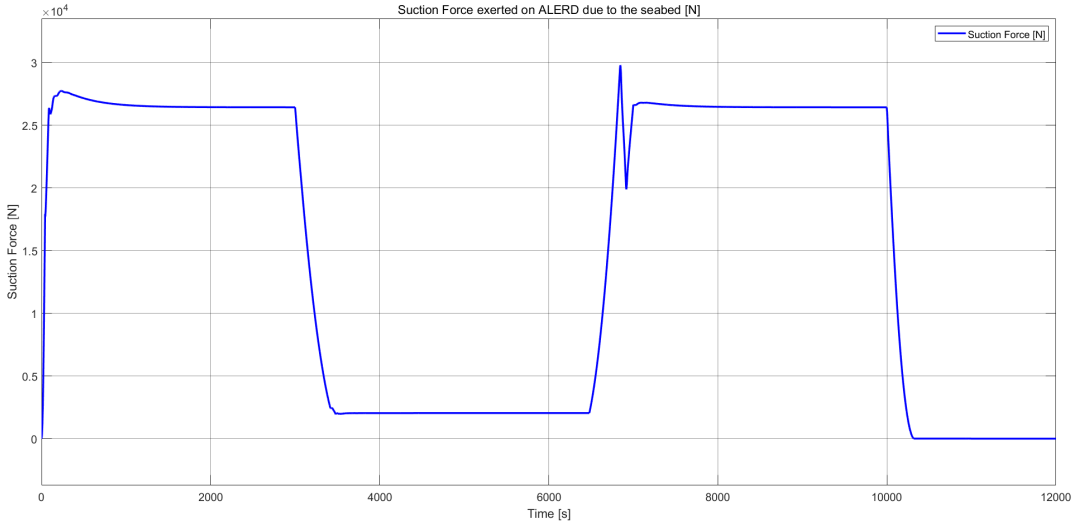

Figure A.7: Suction force created due to seabed exerted on the ALERD

A.2. Trim Tanks

Comparison between the peak velocity from Bakker's study [9] and the current project when the pipe dimeter is $D = 0.4m$.

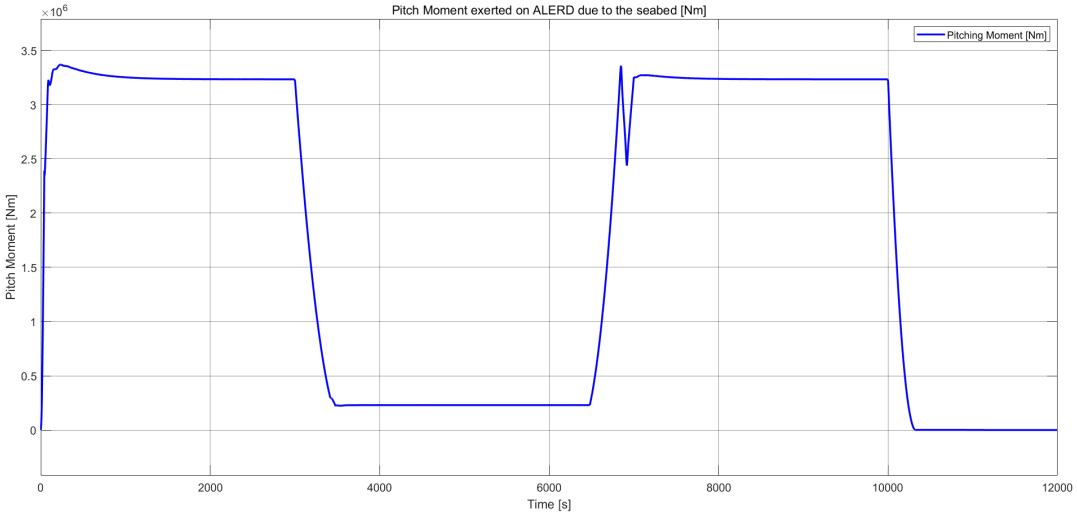

Figure A.8: Pitch moment created due to seabed exerted on the ALERD

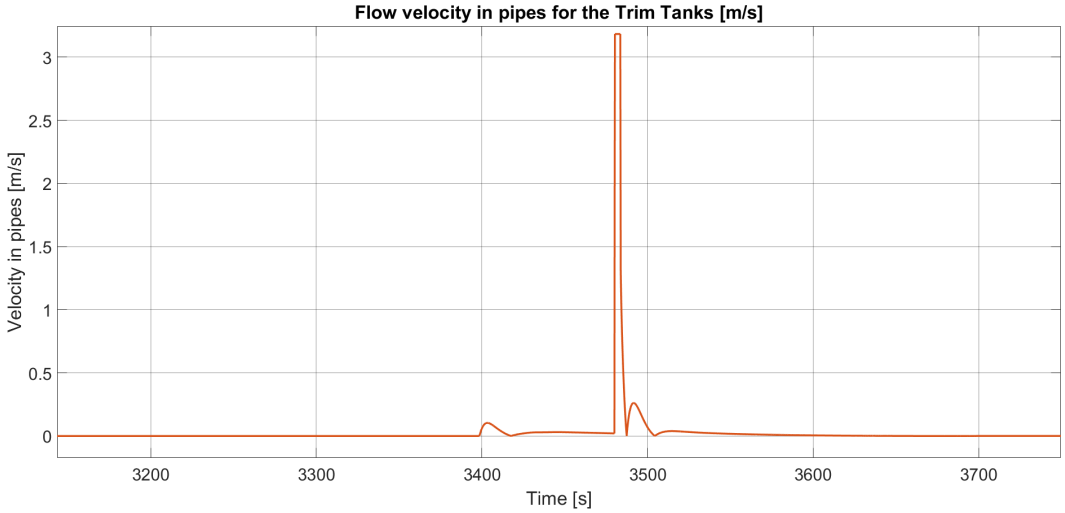

Figure A.9: Peak velocity in the pipes - Trim Tanks Bakker's

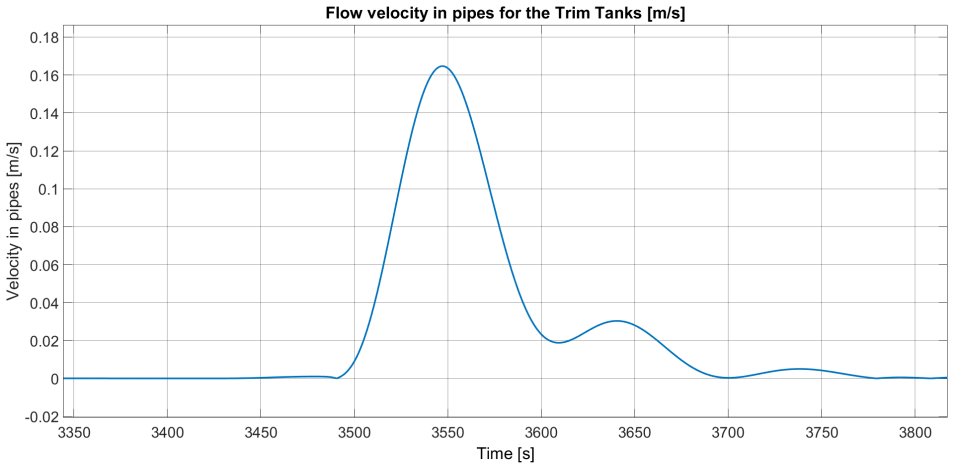

Figure A.10: Peak velocity in the pipes - Trim Tanks $D = 0.4m$

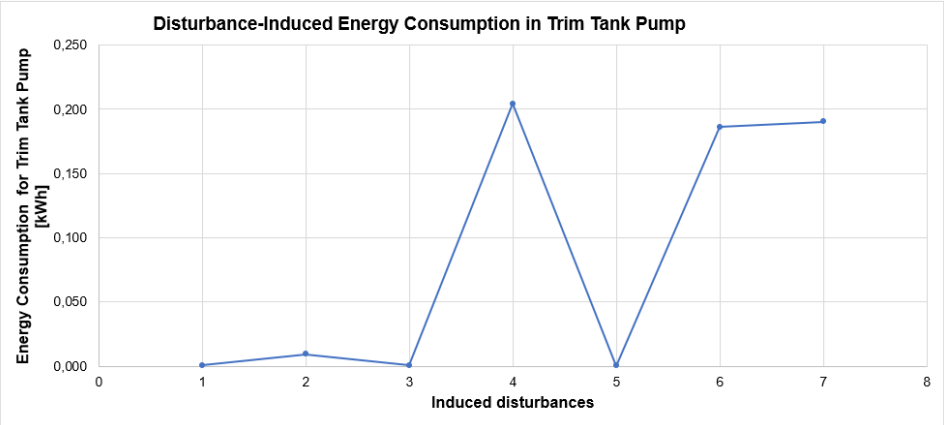

Figure A.11: Disturbance-induced energy consumption in trim tank pump

A.3. Combined scenario

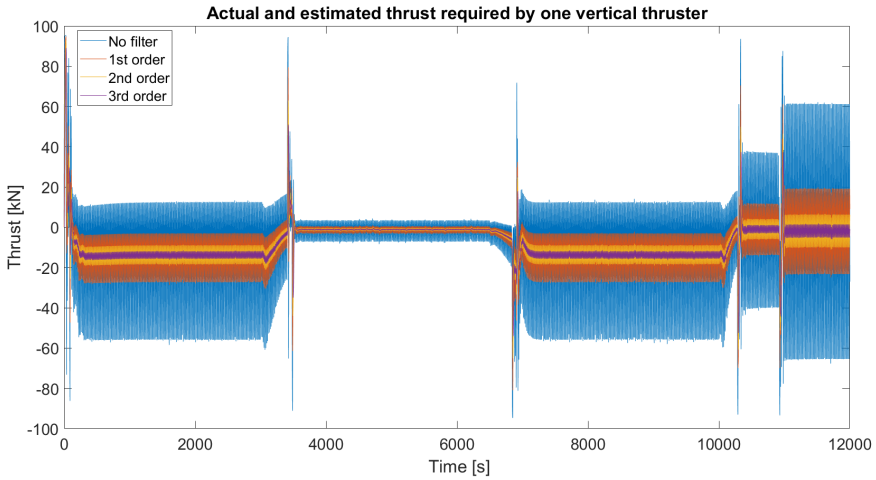

Figure A.12: Combined scenario - Actual and estimated thrust required by one vertical thruster

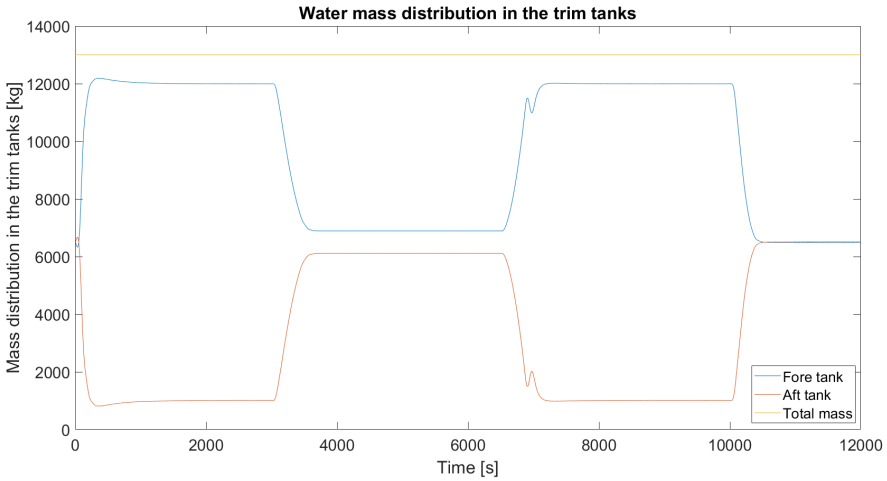

Figure A.13: Combined scenario - Water mass distribution in the trim tanks

A.4. Power according to time per actuator

A.4.1. Track following

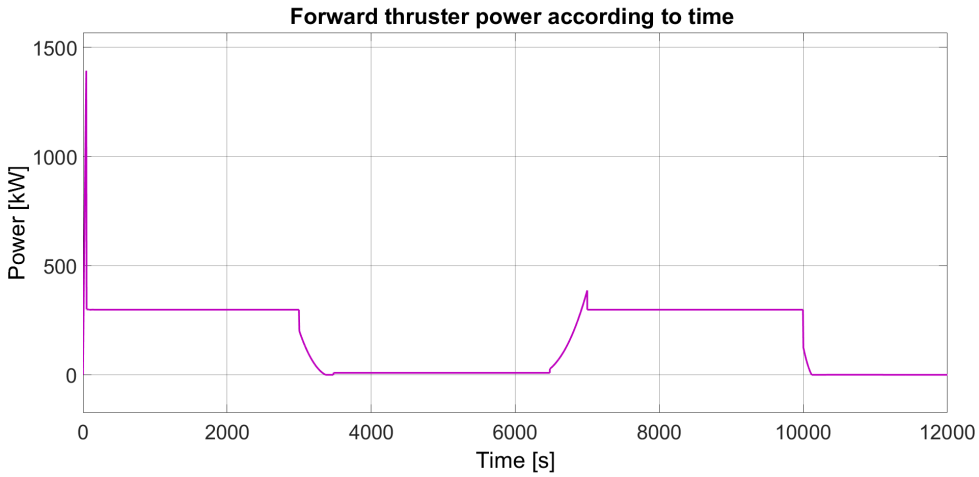

Figure A.14: Tack Following - Forward thruster power according to time

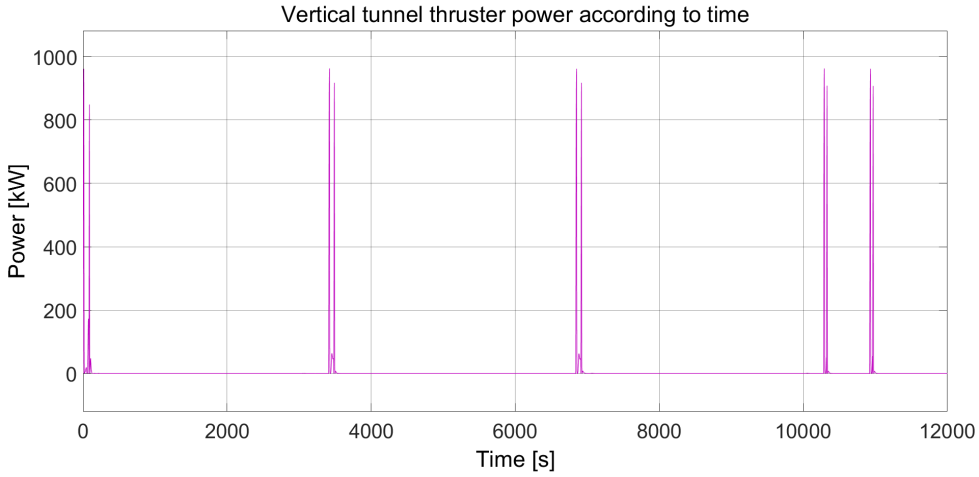

Figure A.15: Tack Following - Vertical tunnel thruster power according to time

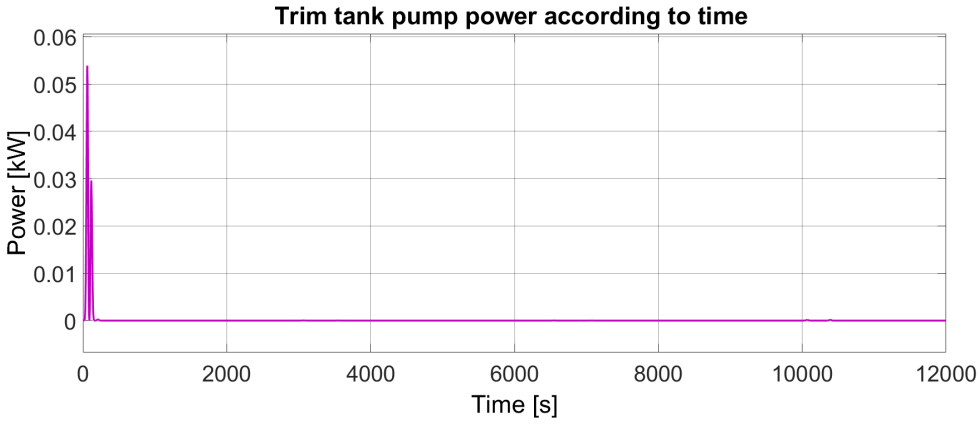

Figure A.16: Tack Following - Trim tank pump power according to time

A.4.2. Draghead Forces/Moments

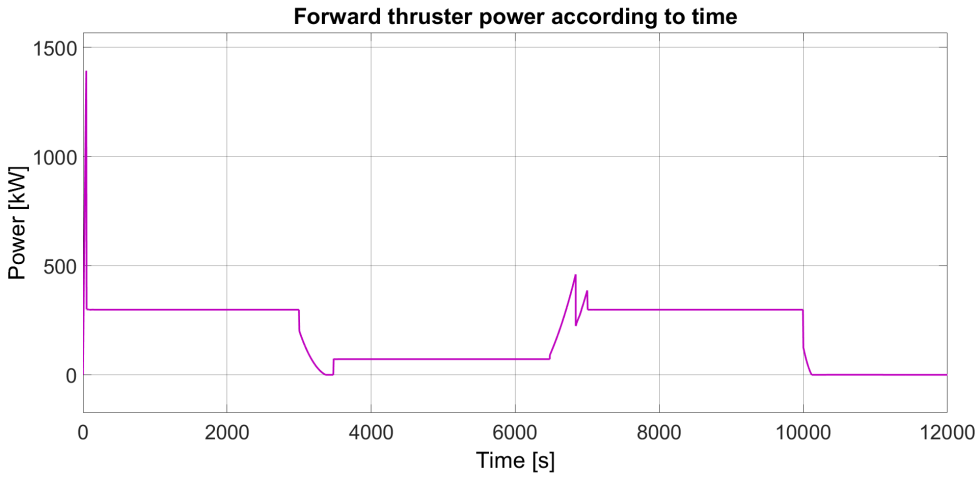

Figure A.17: Draghead Forces/Moments - Forward thruster power according to time

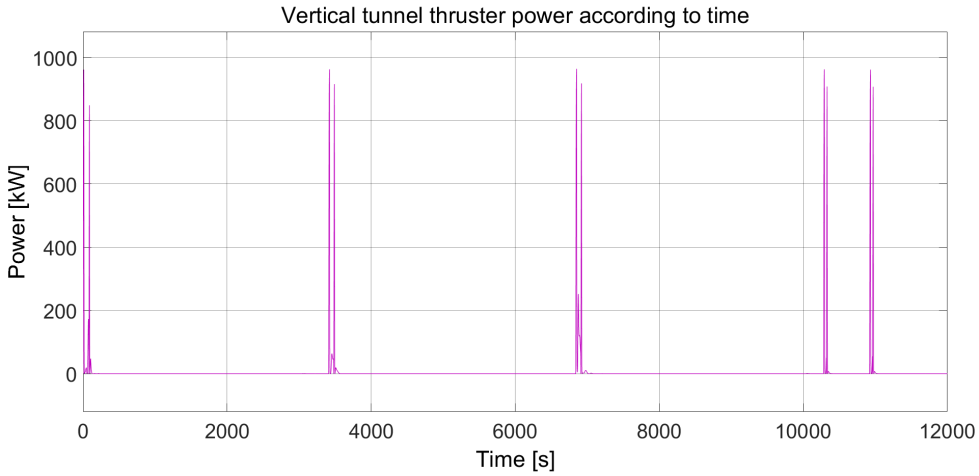

Figure A.18: Draghead Forces/Moments - Vertical tunnel thruster power according to time

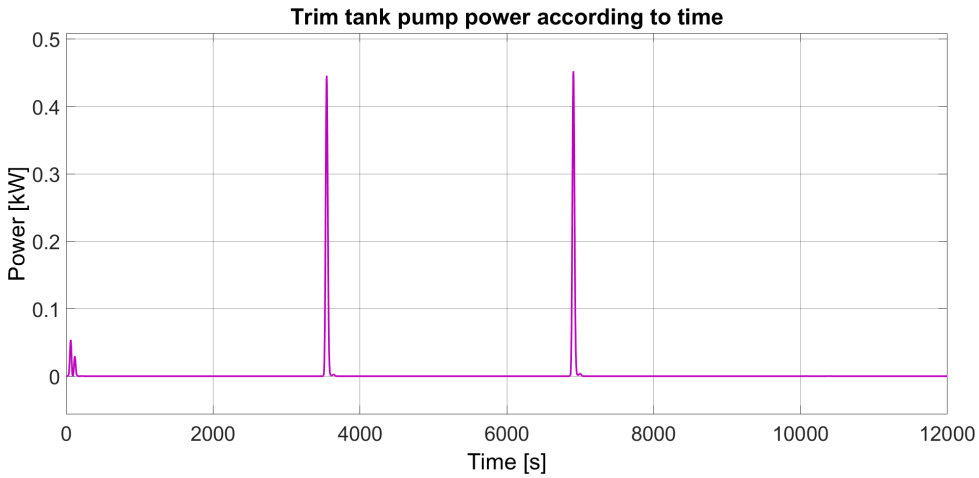

Figure A.19: Draghead Forces/Moments - Trim tank pump power according to time

A.4.3. Ocean Current

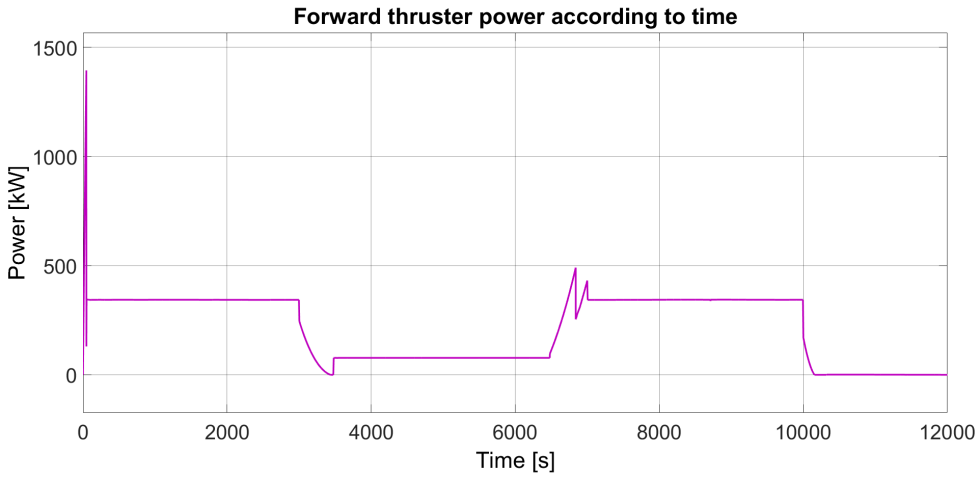

Figure A.20: Ocean Current - Forward thruster power according to time

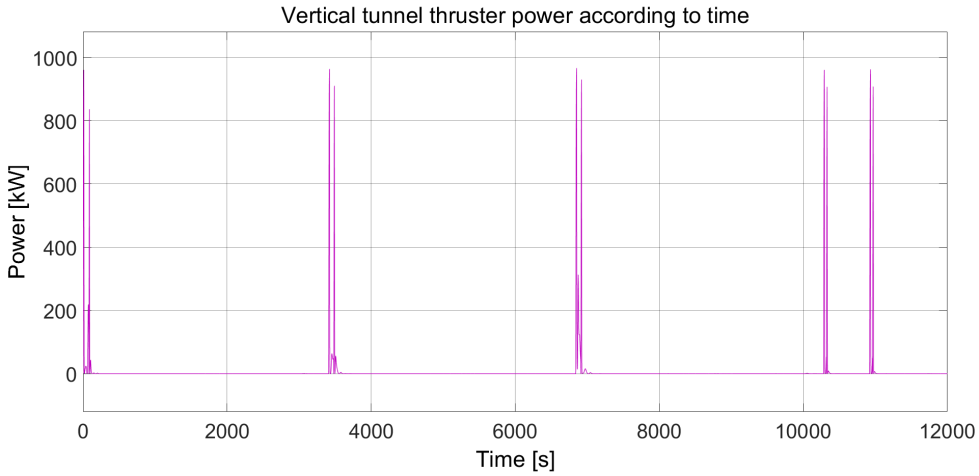

Figure A.21: Ocean Current - Vertical tunnel thruster power according to time

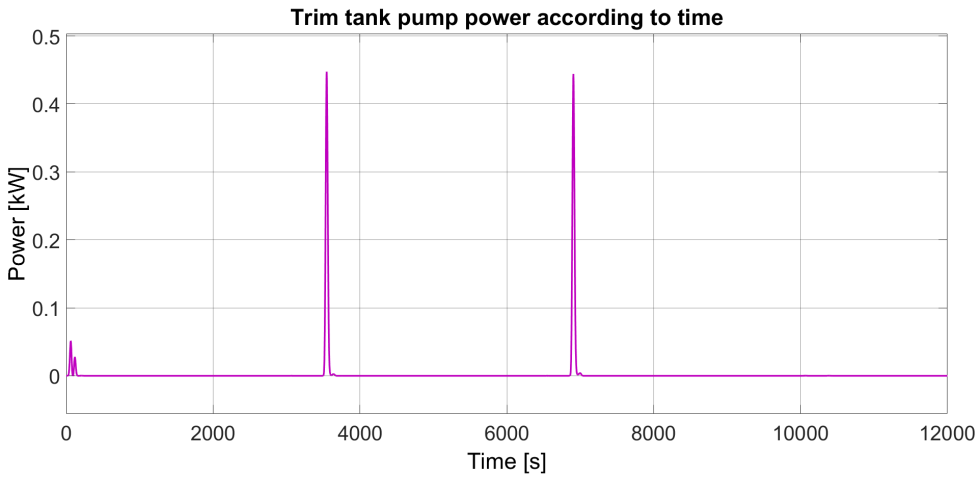

Figure A.22: Ocean Current - Trim tank pump power according to time

A.4.4. Ocean Waves

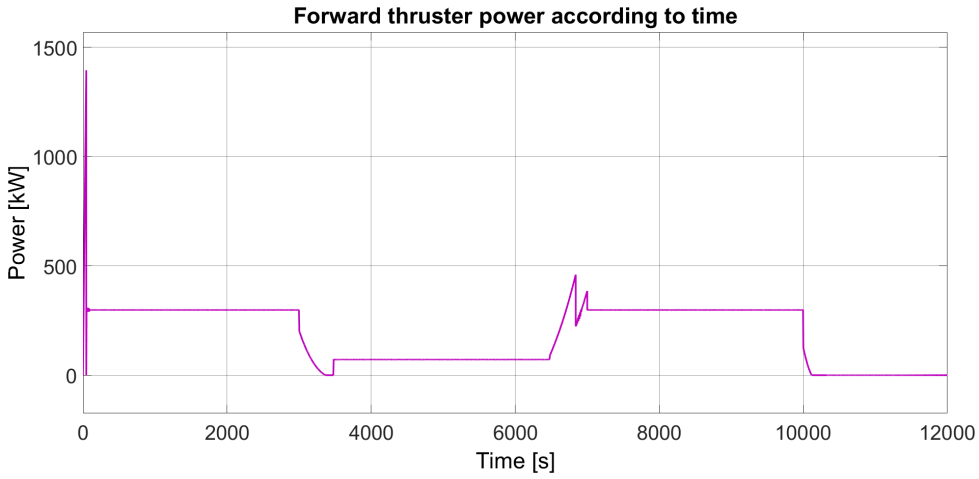

Figure A.23: Ocean Waves - Forward thruster power according to time

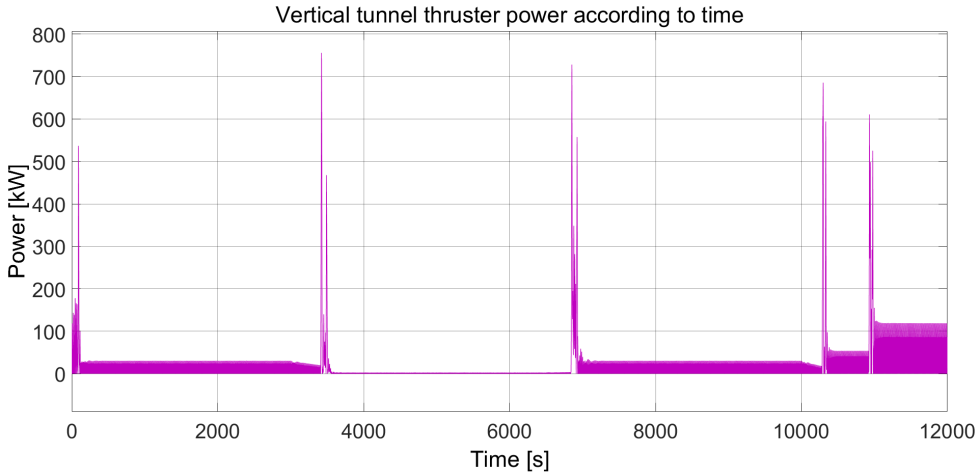

Figure A.24: Ocean Waves - Vertical tunnel thruster power according to time

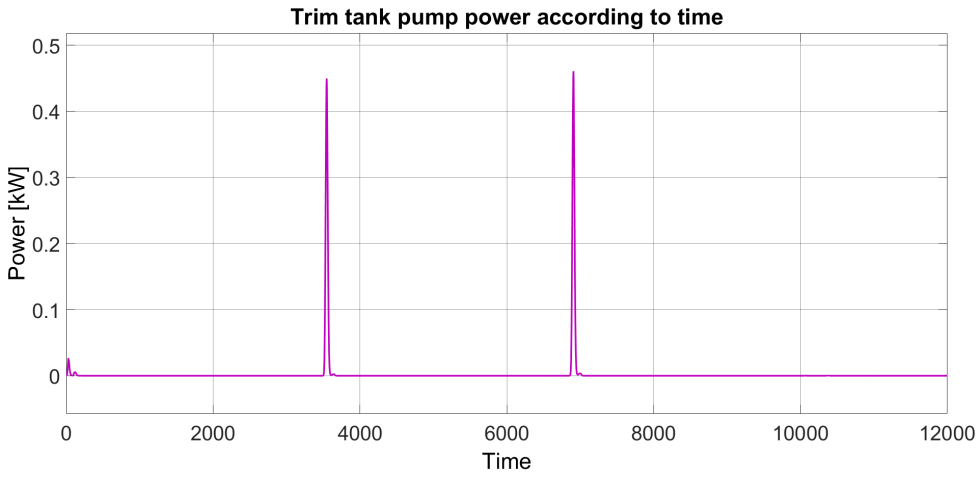

Figure A.25: Ocean Waves - Trim tank pump power according to time

A.4.5. Seabed Interaction

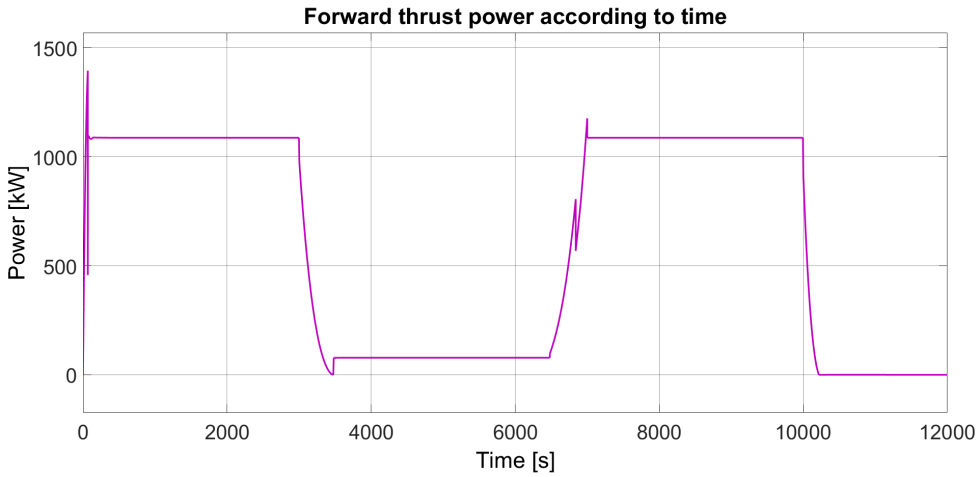

Figure A.26: Seabed Interaction - Forward thruster power according to time

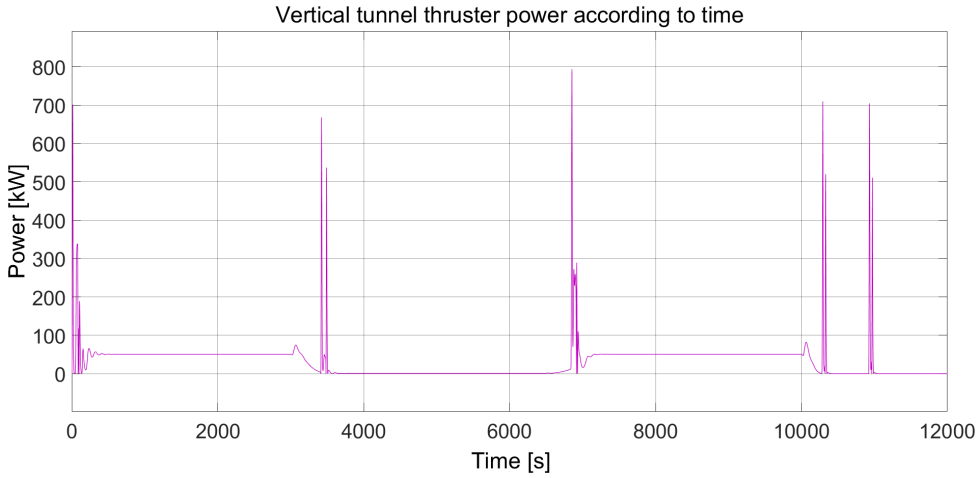

Figure A.27: Seabed Interaction - Vertical tunnel thruster power according to time

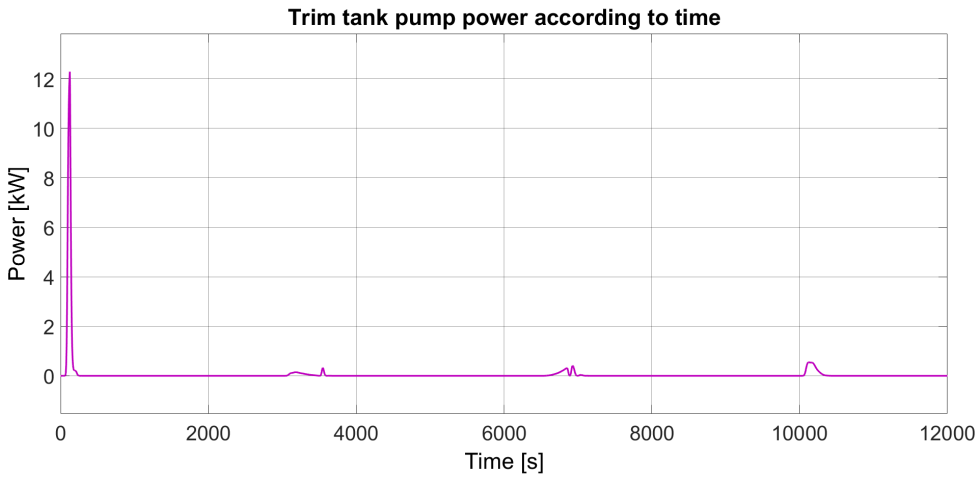

Figure A.28: Seabed Interaction - Trim tank pump power according to time

A.4.6. Combined Scenario wt Draghead

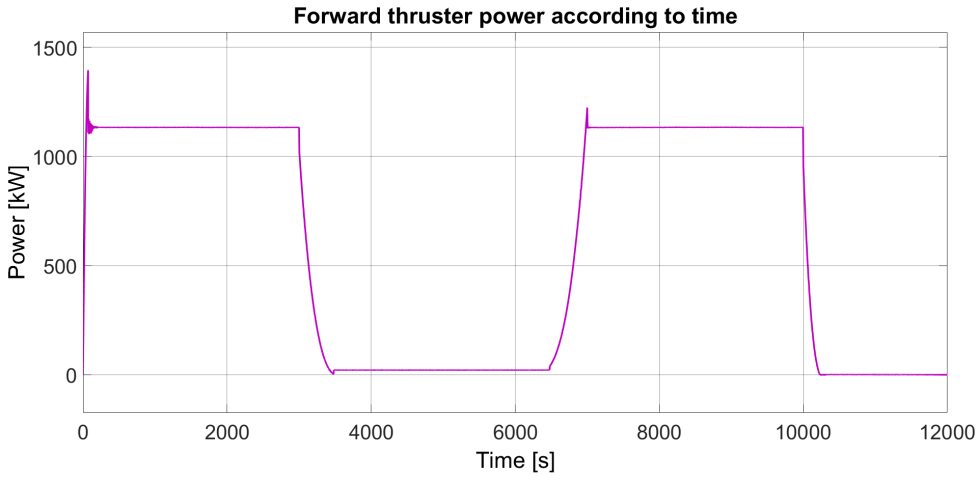

Figure A.29: Combined Scenario wt Draghead - Forward thruster power according to time

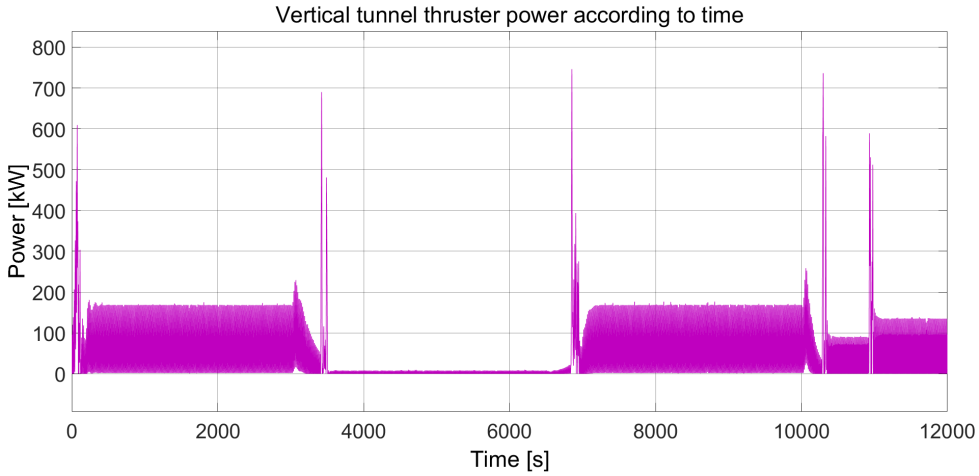

Figure A.30: Combined Scenario wt Draghead - Vertical tunnel thruster power according to time

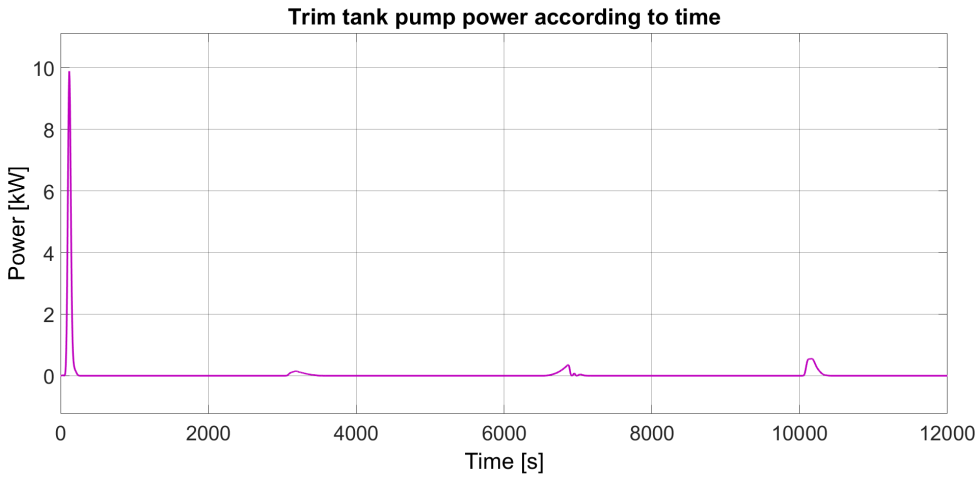

Figure A.31: Combined Scenario wt Draghead - Trim tank pump power according to time

A.4.7. Combined Scenario

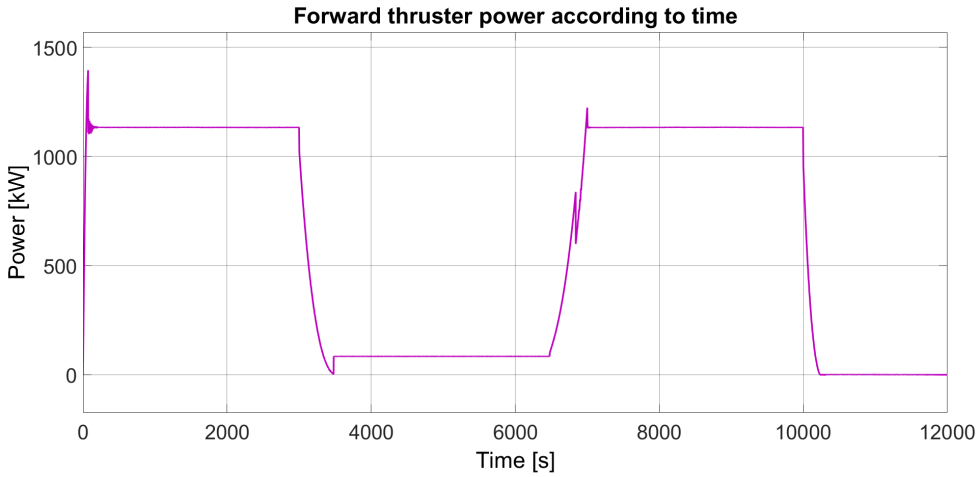

Figure A.32: Combined Scenario - Forward thruster power according to time

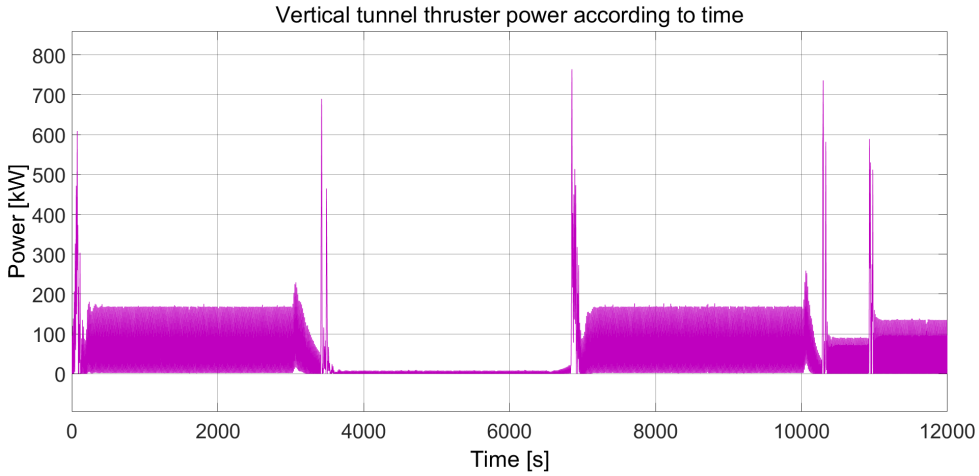

Figure A.33: Combined Scenario - Vertical tunnel thruster power according to time

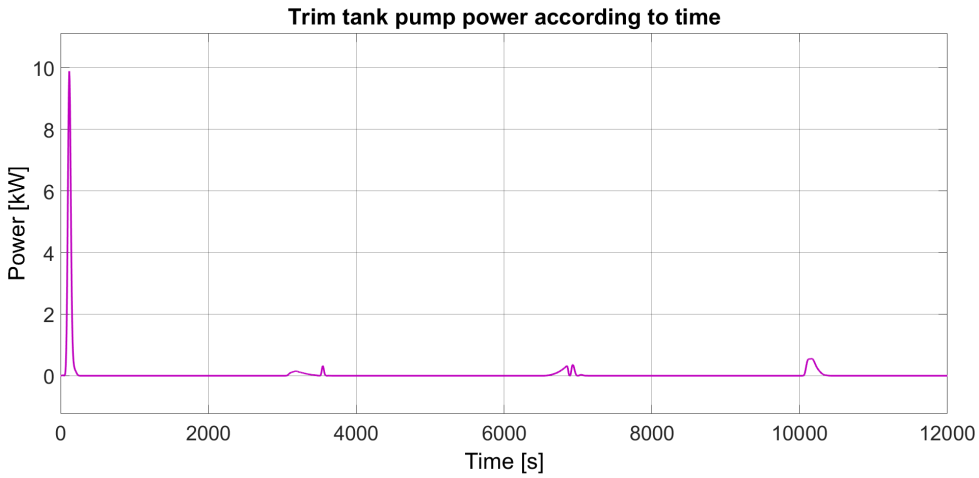

Figure A.34: Combined Scenario - Trim tank pump power according to time